UNIVERSIDADE DE BRASÍLIA – UnB
INSTITUTO DE GEOCIÊNCIAS – IG

GEOLOGIA, PETROLOGIA E GEOQUÍMICA DO CORPO ULTRAMÁFICO CABOCLO DOS MANGUEIROS, NOROESTE DA BAHIA, E SEU DEPÓSITO DE SULFETO DE Ni-Cu.

Vitor Bandeira Martins Matos

Dissertação de Mestrado nº 397

Brasília – DF
2017

UNIVERSIDADE DE BRASÍLIA – UnB
INSTITUTO DE GEOCIÊNCIAS – IG

GEOLOGIA, PETROLOGIA E GEOQUÍMICA DO CORPO ULTRAMÁFICO CABOCLO DOS MANGUEIROS, NOROESTE DA BAHIA, E SEU DEPÓSITO DE SULFETO DE Ni-Cu.

DISSERTAÇÃO DE MESTRADO

Autor: Vitor Bandeira Martins Matos

Orientador: Prof. Dr. Cesar Fonseca Ferreira Filho

Brasília – DF
2017

UNIVERSIDADE DE BRASÍLIA – UnB
INSTITUTO DE GEOCIÊNCIAS – IG

Geologia, petrologia e geoquímica do corpo ultramáfico Caboclo dos Mangueiros, noroeste da Bahia, e seu depósito de sulfeto de Ni-Cu.

Autor: Vitor Bandeira Martins Matos

Examinadores:

Prof. Dr. Cesar Fonseca Ferreira Filho (IG-UnB)
Prof. Dr. Catarina Labouré Bemfica Toledo (IG-UnB)
Prof. Dr. Johildo Salomão Figueiredo Barbosa (IG-UFBA)

Brasília, 25 de Julho de 2017.

“Por ironia do destino, esta conquista se dá ao tempo em que se completa uma década da partida de vocês. Dedico esta obra, mais uma vez, às memórias do meu primo irmão *Diego Martins Matos Nascimento* e da minha eterna educadora e avó *Noeme Martins Matos.*”

AGRADECIMENTOS

Agradeço a Deus, geólogo do universo que tem me guiado por caminhos os quais me tornam, a cada dia, um ser humano mais digno e humilde.

Aos familiares, minha querida mãe Maria Antônia, a quem devo toda gratidão pelos valores ensinados e pelo amor transmitido. Ao meu pai Fernando, meu maior exemplo de caráter e motivador pela busca do conhecimento, muito obrigado pelo incentivo diário. Ao meu irmão Alexandre, um parceiro generoso que sempre se predispõe a me ajudar. Ao primo Lucas (Cafu), quem tenho visto crescer diariamente, muito do que faço é procurando ser um exemplo para você. Aos tios e tias, primos e primas, e avôs, vocês são minha base, muito obrigado.

Agradeço especialmente aos meus amores, minha esposa Samille e filho João Guilherme. Meu convívio diário com vocês tem me tornado um homem generoso e com mais amor no coração. Obrigado pela paciência e apoio incondicionais. Amo vocês! E ao meu cachorro Bobin, companheiro das madrugadas escrevendo este trabalho.

Ao meu orientador, Prof. Dr. Cesar Fonseca Ferreira Filho, exemplo de profissionalismo, ética e dedicação ao trabalho. Obrigado por se engajar neste projeto e pela generosidade em compartilhar cada conhecimento adquirido ao longo de anos envolvido com os depósitos associados ao magmatismo máfico-ultramáfico.

Aos amigos de Brasília-DF. Minha amiga baiana Ticiara que me cedeu seu apartamento nos momentos de dificuldade para me instalar na capital do país. Minha amiga Mariana (Dalit), riquíssimas discussões geológicas você me proporcionou e muitas ajudas foram prestadas enquanto estava na Bahia, obrigado. Agradeço ao amigo Nonato, sempre disposto a me receber nos apartamentos da Colina – UnB.

À Universidade de Brasília, especialmente ao Programa de Pesquisa e Pós-Graduação em Geologia do Instituto de Geociências. A infraestrutura e acessibilidade aos laboratórios me permitiram realizar este trabalho com muita motivação. Agradeço à Jaqueline pelo auxílio em análises na Microssonda Eletrônica e ao Prof. Dr. Elton Dantas pelo apoio no Laboratório de Geocronologia.

À Companhia Baiana de Pesquisa Mineral – CBPM, pelo apoio no projeto, em especial ao Prof. Dr. José Haroldo da Silva Sá, quem deu o *start up* para que este apoio ocorresse e quem me recebeu inúmeras vezes em sua residência para discussões geológicas extremamente enriquecedoras. Sou um admirador seu ainda dos tempos de graduação na Universidade Federal da Bahia. Ao Prof. Dr. Johildo Barbosa pelo apoio na concessão de recursos para análises ao final deste projeto.

Sumário

Índice de Figuras

Índice de Tabelas

RESUMO

O depósito magmático de sulfetos de Ni-Cu Caboclo dos Mangueiros representa recente descoberta feita pela Companhia Baiana de Pesquisa Mineral (CBPM) no ano de 2012, por meio de trabalhos exploratórios no extremo noroeste do estado da Bahia, próximo à divisa com o estado do Piauí. O depósito está situado na borda noroeste do Cráton do São Francisco, próximo à zona de contato com a faixa de dobramentos Neoproterozoica Rio Preto, região em que outros complexos máfico-ultramáficos (M-UM) mineralizados são encontrados, a exemplo do complexo M-UM Campo Alegre de Lourdes, mineralizado a Fe-Ti-V. Quinze furos de sondagem rotativa foram realizados, totalizando 2670 m, e indicaram recurso preliminar de aproximadamente 200Mt@0.20%Ni e 0.13%Cu. A sulfetação de Ni-Cu no depósito compreende um corpo de minério hospedado em intrusão de composição essencialmente ultramáfica com aproximadamente 2 km de comprimento na direção WNW-ESE, ~500 m de largura, chegando a 270 m de profundidade na porção central e ~100 m nas extremidades. A estrutura remete a um *sill* (soleira) alongado em forma de barco. Dados litogeoquímicos de rocha total indicam que a composição das rochas ultramáficas é controlada pelo tipo e proporção modal de minerais cúmulus. Gráficos dos óxidos selecionados de elementos maiores e menores *versus* MgO indicam predominância de olivina e clinopironênio cumulados. Estes por sua vez seguem a seguinte sequência de cristalização: Ol => Ol + Cpx => Cpx, indicando composição insaturada em sílica para o magma parental. A intrusão está fracionada da porção norte, onde dunito e wehrlito prevalecem, para a porção sul em que clinopiroxenito é abundante. O fracionamento é também observado no decréscimo progressivo dos valores de #Mg catiônico (*i.e.*, Mg/[Mg+Fe^{2+}]) de cristais cúmulus de clinopiroxênio em direção à porção sul da intrusão, como indicado pela variação de #Mg catiônico em clinopiroxênios de clinopiroxenito e wehrlito de furos de sondagem localizados na seção central perpendicular à intrusão (*i.e.*, NE-SW). A variação composicional de #Mg catiônico nos clinopiroxênios é entre 0.78 e 0.94, sugerindo composição moderada a muito primitiva para o magma parental. Perfis de elementos terras raras e elementos traço resistentes à alteração, em gráficos normalizados ao manto primitivo, para as rochas cumuláticas ultramáficas mostram enriquecimento em elementos terras raras leves (ETRL) com significativas anomalias negativas de Nb e Ta. Este enriquecimento também é mostrado em perfis de elementos traço resistentes à alteração para o líquido parental estimado, embora anomalias negativas de Nb-Ta não são observadas. Os dados revelam que os padrões de ETRL são dependentes da proporção modal de clinopiroxênio nas rochas cumuláticas, como indicado pela diminuição progressiva nos valores da razão La/Sm (normalizados ao manto primitivo) de dunito, wehrlito, olivina-clinopiroxenito e clinopiroxenito. Significativa assimilação de rochas crustais não é suportada pela sequência de cristalização típica de magmas insaturados em sílica, bem como pela falta de anomalias negativas de Nb-Ta. A mineralização do depósito é dominantemente (*i.e.*, ~99% em volume) de natureza primária e disseminada em forma de agregados (*blebs*) intersticiais, formando associações de pirrotita, pentlandita, calcopirita e pirita. A mineralização secundária consiste da remobilização e recristalização da mineralização primária e compreende em torno de 1% em volume do depósito. Ocorre em forma de brechas, vênulas ou ao longo do plano de foliação da rocha quando associadas a zonas de cisalhamento discretas. As texturas primárias e o conteúdo de sulfetos no depósito, acima da proporção considerada cotética numa intrusão mineralizada, sugerem entradas de magma carreando sulfetos em suspensão através de estrutura de conduto magmático que posteriormente se solidificou como um *sill* alongado em forma de barco. A saturação de sulfetos no magma é entendida como sendo decorrente da diminuição da temperatura, sem assimilação de rocha ou enxofre de origem crustal. Resultados das análises de isótopos de enxofre indicam composição isotópica para os sulfetos disseminados compatível com a composição isotópica do manto. Adicionalmente, o intervalo restrito dos valores da composição isotópica das amostras não sugere diferenças na composição isotópica relacionada a diferentes rochas (*i.e.*, wehrlito ou clinopiroxenito) de diferentes locais da intrusão ultramáfica. O conteúdo depletado de elementos do grupo da platina na composição dos sulfetos, provenientes de magma parental primitivo, é sugestivo que tenha ocorrido segregação prévia de sulfetos em profundidade. Eventos tectônicos e metamorfismo em fácies xisto verde afetaram o *sill* fracionado e suas rochas crustais encaixantes. Apesar da tectônica, a estrutura magmática primária se manteve preservada. Devido à falta de idades absolutas para as rochas ultramáficas, o posicionamento do depósito Caboclo dos Mangueiros na evolução tectônica do cráton do São Francisco permanece incerto.

ABSTRACT

The Caboclo dos Mangueiros magmatic Ni-Cu sulfide deposit represents a recent discovery in the northern Brazil made by Companhia Baiana de Pesquisa Mineral (CBPM) in 2012 by means of greenfield exploration works at the northwestern portion of the Bahia state, close to the limit with the Piauí state. The deposit is situated in the northwestern edge of the São Francisco craton, close to the contact with the Rio Preto Neoproterozoic fold belt, where a cluster of mineralized mafic-ultramafic complexes are found, as exemplified by the Fe-Ti-V Campo Alegre de Lourdes mafic-ultramafic complex. Fifteen drill holes were performed, totalizing 2,670 meters, and indicate preliminary resource of ~ 200Mt@0.20%Ni and 0.13%Cu. The Ni-Cu sulfides comprise an orebody hosted in an ultramafic intrusion with ~2 km long WNW-ESE trending, ~500 m wide, reaching ~270 m depth in central portions and ~100 m in the extremities, resembling an elongated boat-shaped sill. The composition of the ultramafic rocks is controlled by the type and modal proportion of cumulus minerals. The plots of selected major and minor element oxides versus MgO indicate the predominance of olivine and clinopyroxene cumulates. It follows a crystallization sequence consisting of Ol => Ol + Cpx => Cpx, which indicate a silica undersaturated composition for the parental magma. The intrusion is fractionated from the northern portion, where dunite and wehrlite prevail, to the southern where clinopyroxenite is abundant. The fractionating also is observed in the progressively decrease of cationic Mg# values (i.e., $Mg/[Mg+Fe^{2+}]$) in cumulus clinopyroxene crystals toward the southern portion of the intrusion, as indicated by the variation in cationic Mg# in clinopyroxene from clinopyroxenites and wehrlite from bore holes located across a NE-SW section of the intrusion. The compositional range of cationic Mg# of cumulus clinopyroxene from 0.78 to 0.94 supports a moderate to primitive composition for the parental magma. Primitive mantle-normalized REE and primitive mantle-normalized alteration-resistant trace element profiles for the cumulate ultramafic rocks show enrichment in LREE with significant negative Nb and Ta anomalies. This enrichment is also showed in mantle-normalized alteration-resistant trace element profiles estimated to the parental melt, although negative Nb-Ta anomalies are not observed. The data reveal that LREE patterns are dependent of the modal proportion of clinopyroxene in the cumulate rocks, as indicated by progressively lower La/Sm_{PM} from dunite, werhlite, olivine-clinopyroxenite and clinopyroxenite. Significant assimilation of crustal rocks during ascent and emplacement of the magma is not supported by the crystallization sequence typical of silica undersaturated magmas, as well as by the absence of Nb-Ta anomalies. The mineralization of the deposit is mainly (i.e., ~99 vol.%) primary nature and disseminated as interstitial blebs, comprising pyrrhotite, pentlandite, chalcopyrite and minor pyrite. The secondary mineralization consists of remobilization and recrystallization of the primary one and represent about 1 vol.% of the deposit. It occurs in irregular veinlets and breccia, as well as sulfide aggregates or stringers concordant with the foliation in discrete shear zones. The primary textures and the amount of sulfides, well above the cotectic proportion for a mineralized intrusion, suggest emplacement of sulfide droplets-charged magma through a conduit structure that later solidified as an elongated boat-shaped sill. The sulfide saturation of the magma is understood due to the decrease of temperature, with no significant assimilation of crustal-derived rock or sulfur. Results for sulfur isotope indicate isotopic compositions for disseminated sulfides that mainly fit into the mantle range. Additionally, the narrow compositional range of isotopic compositions in our samples does not suggest differences in isotopic compositions related to different host rocks (i.e., wehrlite or clinopyroxenite) of different location in the ultramafic intrusion. The depletion of PGE in the sulfide composition from a moderate to primitive magma is suggestive that has been occurred previous sulfide segregation at depth. Tectonic events and greenschist facies metamorphism may have affected the fractionated ultramafic sill and its sedimentary country rocks. Despite the tectonics the primary magmatic structure remains well preserved. Due to the lack of an absolute age for the ultramafic rocks the positioning of the Caboclo dos Mangueiros deposit in the tectonic evolution of the São Francisco craton remains uncertain.

CONSIDERAÇÕES GERAIS

1. Introdução

Depósitos de Ni-Cu hospedados em intrusões de composição máfico-ultramáfica são amplamente classificados dentre aqueles associados a condutos magmáticos ou a intrusões acamadadas (Beresford and Hronsky, 2014). Contudo, nenhum grande depósito sulfetado de Ni-Cu tem sido descoberto em zonas basais de grandes intrusões acamadadas de natureza máfico-ultramáfica em mais de meio século, portanto sistemas magmáticos dinâmicos ascendentes através de estruturas de condutos têm se tornado alvos favoráveis para exploração de depósitos sulfetados de Ni-Cu (Maier et al., 2001; Song et al., 2012). Significativa importância também é atribuída ao ambiente tectônico favorável para este tipo de depósito. Begg et al. (2010) reconheceram associação espacial empírica entre diversos depósitos sulfetados de Ni-Cu-EGP (*e.g.*, Niril'sk, Naldrett, 1992; Voisey's Bay, Li and Naldrett, 1999), desde grandes campos a pequenos depósitos, e zonas de bordas litosféricas, mais especificamente com margens de blocos cratônicos Arqueanos, independente se formaram riftes ou não.

O depósito magmático de sulfetos de Ni-Cu Caboclo dos Mangueiros foi descoberto no ano de 2012, pela Companhia Baiana de Pesquisa Mineral (CBPM), por meio de trabalhos exploratórios desenvolvidos no extremo noroeste do estado da Bahia, próximo à divisa com o estado do Piauí. Esta região consiste na zona da borda norte-noroeste do Cráton do São Francisco (Almeida, 1977) próximo ao contato com a faixa de dobramentos Rio Preto (Uhlein et al., 2011), região em que outros complexos máfico-ultramáficos mineralizados são encontrados (*e.g.*, Complexo de Campo alegre de Lourdes, Sampaio et al., 1986).

O depósito consiste de corpo de minério com recurso preliminar de ~200Mt@0.20%Ni e 0.13%Cu (Projeto Valorização de Alvos Geofísicos; relatório interno da CBPM não publicado). A mineralização do depósito é dominantemente de natureza primária disseminada e está hospedada em rochas de composição essencialmente ultramáfica que compõem uma intrusão alongada com aproximadamente 2 km de comprimento, ~500 m de largura, chegando a 270 m de profundidade na porção central e ~100 m nas extremidades. Sulfetos disseminados ocorrem ao longo de toda a porção sondada da intrusão com conteúdo médio entre 1 e 5 % em volume, sugerindo um corpo de minério de baixo teor e grande volume, coincidente com a intrusão alongada. Este conteúdo de sulfetos em volume pode ser considerado acima da proporção cotética de sulfetos para uma intrusão magmática mineralizada (Ripley & Li, 2013).

Esta recente descoberta motivou a realização do presente trabalho que consiste na primeira descrição e caracterização detalhada da estrutura magmática e da mineralização de Ni-Cu do depósito Caboclo dos Mangueiros. Para tanto foram feitas novas avaliações do banco de dados da CBPM (*e.g.*, furos de sondagem, geoquímica dos furos, lâminas petrográficas e levantamentos geofísicos), além de estudos analíticos adicionais como descrição de novas seções delgadas polidas, litogeoquímica, química mineral e estudos isotópicos de enxofre. Os resultados culminaram na reinterpretação da estruturação e gênese do depósito, como sendo

de natureza magmática primária, depletada em elementos do grupo da platina (EGP) e hospedada em estrutura de conduto que posteriormente se solidificou como um *sill* (soleira) alongado.

2. Localização e Fisiografia

A área do depósito sulfetado de Ni-Cu Caboclo dos Mangueiros, objeto deste estudo, localiza-se no extremo noroeste do estado da Bahia a 880 km da capital Salvador, próximo à divisa com o sul do estado do Piauí, nordeste do Brasil. O vilarejo homônimo está inserido no município de Campo Alegre de Lourdes, localizado aproximadamente 50 km em linha reta a nordeste (Figura i.1).

O depósito de Ni-Cu Caboclo dos Mangueiros está inserido na região climática do semi-árido, a qual apresenta baixos índices de chuvas, normalmente com média anual abaixo de 850 mm, associados a elevadas taxas de evapotranspiração e altas temperaturas, com médias anuais acima dos 25ºC. O relevo regional que hospeda o depósito, dominantemente plano arrasado com pequenas elevações também planas, compõe o domínio geomorfológico pediplano sertanejo. As porções planas arrasadas apresentam média de cotas altimétricas de 480 m e estão associadas à extensa cobertura sedimentar inconsolidada tércio-quaternária, enquanto que as áreas mais elevadas (~500 m) são sustentadas por crostas lateríticas ferruginosas.

3. Justificativas e Objetivos

A região noroeste do estado da Bahia, em que o depósito de Ni-Cu sulfetado Caboclo dos Mangueiros está localizado, possui diversas intrusões de natureza máfico-ultramáficas hospedeiras de importantes depósitos minerais, a exemplo do depósito de Fe-Ti-V do Complexo Máfico-Ultramáfico de Campo Alegre de Lourdes (Sampaio et al., 1986) e do depósito de P_2O_5 do Complexo Carbonatítico Angico dos Dias (Silva et al., 1987, 1988, 1997; Antonini et al., 2003), atualmente explotado pela Mineração Galvani S.A., além de ocorrências de mineralizações de Fe-Ti-V do Complexo Máfico-Ultramáfico Peixe (Leite et al. 1993, 1997). Portanto, trata-se de um cenário geológico altamente favorável para exploração mineral que, em contrapartida, é pouco conhecido e carece de estudos acadêmicos sistemáticos. Este trabalho é desenvolvido em cooperação com a Companhia Baiana de Pesquisa Mineral, empresa de exploração mineral responsável pelas pesquisas que resultaram na descoberta do depósito.

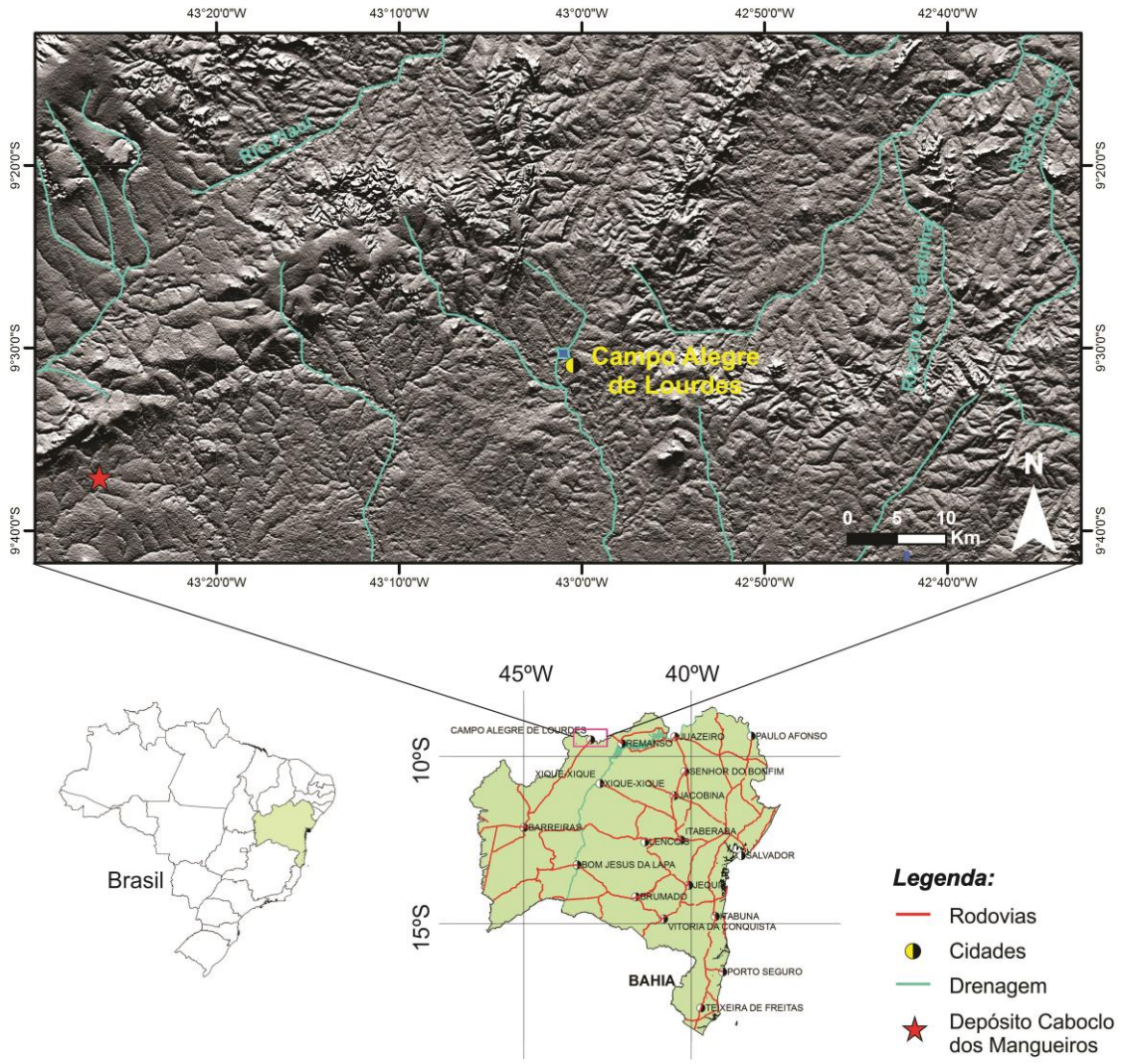

Figura i.1: Mapa de localização da área com principais drenagens e modelo digital de terreno.

O estudo sistemático do depósito Caboclo dos Mangueiros, de caráter inédito, apresenta importância tanto de cunho exploratório para empresas de mineração, como acadêmico. Além de proporcionar a abertura de novas perspectivas metalogenéticas em corpos máficos e/ou ultramáficos adajecentes, e por fim, os trabalhos contribuem para o conhecimento da metalogênese de depósitos de Ni-Cu sulfetado.

O principal objetivo deste estudo é definir a gênese e os controles da mineralização de Ni-Cu sulfetado do depósito Caboclo dos Mangueiros. Para isto serão fornecidas informações de caráter geológico, petrográfico e petrológico, incluindo dados litogeoquímicos, isotópicos e de química mineral, tanto da intrusão como do corpo de minério sulfetado. Estas informações também servirão de suporte para o entendimento integrado da evolução e estruturação magmática do corpo ultramáfico hospedeiro, bem como dos processos magmáticos responsáveis pela mineralização.

4. Métodos

Para alcançar os objetivos pré-estabelecidos neste estudo, os trabalhos iniciaram-se com revisão bibliográfica. Esta etapa incluiu revisão e compilação do acervo de dados da CBPM (relatórios internos, descrições e litogeoquímica dos furos de sondagem e lâminas petrográficas), bem como o estudo das informações disponíveis sobre depósitos magmáticos de Ni-Cu sulfetado e do conhecimento geológico da região por meio de artigos científicos.

No intuito de apresentar o detalhamento geológico da intrusão, foram feitas duas etapas de campo. Durante a primeira etapa, realizaram-se novas descrições dos 15 furos de sondagem, disponíveis na litoteca da CBPM, em Salvador, Bahia. Nestas atividades foram adotadas sistemáticas de trabalho próprias, visando o entendimento da estruturação magmática da intrusão e da mineralização. Estes trabalhos contaram com a participação do orientador e apoio logístico da CBPM, e foram realizados com auxílio dos resultados de litogeoquímica dos furos de sondagem e após descrição prévia das lâminas petrográficas, ambos disponibilizados pela empresa. Ainda nesta etapa foram feitas novas amostragens para estudos analíticos petrográficos / química mineral, litogeoquímicos e isotópicos. A segunda etapa de campo consistiu em campanha de seis dias *brownfield*, com descrição e amostragem de afloramentos da intrusão ultramáfica e das rochas encaixantes, bem como das rochas que compunham o cenário geológico e tectônico regional.

Os estudos petrográficos consistiram de duas etapas, uma inicial realizada no laboratório de microscopia da CBPM, utilizando as 32 lâminas delgadas polidas disponibilizadas pela empresa e uma etapa final realizada nos laboratórios de microscopia do Instituto de Geociências da Universidade de Brasília (IG-UnB). Esta segunda etapa consistiu do estudo de 40 novas lâminas delgadas polidas, confeccionadas no Laboratório de Laminação do IG-UnB. Os estudos petrográficos forneceram suporte na seleção de amostras para estudos de química mineral e litogeoquímica.

Análises de química mineral utilizando microssonda eletrônica foram realizadas no Laboratório de Microssonda Eletrônica do IG-UnB, em equipamento JEOL JXA-8230. Foram analisados de forma sistemática cristais de clinopiroxênio, anfibólio e sulfetos (calcopirita, pentlandita, pirrotita e pirita / marcassita). O tratamento dos dados foi feito por meio de planilha eletrônica *Microsoft Excel*® e os resultados analíticos encontram-se nos Apêndices 1, 2 e 3.

As análises litogeoquímicas de rocha total e a preparação do total de 13 amostras para elementos maiores, menores e traços foram realizadas nos laboratórios da SGS GEOSOL. Os elementos maiores foram analisados por fluorescência de raios X (XRF) em amostras decompostas através de fusão com tetraborato de lítio. Elementos menores e traços foram analisados por Espectrometria de Emissão Ótica por Plasma Acoplado Indutivamente (ICP-OES) após digestão multi-ácida (HCl-HNO_3-$HClO_4$-HF). Os elementos terras raras (ETR), nióbio (Nb), tântalo (Ta), háfnio (Hf) e rubídio (Rb) foram analisados por Espectrometria de Massa por Plasma Acoplado Indutivamente (ICP-MS), após fusão com metaborato de lítio. As concentrações de enxofre (S) foram determinadas pelo método LECO. Para determinação dos conteúdos dos elementos ouro (Au), platina (Pt) e paládio (Pd) foi utilizado ICP-OES após

concentração prévia padrão por fusão *Fire Assay*. O tratamento dos dados foi feito por meio de planilha eletrônica *Microsoft Excel*® e os resultados analíticos encontram-se na Tabela 1.

Seis amostras, representativas da mineralização, foram coletadas do depósito Caboclo dos Mangueiros para estudos isotópicos de enxofre. Estas análises foram realizadas no Laboratório de Geocronologia do IG-UnB. As composições isotópicas de enxofre foram determinadas por Espectrometria de Massa de Razão Isotópica (IRMS), utilizando o espectrômetro Thermo Scientific MAT253 IRMS. O tratamento dos dados foi feito por meio de planilha eletrônica *Microsoft Excel*® e os resultados analíticos encontram-se na Tabela 2.

5. Escopo do Estudo

Conforme previsto no regulamento do Curso de Pós-graduação em Geologia da Universidade de Brasília e por sugestão do Orientador, esta dissertação de mestrado apresenta-se estruturada na forma de artigo a ser submetido para publicação em periódico com corpo editorial. O artigo é apresentado na forma que será submetido, mantendo o estilo e o formato previstos no periódico.

O artigo, intitulado **"*The Caboclo dos Mangueiros Deposit: Ni-Cu sulfide mineralization hosted in ultramafic cumulates in the northern edge of the São Francisco Craton, Brazil.*"** foi elaborado durante o ano de 2017 e será submetido à revista ***Economic Geology.*** Este artigo tem como principal objetivo definir a gênese e os controles da mineralização de Ni-Cu sulfetado do depósito Caboclo dos Mangueiros, bem como sua contextualização no cenário global dos depósitos de Ni-Cu sulfetado.

Referências

Almeida, F.F.M., 1977, O Cráton do São Francisco: Revista Brasileira Geociências, v. 7, n. 4, p. 349-364.

Antonini, P., Comin-Chiaramonti, P., Gomes, C.B., Censi, P., Riffel, B.F., and Yamamoto, E., 2003, The Early Proterozoic carbonatite complex of Angico dos Dias, Bahia State, Brazil: geochemical and Sr-Nd isotopic evidence for an enriched mantle origin: Mineralogical Magazine, v. 67, n. 5, p. 1039-1057.

Begg, G.C., Hronsky, J.A.M., Arndt, N.T., Griffin, W.L., O'Reilly, S.Y., and Hayward, N., 2010, Lithospheric, cratonic and geodynamic setting of Ni–Cu–PGE sulfide deposits: Economic Geology, v. 105, p. 1057–1070.

Beresford, S.W., and Hronsky, J.M.A., 2014, The chonolith Ni–Cu model: expanding the footprint of Ni–Cu deposits [ext. abs.]: International Platinum Symposium, 12th, Yekaterinburg, Russia, 2014, Extended Abstracts, p. 102–103.

Leite, C.M.M., Santos, R.A., and Conceição, H., 1993, A província toleítica-alcalina de Campo Alegre de Lourdes: geologia e evolução tectônica, in: Simpósio Sobre o Cráton São Francisco, 2, Anais, Salvador: SBG, SGM, v. 1, p. 56-59.

Leite, C. M. M. (Org.), 1997, Campo Alegre de Lourdes, folha SC.23-X-DIV, Peixe, folha SC.23-X-D-I: Estado da Bahia. Brasília, DF: CPRM, Programa Levantamentos Geológicos Básicos do Brasil.

Li, C., and Naldrett, A.J., 1999, Geology and petrology of the Voisey's Bay intrusion: Reaction of olivine with sulfide and silicate liquids: Lithos, v. 47, p. 1–31.

Maier, W., Li, C., and De Waal, S.A., 2001, Why are there no major Ni-Cu sulfide deposits in large layered mafic-ultramafic intrusions?: The Canadian Mineralogist, v. 39, p. 547–556.

Naldrett, A.J., 1992, A model for the Ni-Cu-PGE ores of the Noril'sk region and its application to other areas of flood basalts: Economic Geology, v. 87, p. 1945−1962.

Ripley, E.M., and Li, C., 2013, Sulfide saturation in mafic magmas: is external sulfur required for magmatic Ni–Cu–(PGE) ore genesis?: Economic Geology, v. 108, p. 45–58.

Sampaio, D.R., Lima, R.F.F.F., and Moreira, J.F.C., 1986, Os depósitos de ferro, titânio e vanádio de Campo Alegre de Lourdes, Bahia, *in*: Schobbenhaus, C.; and Coelho, C.E.S. (Coords.), Principais Depósitos Minerais do Brasil, Brasília, DNPM-CVRD, v. II, p. 481-491.

Silva, A.B., Liberal, G.S., Issa Filho, A., Rodrigues, C.S., and Riffel B.F., 1987, Depósito de fosfato em carbonatito pré-cambriano, Angico dos Dias-Ba: Soc. Bras. Geol., Núcleo da Bahia, Salvador, 15 p.

Silva, A.B., Liberal, G.S., Grossi Sad, J.H., Issa Filho, A., Rodrigues, C.S., and Riffel, B.F., 1988, Geologia e petrologia do Complexo Angico dos Dias (Bahia, Brasil), uma associação metacarbonatítica pré-cambriana: Geochimica Brasiliensis, v.2, n. 1, p. 81-108.

Silva, A.B., Liberal, G.S., Riffel, B.F., and Issa Filho, A., 1997, Depósito de fosfato de Angico dos Dias, Campo Alegre de Lourdes, Bahia, *in*: Schobbenhaus, C., and Coelho, C.E.S. (Coords.), Principais Depósitos Minerais do Brasil, Brasília, DNPM-CPRM, v. IV-C, p. 123-130.

Song, X-Y., Danyushevsky, L.V., Keays, R.R., Chen, L-M., Wang, Y-S., Tian, Y-L., and Xiao. J-F., 2012, Structural, lithological, and geochemical constraints on the dynamic magma plumbing system of the Jinchuan Ni-Cu sulfide deposit, NW China: Mineralium Deposita, v. 47, p. 277–297.

Uhlein, A., Caxito, F.A., Sanglard, J.C.D., Uhlein, G.J., and Suckau, G.L., 2011, Estratigrafia e tectônica das faixas neoproterozoicas da porção norte do Cráton do São Francisco: Geonomos, v. 19, n. 2, p. 8-31.

To be submitted to ECONOMIC GEOLOGY

The Caboclo dos Mangueiros Deposit: Ni-Cu sulfide mineralization hosted in ultramafic cumulates in the northern edge of the São Francisco Craton, Brazil.

Vitor Bandeira Martins Matos[1]; Cesar Fonseca Ferreira Filho[1]

1 *Instituto de Geociências, Universidade de Brasília, Brasília, DF. 70910-900, Brazil.*

Abstract

The Caboclo dos Mangueiros magmatic Ni-Cu sulfide deposit is a recent discovery in the northern Brazil made by Companhia Baiana de Pesquisa Mineral (CBPM) in 2012. The deposit is situated in the northwestern edge of the São Francisco craton, close to the contact with the Rio Preto Neoproterozoic fold belt, where a cluster of mineralized mafic-ultramafic complexes are found. Drilling results indicate a preliminary resource of ~ 200Mt@0.20%Ni and 0.13%Cu. The Ni-Cu sulfides comprise an orebody hosted in an ultramafic intrusion with ~2 km long, ~500 m wide and ~270 m depth in central portions and ~100 m in the extremities, resembling an elongated boat-shaped sill. The intrusion is fractionated from the northern portion, where dunite and wehrlite prevail, to the southern where clinopyroxenite is abundant. It follows a crystallization sequence consisting of Ol => Ol + Cpx => Cpx, which indicate a silica undersaturated composition for the parental magma. The compositional range of cationic Mg# of cumulus clinopyroxene from 0.78 to 0.94 supports a moderate to primitive composition for the parental magma. Mantle-normalized REE and mantle-normalized alteration-resistant trace element profiles for the cumulate ultramafic rocks show enrichment in LREE with significant negative Nb and Ta anomalies. This enrichment is also showed in mantle-normalized alteration-resistant trace element profiles estimated to the parental melt. The data reveal that LREE patterns are dependent of the modal proportion of clinopyroxene in the cumulate rocks. Significant assimilation of crustal rocks during ascent and emplacement of the magma is not supported by the crystallization sequence typical of silica undersaturated magmas, as well as by the absence of Nb-Ta anomalies. The primary textures and the amount of sulfides, well above the cotectic proportion, suggest emplacement of sulfide droplets-charged magma through a conduit structure that later solidified as an elongated boat-shaped sill. Sulfur isotope compositional characteristics of the deposit reflect the mantle source of sulfides with no significant addition of crustal-derived sulfur. The depletion of PGE in the sulfide composition from a moderate to primitive magma is suggestive that has been occurred previous sulfide segregation at depth. Tectonic events and greenschist facies metamorphism may have affected the fractionated ultramafic sill and its sedimentary country rocks. Despite the tectonics the primary magmatic structure remains well preserved. Due to the lack of an absolute age for the ultramafic rocks the positioning of the Caboclo dos Mangueiros deposit in the tectonic evolution of the São Francisco craton remains uncertain.

Introduction

Ni-Cu deposits hosted in mafic-ultramafic intrusions are broadly classified into those associated with magma conduits and those associated with layered intrusions (Beresford and Hronsky, 2014). However, no major Ni-Cu sulfide deposits have been discovered within or at the basis of large mafic-ultramafic layered intrusions in more than half a century, thus dynamic ascending magma systems through conduit structures have become the favored exploration targets for Ni-Cu sulfide deposits (Maier et al., 2001; Song et al., 2012).

The Caboclo dos Mangueiros Ni-Cu magmatic sulfide deposit was discovered in northeastern Brazil by Companhia Bahiana de Pesquisa Mineral (CBPM) in 2012 and consists of an orebody with a significant preliminary resource of ~ 200Mt@0.20%Ni and 0.13%Cu (Projeto Valorização de Alvos Geofísicos; CBPM unpublished internal report). The orebody is hosted in a relatively small size elongated ultramafic intrusion with ~2 km long WNW-ESE trending and ~500 m wide that reaches ~270 m depth in central portions, resembling an elongated boat-shaped sill. The orebody reflects the intrusion shape with 1 to 5 vol.% of sulfides, which is considered well above the cotectic proportion for mineralized magmatic intrusion (Ripley and Li, 2013).

This deposit represents a recent Ni-Cu sulfide discovery located in the northwestern edge of the São Francisco Craton (Almeida, 1977), close to the contact with the Rio Preto fold belt (Uhlein et al., 2011). The intrusion is located close to a cluster of mineralized mafic-ultramafic complexes, exemplified by the Fe-Ti-V magmatic deposit of the Campo Alegre de Lourdes mafic-ultramafic Complex (Sampaio et al., 1986) and the P_2O_5 deposit of the Angico dos Dias Carbonatite Complex (Silva et al., 1988; 1997; Antonini et al., 2003). Several Ni-Cu-PGE sulfide deposits are located in similar tectonic setting (e.g., Noril'sk, Naldrett, 1992; Voisey's Bay, Li and Naldrett, 1999) and significant attention has been given to this as a promising mineral exploration target for Ni-Cu-PGE deposits (e.g., Begg et al., 2010). It is worth mentioning that the northwestern region of the São Francisco Craton is widely covered by tertiary-quaternary sediments and the Caboclo dos Mangueiros deposit do not outcrops.

In this study we present the first description of the magmatic structure and Ni-Cu mineralization of the Caboclo dos Mangueiros deposit. Geological descriptions supported by exploration data (drill core, geophysical surveys and whole-rock assay results of drill cores), together with petrographic studies and geochemical data (whole-rock analyses, mineral compositions and sulfur isotopes) are used to propose a model for the origin of the Ni-Cu sulfide deposit. Our results indicate that the mineralization is associated with a dynamic magma conduit, possibly representing a small portion of larger magmatic systems. The implication of these results for mineral exploration in the northern edge of the São Francisco Craton is discussed.

Discovery History

The occurrence of pyroxenite close to the Caboclo dos Mangueiros village was first reported by Companhia Baiana de Pesquisa Mineral (CBPM) during a regional mapping project in 1987 (Projeto Remanso - Fase I; CBPM unpublished internal report). Several aeromagnetic anomalies were identified in a regional aerogeophysical survey developed in the northern portion of the Bahia state by CBPM/CPRM-Brazilian Geological Survey in 2005-2006 (LASA, 2006). Follow up exploration of aeromagnetic anomalies carried out by CBPM in 2009, including surface recognition campaigns and lithogeochemical analyses, identified Ni-Cu anomalies associated with ultramafic rocks in the Caboclo dos Mangueiros target. In 2012, CBPM carried out ground geophysical (magnetic, induced polarization and time-domain electromagnetic) and soil geochemical surveys that supported the following drilling program for Ni-Cu sulfides. The drilling program totaling 2,670 m (15 drill holes), completed in 2015 by CBPM, intersected up to 213 m of disseminated sulfides grading 0.22 wt.% Ni and 0.13 wt.% Cu. Drilling results indicate a preliminary resource of ~ 200Mt@0.20%Ni and 0.13%Cu (Projeto Valorização de Alvos Geofísicos; CBPM unpublished internal report). Additional drilling carried on by CBPM in 2017 (7 drill holes) indicated a southeastern extension of the mineralization evaluated in 2015.

Geological Setting

The Caboclo dos Mangueiros Deposit is located in the northwestern edge of the São Francisco Craton (Almeida, 1977), close to the contact with the Rio Preto fold belt (Uhlein et al., 2011) (Fig. 1). The basement of the São Francisco Craton consists of four crustal segments assembled during the Paleoproterozoic (ca. 2.0 Ga) orogenic cycle (Barbosa and Sabaté, 2004; Peucat et al., 2011). These crustal segments, designated as (i) Gavião Block, (ii) Jequié Block, (iii) Itabuna-Salvador-Curaçá Belt and (iv) Serrinha Block, are limited by Neoproterozoic fold belts that surround the São Francisco Craton (Uhlein et al., 2011). These crustal segments consist mainly of amphibolite to granulite facies orthogneiss and migmatites originated during the 2,0 Ga orogeny. The older rocks of the São Francisco Craton consist of Archean tonalite-trondhjemite-granodiorite terrains and greenstone belts, partially to extensively transformed during the Paleoproterozoic orogeny (Barbosa and Sabaté, 2004). Large portions of the São Francisco Craton are covered by Proterozoic and Phanerozoic sedimentary sequences (Fig. 1).

The northwest portion of the São Francisco Craton (Fig. 2), where the Caboclo dos Mangueiros deposit is located, belongs to the Archean-Paleoproterozoic Gavião Block. The following description and Figure 2A are based on the regional mapping project carried on by the Brazilian Geological Survey (Leite et al., 1997). The Archean Sobradinho-Remanso Complex, interpreted as a tonalite-trondhjemite-granodiorite terrain affected by the Paleoproterozoic orogeny, consists of orthogneiss and migmatite. Dantas et al. (2010) obtained U-Pb zircon ages of 2,564±11 Ma and 3,537±8 Ma for these rocks. The Serra da Boa Esperança Complex consists of carbonate schist with lens of marble, as well as minor mica schist and mica-quartz schist (Leite et al., 1997; Barbosa et al., 2012). This carbonatic-pelitic sedimentary sequence

has greenschist facies metamorphic parageneses and is correlated with Paleo or Mesoproterozoic sedimentary covers of the São Francisco Craton.

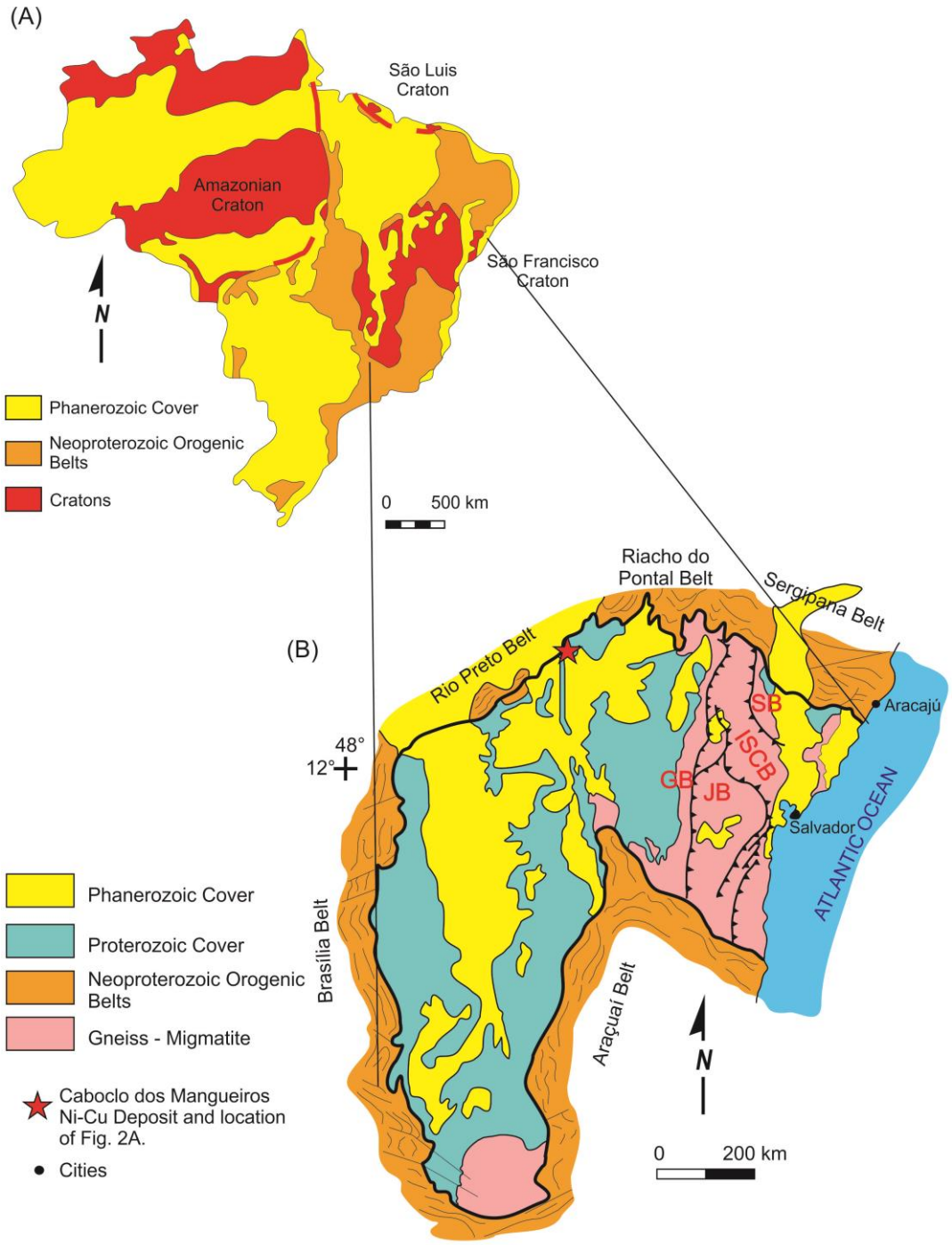

Fig. 1: Geological setting. (A) Brazilian cratons. (B) Sketch showing the main domains of the São Francisco Craton and surrounding Neoproterozoic belts. Modified from Alkmim et al. (1993). Abbreviations: GB - Gavião Block; JB - Jequié Block; ISCB - Itabuna-Salvador-Curaçá Belt; SB - Serrinha Block.

Several mafic-ultramafic intrusions occur within the Sobradinho-Remanso and Serra da Boa Esperança Complexes. Mafic-ultramafic intrusions are usually weathered and/or largely covered by Cenozoic sedimentary sequences (Fig. 2A). Except for the U-Pb zircon and baddeleyite 2,010±6 Ma age of the Angico dos Dias carbonatite complex (Silva et al., 1987), no

robust age dating is available for these intrusions. The mafic-ultramafic complexes indicated in Figure 2A are briefly described as follow:

a) The Angico dos Dias carbonatite complex consists of pyroxenite, alkali diorite, syenite, carbonatite and lamprophyre (Silva et al., 1988; 1997; Antonini et al., 2003). The complex host a phosphate deposit developed in the weathered profile of apatite-rich carbonatite. This 15Mt@15.4%P_2O_5 deposit is currently mined by Mineração Galvani S.A.

b) The Campo Alegre de Lourdes Mafic-Ultramafic Complex is a gabbro-anorthositic intrusion hosting a large Fe-Ti-V deposit (Sampaio et al., 1986). This elongate 11 km long intrusion consists of interlayered pyroxenite, gabbro, anorthosite and ilmenite-magnetitite metamorphosed under greenschist to amphibolite facies. Fe-Ti-V mineralization occurs in several individual bodies of massive to banded ilmenite-magnetitite, with total resources of 100Mt@45%Fe, 21%TiO_2, 0.71% V_2O_5 (Sampaio et al., 1986).

c) The Fe-Ti-V mineralized Peixe Mafic-Ultramafic Complex is largely covered by Cenozoic eluvial/colluvial sediments. Geological limits are based upon an aeromagnetic anomaly (Leite et al. 1993, 1997) and geological descriptions limited to exploratory drilling carried on by CBPM in 1988. Drill core consists of interlayered metagabbro, metapyroxenite and massive ilmenite-magnetitite.

d) The Caboclo dos Mangueiros Intrusion outcrops as rare weathered pyroxenite and peridotite blocks within a flat region covered by eluvial/colluvial sediments (Fig. 2A). Additional occurrences of these rock types mapped by Leite et al. (1997) suggest that they belong to a cluster of small ultramafic bodies.

The Serra do Meio Alkaline Suite, intrusive into mica-quartz schists of the Serra da Boa Esperança Complex, consists of alkali granite with subordinated syenite (Plá Cid, 1994). This felsic suite corresponds to Neoproterozoic to Cambrian anorogenic plutons (Plá Cid, 1994).

Paleozoic sedimentary rocks of the southern border of the Parnaíba Basin outcrop in the northwest portion of Figure 2A. This sedimentary basin discordantly covers the Precambrian rocks of the São Francisco Craton and adjacent Brasiliano belts in the region.

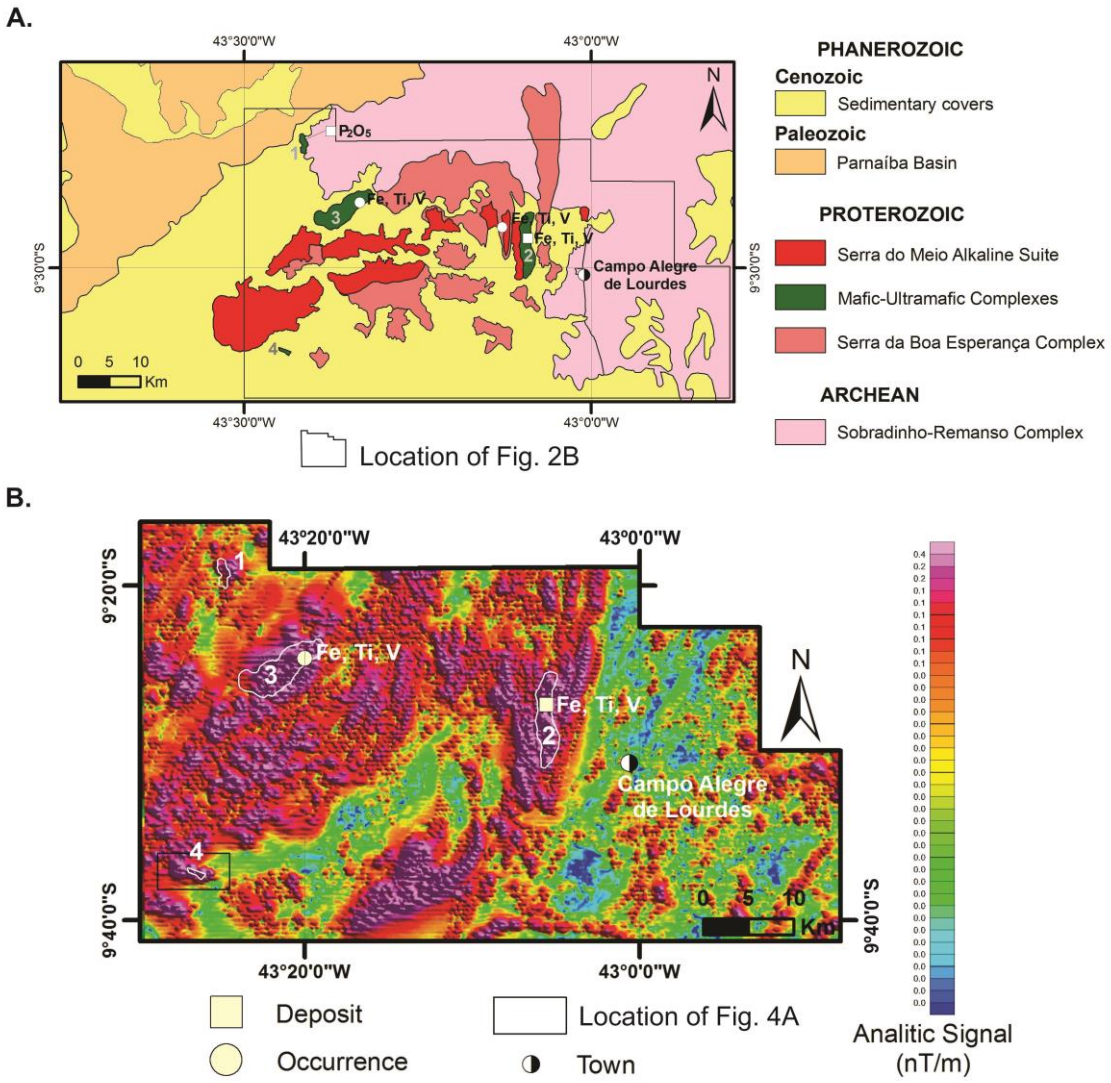

Fig. 2: Local Geology. (A) Geology of the northwest portion of the São Francisco Craton. 1 = Angico dos Dias carbonatite complex; 3 = Peixe mafic-Ultramafic Complex; 2 Campo Alegre de Lourdes Mafic-Ultramafic Complex; 4 = Caboclo dos Mangueiros Intrusion. Modified from Vasconcelos et al. (2004). (B) Analytical signal amplitude (nT/m) image of the area indicated in Figure 2A. Modified from LASA (2006). White lines indicate mapped limits of mafic-ultramafic complexes.

Materials and Methods

Geological characterization of the Caboclo dos Mangueiros ultramafic intrusion was supported by the exploration program carried on by Companhia Baiana de Pesquisa Mineral. This program included geological mapping, soil geochemical grids, ground geophysical surveys, petrographical studies and drilling. For this study, all drill holes were described to provide representative samples for analytical studies. Petrographic studies of 40 additional polished thin sections were carried on in the Microscopy Laboratory of the Universidade de Brasília.

Mineral analyses were performed on polished thin section using a JEOLJXA-8230 SuperProbe with 5 wavelength dispersive (WDS) spectrometers at the Electron Microprobe Laboratory of the University of Brasília (Brazil). The wavelength dispersive (WDS) analyses were performed at an accelerating voltage of 15 kV and a beam current of 10 nA. Energy dispersive X-ray spectroscopy (EDS) of several minerals was also adopted to support

petrographic studies. Systematic WDS analyses were obtained for clinopyroxene, amphibole and sulfides. Both synthetic and natural mineral standards were used for the analyses and the same standards and procedure were retained throughout the analytical work.

Whole-rock chemical analyses and sample preparation for major, minor and trace elements were carried out at SGS GEOSOL Laboratory in Brazil. The major elements were analysed by X-ray fluorescence (XRF) on dissolved samples, fused by lithium tetraborate. The minor and trace elements were analysed by inductively-coupled plasma optical emission spectroscopy (ICP-OES) after multi-acid (HCl-HNO_3-$HClO_4$-HF) digestion. The REE, Nb, Ta, Hf and Rb were analysed by inductively-coupled plasma mass spectroscopy (ICP-MS), after fusing with lithium metaborate. The concentrations of S were determined by the LECO method. The concentrations of Au, Pt and Pd were determined by ICP-OES after standard lead oxide fire assay preconcentration. A total of 13 representative drill core samples were analysed.

It was used 429 quarter drill core whole-rock assay results of Mg, Cr, Ni and Cu from two drill holes from the Companhia Baiana de Pesquisa Mineral database. They were sampled continuously at approximately 1-m intervals, respecting geologic contacts. These samples were analysed by ICP-OES after aqua regia digestion at SGS Geosol Laboratory in Brazil.

Sulfur isotopic analyses were carried out at the Geochronology Laboratory of the Geosciences Institute of the University of Brasilia, Brazil. A total of six representative ore samples were collected from the Caboclo dos Mangueiros deposit for sulfur isotopic study. Sulfides consisting of pyrrhotite, chalcopyrite, pyrite and pentlandite from interstitial blebs were hand-picked and individually mounted. The sulfur isotope compositions were determined by isotopic ratio mass spectrometry (IRMS), utilizing a Thermo Scientific MAT253 IRMS, after the samples get diluted in the elementary analyser Thermo Scientific Flash 2000.

The Ultramafic Intrusion

The Caboclo dos Mangueiros intrusion consists of a ~2 km long and ~500 m wide (~1 km^2) WNW-ESE trending ultramafic body. The magmatic structure is mainly delineated by geological descriptions of drill holes and extends to a maximum depth of 270 m (Fig. 3A). The ultramafic intrusion is widely covered by tertiary-quaternary sediments and ferruginous lateritic crusts (Fig. 3B). The latter outcrops as ferruginous silexites (Fig. 3C) that sustain smooth hills, up to 20 m higher than surrounding flat terrains where unconsolidated sediments prevail (Fig 3B). Ultramafic rocks occur as scattered blocks of partially weathered wehrlite and pyroxenite.

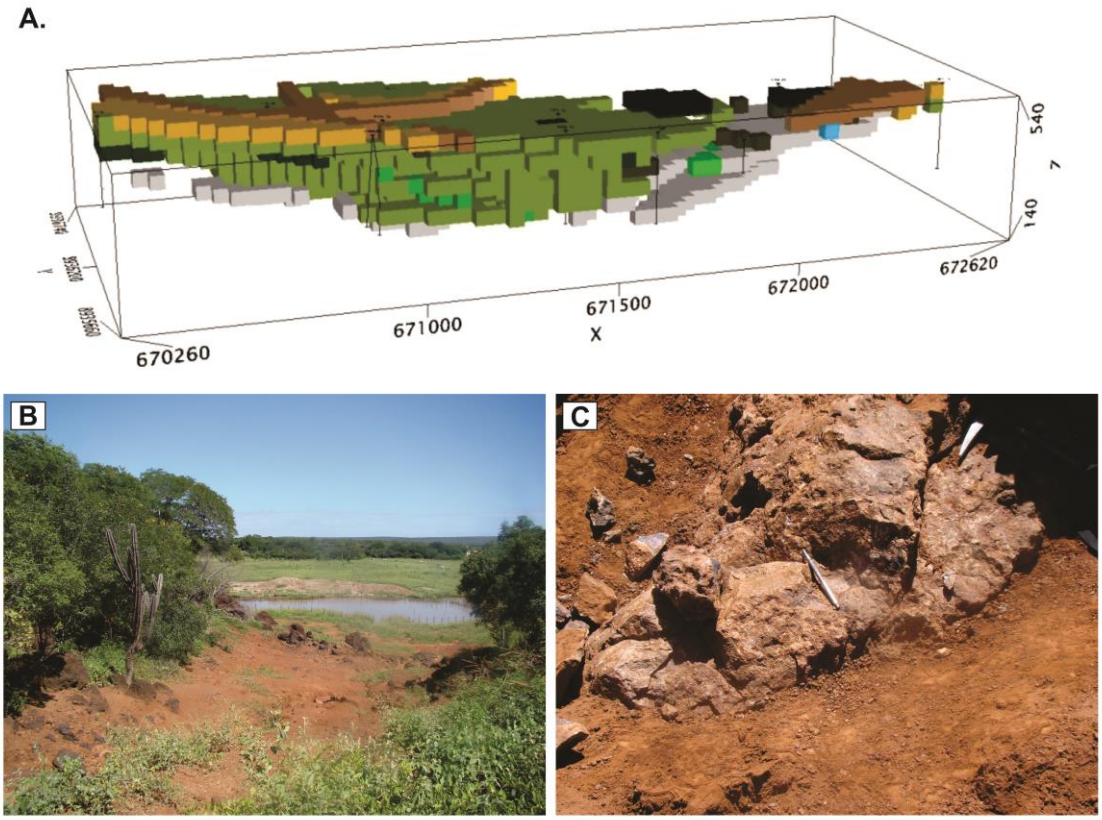

Fig. 3: (A) Tridimensional model of the Caboclo dos Mangueiros intrusion (CBPM, unpublished internal report). Green = ultramafic rocks, grey and blue = country rocks, yellow = saprolite, brown = soil, black = ferruginous lateritic crust. (B) Panoramic view of the flat terrain and ferruginous lateritic crust (scale = 8-m-wide dirty path). (C) Outcrop of silexite from ultramafic rocks.

Ultramafic rocks consist of olivine and clinopyroxene cumulates with disseminated sulfides. Cumulus minerals are partially to extensively altered to hydrous minerals, as indicated by pseudomorphs of olivine replaced by serpentine + magnetite and pseudomorphs of clinopyroxene replaced by tremolite-actinolite, but igneous textures are preserved throughout the intrusion. Penetrative fabric is restricted to narrow sheared domains of up to few meters across, and igneous minerals and/or pseudomorphs are identified in adjacent nondeformed domains. Because the original igneous texture is largely preserved in ultramafic rocks, such that original cumulate minerals can be identified, these rocks are described using igneous terminology. The contact of the intrusion intersected in drill core consists of up to 4 meters thick zones of fine-grained chlorite-actinolitite or chlorite-actinolite schist. Country rocks of the Caboclo dos Mangueiros intrusion are foliated and folded graphite-bearing quartz-biotite schists. Country rocks are crosscut by rare veins or dykes (up to 1-2 m thick) with granitic composition.

The Caboclo dos Mangueiros intrusion is thicker in the central portion and become progressively thinner toward the extremities, resembling a boat-shaped structure (Fig. 3A). The elongated intrusion is partially coincident with a 5-km-long discrete magnetic anomaly (Fig. 4A). The latter extends to the northwest of the delineated ultramafic intrusion, suggesting that ultramafic rocks may extend beyond the actual limits. Geological sections and drill core logs

(e.g., Fig. 4B and 4C) across de central portion of the intrusion indicate that dunite and wehrlite predominate in the northern portion, while clinopyroxenite predominates in the southern portion. These features indicate a progressive fractionation from olivine cumulates to clinopyroxene cumulates toward the southern portion of the intrusion. A schematic block diagram illustrates the magmatic structure of the intrusion (Fig. 5). The mineralogical and textural characteristics of the ultramafic and their country rocks are briefly described as follow.

Dunite is a massive dark-green olivine cumulate with interstitial sulfides (up to 5 vol.%). Medium-grained adcumulate to mesocumulate textures (Fig. 6A and 6B) predominate with minor medium- to coarse-grained orthocumulate textures (Fig 6C and 6D). The latter consists of large clinopyroxene oikocrysts (up to several centimeters) enclosing euhedral olivine. Olivine occurs as pseudomorphs completely replaced by fine-grained aggregates of serpentine and magnetite.

Wehrlite is a massive medium- to coarse-grained grayish green cumulate with interstitial sulfides (up to 5 vol.%). Few meters thick lenses of dunite or clinopyroxenite are commonly interlayered in wehrlite. Contacts with both dunite and clinopyroxenite are mainly gradational and characterized by intermediate compositions (i.e., olivine clinopyroxenite; clinopyroxene-bearing dunite). Adcumulate textures, consisting of cumulus olivine and clinopyroxene, predominate in wehrlite (Fig. 6C). Meso- to orthocumulate textures, characterized by abundant clinopyroxene oikocrysts enclosing cumulus olivine, occur in wehrlite closely associated with dunite (Fig. 6D) in the northern portion of the intrusion. Olivine occurs as pseudomorphs completely replaced by fine-grained aggregates of serpentine and magnetite, whereas clinopyroxene is variably replaced by tremolite-actinolite.

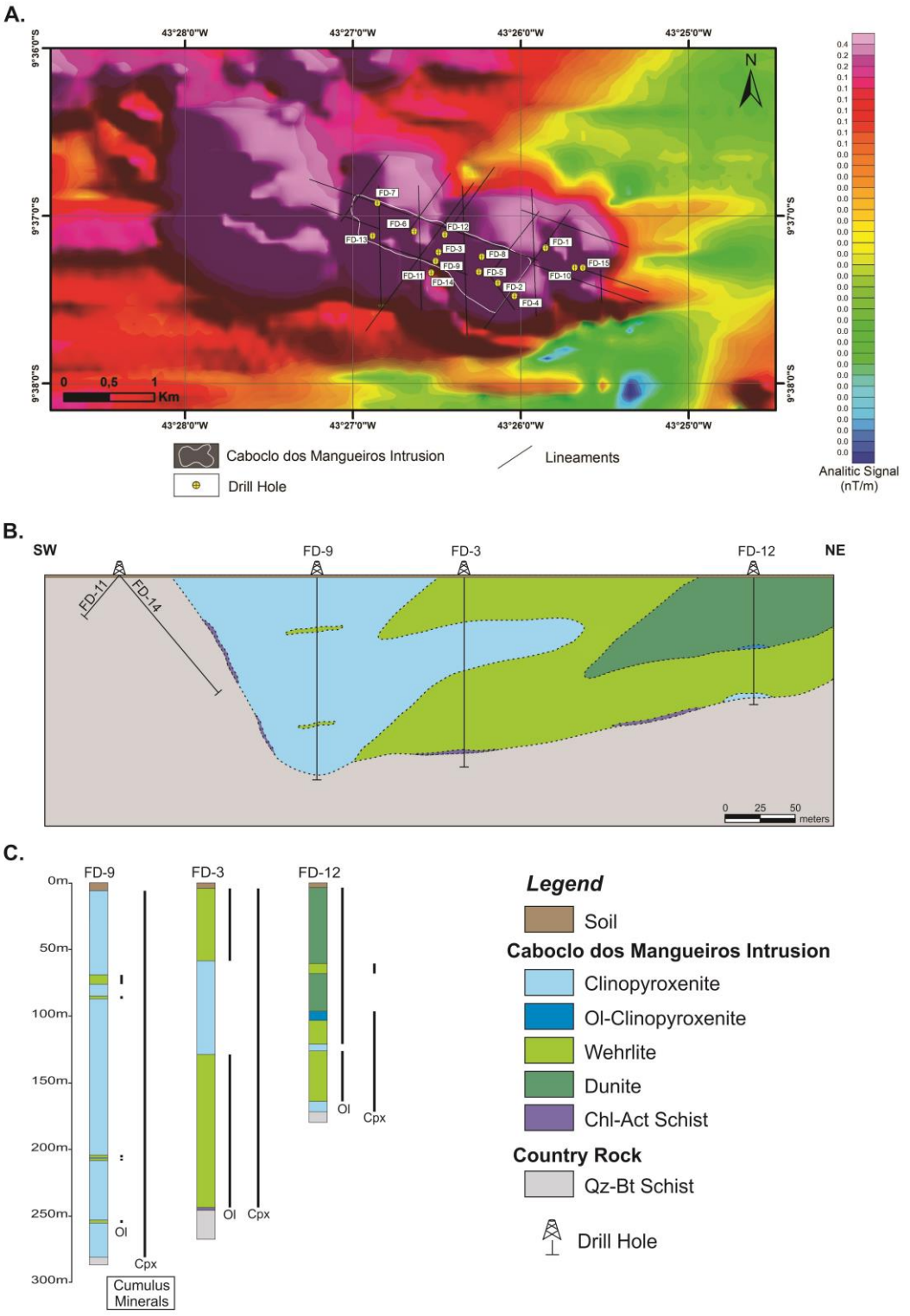

Fig. 4: (A) Analytical signal amplitude (nT/m) image of the area indicated in Fig. 2B. Modified from LASA (2006). (B) Transversal schematic geological section of the ultramafic intrusion, showing the progressively more primitive rocks toward the northern edge of the intrusion. (C) FD-9, FD-3 and FD-12 drill holes strip log. The distribution of cumulus minerals along the drill holes is indicated.

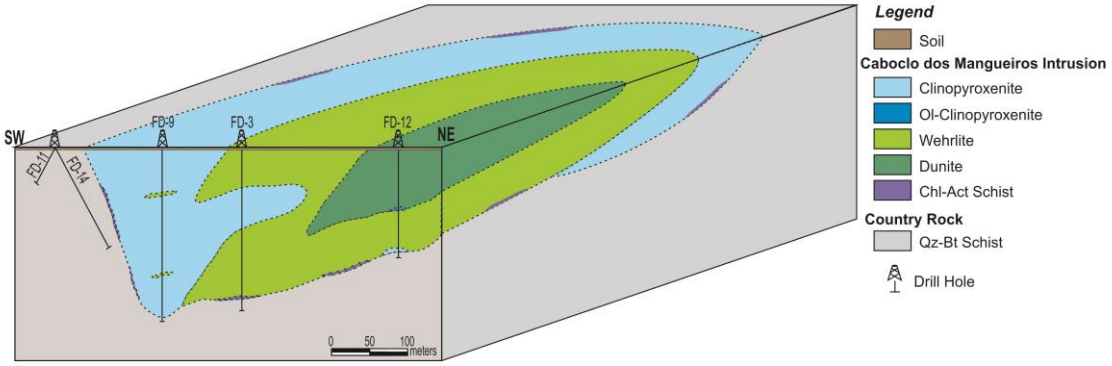

Fig. 5: Schematic tridimensional model of the Caboclo dos Mangueiros intrusion. The model shows the northwestern half of the NW-SE elongated intrusion.

Clinopyroxenite is a massive light greenish gray medium- to coarse-grained clinopyroxene adcumulate with interstitial sulfides (Fig. 6E and 6F). Clinopyroxene commonly have preserved cores with rims variably replaced by tremolite-actinolite (Fig. 6F). Clinopyroxene is usually twinned and eventually have tiny acicular exsolutions of ilmenite.

Chlorite-actinolite schists are fine-grained greenish rocks (Fig. 6G and 6H) located in the contact of the ultramafic intrusion and country rocks. They form up to 4 meters thick zones of variable rocks. Although chlorite-actinolite schist with > 70 vol.% actinolite prevail, rocks with less prominent foliation and/or abundant biotite also occur. The contacts of ultramafic and country rocks are usually sharp and characterized by abrupt changes in texture, mineral composition and grain size. The disseminated sulfides (1-5 vol.%) that occur throughout the ultramafic intrusion sharply disappear in the chlorite-actinolite schist.

Country rocks are fine- to medium-grained graphite-bearing quartz-biotite schists with prominent foliation (Fig. 6I and 6J). The tectonic foliation is parallel to a lamination consisting of alternating darker graphite-rich and lighter quartz-plagioclase-rich irregular laminae. Quartz-biotite schist consists mainly of variable proportions of quartz (30-35 vol.%), biotite (20-25 vol.%), albite (20-25 vol.%), muscovite (up to 20 vol.%) and graphite (up to 10 vol.%). Common accessory minerals include epidote, chlorite, ilmenite, pyrite and garnet. Chlorite is a common alteration mineral replacing biotite. Disseminated fine- to medium-grained syn-cinematic euhedral garnet was identified in just one sample of the country rocks. Metamorphic parageneses consisting of albite + quartz + biotite + muscovite + epidote ± garnet are typical of metasediments submitted to the upper greenschist facies of regional metamorphism (Bucher and Grapes, 2011). The upper greenschist facies is also indicated by the absence of chlorite in the metamorphic parageneses of the metasediments (Bucher and Grapes, 2011).

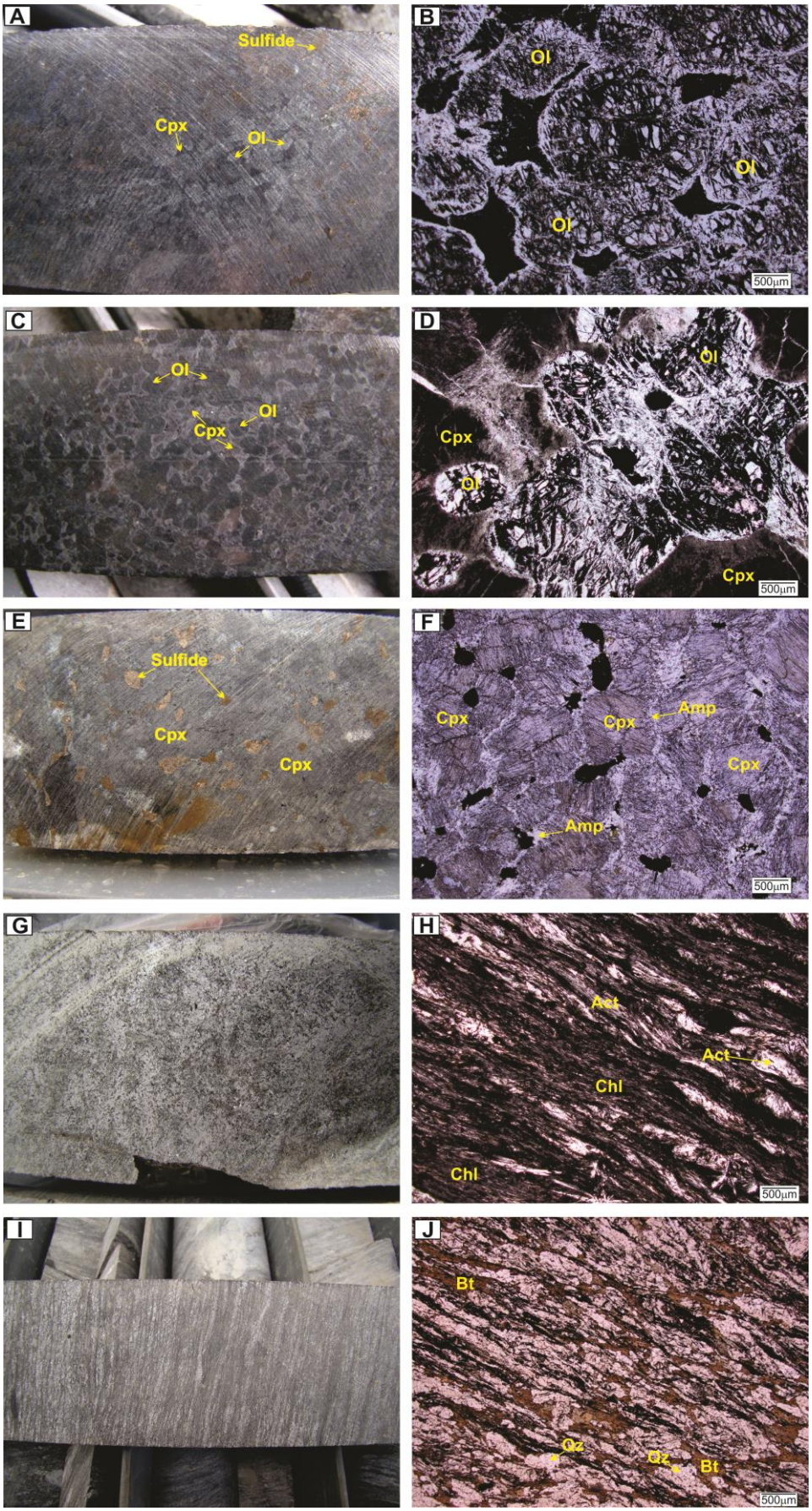

Fig. 6: Photos of core samples (left column) and photomicrographs (right column). (A) Medium-grained dunite with disseminated sulfides. (B) Adcumulate dunite consisting of euhedral pseudomorphs of cumulus olivine and interstitial sulfides (opaques). (C) Coarse-grained orthocumulate wehrlite consisting of

pseudomorphs of cumulus olivine (dark color) and clinopyroxene oikocrysts. (D) Coarse-grained wehrlite with orthocumulate texture. Note peseudomorphs of euhedral cumulus olivine and intercumulus clinopyroxene. (E) Typical coarse-grained clinopyroxenite with interstitial sulfide blebs. (F) Adcumulate clinopyroxenite with interstitial sulfides (opaques). Note metamorphic amphiboles developed in the outer rim of clinopyroxene. (G) Fine-grained chlorite–actinolite schist from the contact zone of the intrusion. (H) Chlorite-actinolite schist with prominent foliation. (I) Typical country rock. Fine-grained graphite-bearing quartz–biotite schist. (J) Lepidoblastic texture in graphite-bearing quartz–biotite schist. Mineral symbols in accordance with classification of Whitney (2010).

Geochemistry of the Ultramafic Rocks

Mineral composition

Systematic analyses of clinopyroxene and amphibole were performed in unweathered samples troughout the Caboclo dos Mangueiros intrusion. Representative analyses for minerals of the intrusion are provided in Appendixes 1 and 2.

Clinopyroxene compositions are essentially calcic and magnesian, ranging from 17.64 to 24.51 wt.% CaO and from 14.35 to 18.89 wt.% MgO. The cationic Mg# (i.e., $Mg/[Mg+Fe^{2+}]$) of clinopyroxene throughout the intrusion range from 0.78 to 0.94, which is characteristic of primitive to moderately primitive compositions. These values progressively decrease toward the southern portion of the intrusion, as indicated by the variation in cationic Mg# in clinopyroxene from clinopyroxenites (Fig. 7A) and wehrlite (Fig. 7B) from bore holes located across a NE-SW section of the intrusion (see Fig. 4 for the location of bore holes). The decrease of Mg# in clinopyroxene matches the progressive fractionation from olivine cumulates to clinopyroxene cumulates toward the southern portion of the intrusion (Fig. 4B and 4C). Clinopyroxene has Cr_2O_3 contents ranging from 0.22 to 0.64 wt.% (Fig. 7C), with higher values associated with more primitive rocks (i.e., wehrlite).

Amphibole compositions are essentially calcic (11.35 to 13.50 wt.% CaO) and magnesian (17.57 to 22.08 wt.%) with cationic Mg# ranging from 0.78 to 0.91 (Fig. 7D). These compositions range from actinolite to tremolite. The similar range of cationic Mg# of clinopyroxene and amphibole is consistent with the replacement of clinopyroxene by amphibole indicated in petrographic studies. Amphiboles also have higher values of cationic Mg# in wehrlites than in clinopyroxenites (Fig. 7D). Values of Si^{iv} close to 8 (Fig. 7D) indicate that the tetrahedral site is fulfilled by Si with none to minor Al^{iv}.

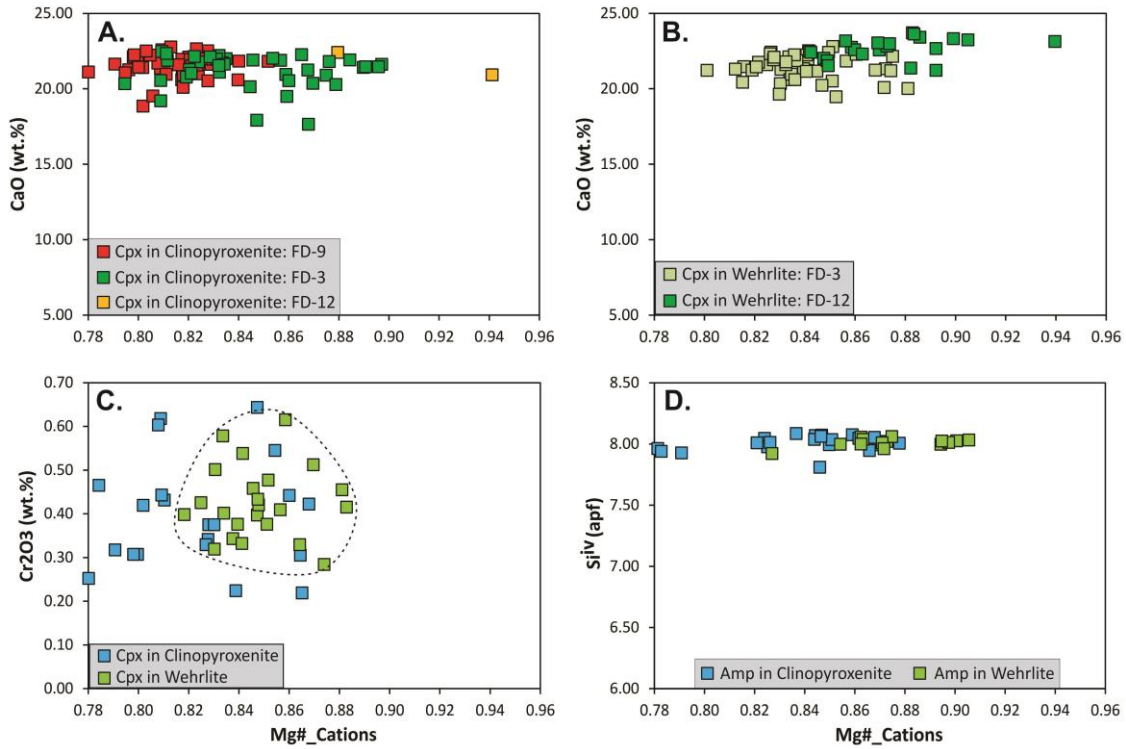

Fig. 7: Mineral compositions. (A) Plot of cationic Mg# versus CaO for clinopyroxene in clinopyroxenites from drill holes FD-9, FD-3 and FD-12. (B) Plot of cationic Mg# versus CaO for clinopyroxene in wehrlites from drill holes FD-3 and FD-12. (C) Plot of cationic Mg# versus Cr_2O_3 for clinopyroxene in clinopyroxenite and peridotite. (D) Plot of cationic Mg# versus Si^{iv} for amphiboles in clinopyroxenites and wehrlites. Data from Appendix 2.

Major and minor element whole-rock compositions

Assay results from the Companhia Bahiana de Pesquisa Mineral exploration database for Mg, Cr, Ni and Cu throughout two representative drill cores (FD-3 and FD-12) are indicated to point out critical features of the stratigraphy of the Caboclo dos Mangueiros intrusion (Fig. 8).

The drill hole FD-3 (Fig. 8A) is representative of the central portion of the intrusion. Mg contents show a flat pattern in clinopyroxenite (average ~3 wt.%) that contrast with higher and variable contents in wehrlite (average ~ 6 wt.%). Variable Mg contents in wehrlites are consistent with their variable modal composition along the drill hole. Cr contents in these rocks are low (< 1500 ppm), except for higher contents (up to 2800 ppm) in weathered rocks close to the surface (Fig. 8A). Cr contents are slightly higher in clinopyroxenite (average ~ 1200 ppm) than in wehrlites (average ~ 900 ppm), suggesting that Cr contents correlate mainly with the modal proportion of clinopyroxene. Similar Ni contents in clinopyronenite and wehrlite indicate that Ni is mainly contained in sulfides. This feature, together with consistently high Cu contents (1000-2000 ppm) and positive Ni-Cu correlation, results from the occurrence of disseminated Ni-Cu sulfides throughout FD-3.

The drill hole FD-12 (Fig. 8B), representative of the northern portion of the intrusion, consists mainly of dunite and wehrlite with minor clinopyroxenite. High Mg contents, including intervals above the upper detection limit of our analyses (i.e., >15 wt.% Mg), are restricted to dunite, while progressively lower contents occur in wehrlite and clinopyroxenite. Mg contents in wehrlite from drill hole FD-12 are commonly higher than 10 wt.% and, consequently,

significantly higher than those reported in wehrlite from drill hole FD-3 located at the central portion of the intrusion (< 10 wt.%). Cr contents in these rocks are commonly low (< 2000 ppm), except for higher contents (up to 3500 ppm) in weathered rocks close to the surface and in one interval of dunite with 3500-5000 ppm (Fig. 8B). The latter results from strong alteration within a narrow zone of sheared dunite enriched in magnetite (~ 4 meter). Similar to FD-3, consistently high Cu contents (1000-2000 ppm) and positive Ni-Cu correlation, results from disseminated Ni-Cu sulfides throughout FD-12 (Fig. 8B).

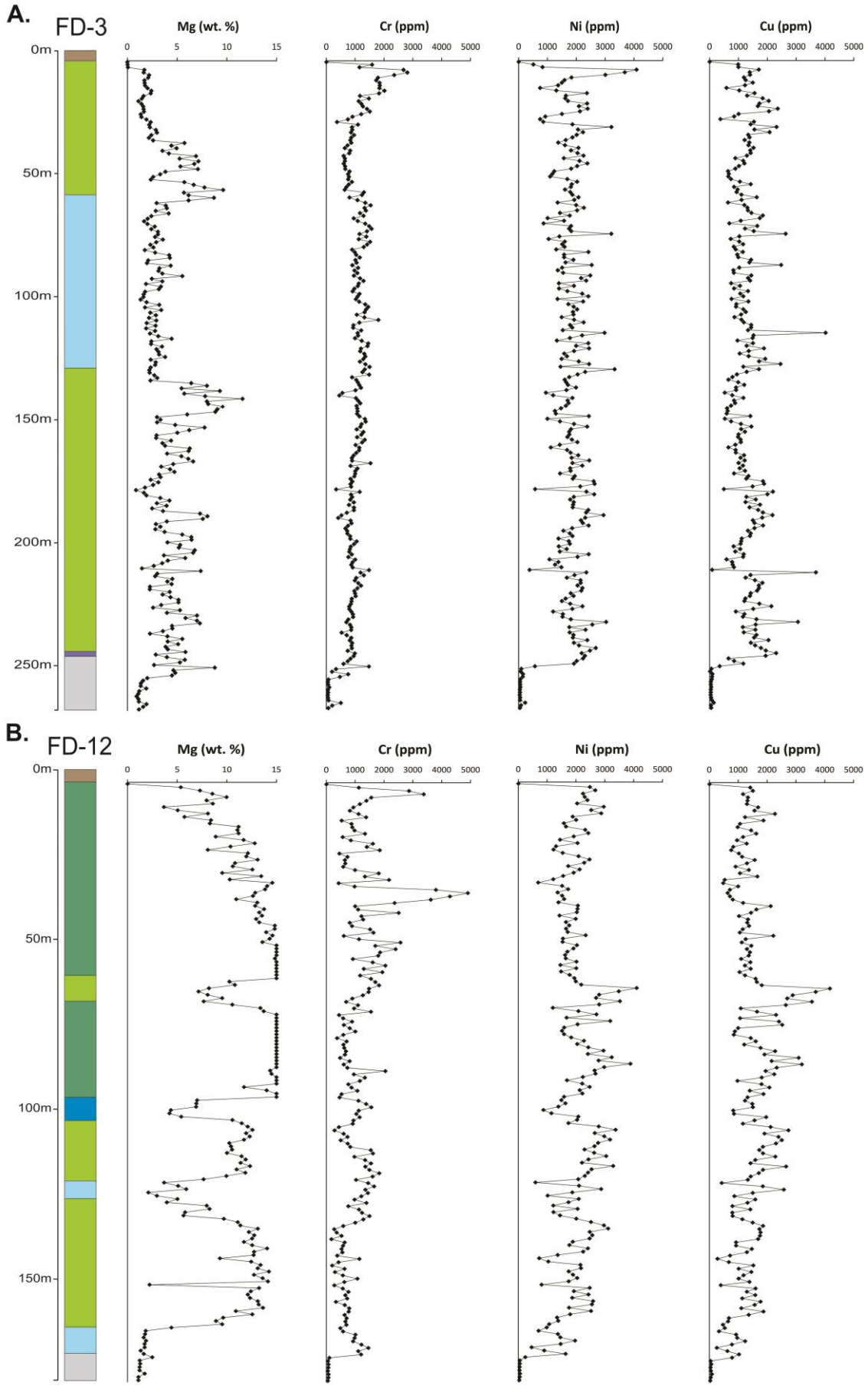

Fig. 8: FD-3 and FD-12 drill holes strip log and its Mg, Cr, Ni and Cu assay results.

Whole-rock chemical compositions were obtained from 12 samples representative of ultramafic rocks and one country rock (Table 1). Variable amounts of loss on ignition reflect the degree of alteration and/or different alteration minerals for distinct rock types. Hence, the compositions of major and minor elements are normalized to 100% on an anhydrous base. This normalization is necessary to equilibrate differences originated by various degrees of alteration, especially when clinopyroxene cumulates (i.e., < 3 wt.% LOI) are compared with olivine cumulate (i.e., ~ 10 wt.% LOI). The composition of the ultramafic rocks is controlled by the type and modal proportion of cumulus minerals. The plots of selected major and minor element oxides versus MgO (Fig. 9) indicate the predominance of olivine and clinopyroxene cumulates. This result, supported by comparing whole rock and clinopyroxene compositions in clinopyroxenite, wehrlite and dunite (Fig. 9), is consistent with petrographic studies. The progressive variation from olivine cumulate (i.e., dunite) to olivine + clinopyroxene cumulate (i.e., wehrlite) and clinopyroxene cumulate (i.e., clinopyroxenite) is well illustrated by the decrease of SiO_2, Al_2O_3 and CaO, and increase in FeO, versus MgO (Fig. 9). Displacement of whole-rock compositions from the expected clinopyroxene-olivine trends are partially explained by disseminated sulfides (1-5 vol.%) in these cumulate rocks. For example, the present of Fe-rich or Ni-rich sulfides result in clinopyroxenites with FeO and Ni contents higher than the composition of clinopyroxene (Fig. 9D and 9G), as well as a minor dilution effect in whole-rock contents of elements not contained in sulfides (e.g., CaO and SiO_2). Whole-rock contents of TiO_2 and Cr_2O_3 have positive correlation with the modal proportion of clinopyroxene. These features are consistent with the reported contents of TiO_2 and Cr_2O_3 in clinopyroxene (Fig. 9E and 9F), as well as the lack of chromite and magmatic Fe-Ti oxides in the cumulate rocks.

Whole-rock compositions of chlorite-actinolite schists from the border zone of the ultramafic intrusion are comparable with compositions of ultramafic cumulates (Fig. 9). However, relatively higher Al_2O_3 (Fig. 9B) and lower CaO (Fig. 9C), together with distinctively higher K_2O content in one sample, suggests some contamination with quartz-biotite schist (Fig. 9 and Table 1). Chlorite-actinolite schists have remarkably low contents of Cu and S (Table 1), which are consistent with the sharp decrease in sulfides described in the fine-grained border zone of the ultramafic intrusion.

Table 1: Whole-rock analyses of representative samples from the Caboclo dos Mangueiros intrusion.

Sample		BM-013	BM-016	BM-027	BM-042	BM-009	BM-033	BM-010	BM-030	BM-041	BM-035	BM-022	BM-039	BM-001
Drill Hole		FD-9	FD-9	FD-6	FD-5	FD-3	FD-12	FD-3	FD-6	FD-5	FD-12	FD-6	FD-5	FD-3
Depth (m)		258.60	227.20	112.20	132.80	104.10	131.50	86.20	25.70	202.50	93.30	222.70	234.70	262.30
Rock Code		Cpxt	Cpxt	Cpxt	Cpxt	Ol-Cpxt	Ol-Cpxt	Wrlt	Wrlt	Wrlt	Dun	Chl-Act Schist	Chl-Act Schist	Qz-Bt Schist
SiO2	%	48.00	50.50	48.00	45.20	46.90	41.50	45.20	42.40	39.20	35.60	40.80	50.80	62.60
Al2O3	%	2.35	2.31	1.88	1.96	1.79	1.70	1.44	1.87	1.36	1.03	12.00	3.42	15.80
Fe2O3	%	14.10	11.00	11.90	15.20	13.30	11.90	16.20	15.90	18.30	18.10	12.10	11.50	7.61
CaO	%	15.90	16.10	16.20	15.60	12.70	14.80	9.27	6.55	5.70	3.53	6.22	11.60	1.74
MgO	%	15.90	16.40	16.90	16.10	19.20	20.00	22.30	25.40	24.80	28.60	19.50	18.20	2.10
TiO2	%	1.07	0.93	0.88	0.92	0.82	1.03	0.67	0.51	0.46	0.48	0.71	1.18	0.74
P2O5	%	<0.01	0.03	0.03	0.02	0.02	0.05	0.05	0.03	<0.01	0.09	0.07	0.05	0.06
Na2O	%	0.19	0.25	0.18	0.12	0.12	<0.10	<0.10	<0.10	<0.10	<0.10	<0.10	<0.10	5.23
K2O	%	0.02	0.04	<0.01	<0.01	0.02	<0.01	<0.01	<0.01	<0.01	<0.01	0.49	0.05	2.07
MnO	%	0.18	0.21	0.18	0.18	0.20	0.22	0.22	0.20	0.19	0.21	0.19	0.21	0.07
Cr2O3	%	0.43	0.27	0.30	0.34	0.37	0.44	0.25	0.21	0.18	0.05	0.36	0.15	0.02
NiO	%	0.24	0.05	0.22	0.34	0.15	0.15	0.21	0.20	0.42	0.54	0.06	0.02	0.01
V2O5	%	0.06	0.07	0.05	0.06	0.05	0.04	0.04	0.03	0.03	0.02	0.05	0.08	0.03
LOI	%	1.87	1.35	2.19	3.00	2.69	8.02	4.88	6.78	7.86	10.08	5.95	2.56	2.49
Total	%	100.32	99.51	98.92	99.05	98.33	99.96	100.84	100.19	98.61	98.44	98.60	99.92	100.57
S	%	2.04	0.61	1.59	3.65	1.01	0.38	1.74	1.60	2.17	2.47	0.05	0.01	0.11
Au	ppb	8.00	<5.00	20.00	19.00	<5.00	<5.00	14.00	20.00	N.A.	14.00	<5.00	<5.00	<5.00
Pd	ppb	9.00	<5.00	14.00	33.00	6.00	<5.00	8.00	7.00	N.A.	17.00	<5.00	<5.00	<5.00
Pt	ppb	14.00	<5.00	14.00	29.00	<5.00	<5.00	5.00	7.00	N.A.	27.00	<5.00	<5.00	<5.00
Ni	ppm	1658.00	303.00	1486.00	2777.00	953.00	991.00	1427.00	1274.00	2912.00	3662.00	382.00	143.00	41.00
Cu	ppm	969.00	129.00	879.00	2937.00	724.00	524.00	899.00	1334.00	1904.00	3153.00	87.00	4.00	32.00
Ag	ppm	<3.00	<3.00	<3.00	<3.00	<3.00	<3.00	<3.00	<3.00	<3.00	<3.00	<3.00	<3.00	<3.00
As	ppm	<10.00	20.00	<10.00	<10.00	<10.00	<10.00	<10.00	23.00	<10.00	<10.00	<10.00	<10.00	<10.00
Ba	ppm	5.00	<3.00	<3.00	<3.00	<3.00	<3.00	<3.00	<3.00	<3.00	7.00	320	<3.00	551.00
Be	ppm	<3.00	<3.00	<3.00	<3.00	<3.00	<3.00	<3.00	<3.00	<3.00	<3.00	<3.00	<3.00	<3.00
Bi	ppm	<20.00	<20.00	<20.00	<20.00	<20.00	<20.00	<20.00	<20.00	<20.00	<20.00	<20.00	<20.00	<20.00
Cd	ppm	<3.00	<3.00	<3.00	4.00	<3.00	<3.00	4.00	<3.00	<3.00	<3.00	<3.00	<3.00	<3.00
Co	ppm	135.20	79.20	121.20	209.00	96.70	90.80	151.70	160.20	214.30	245.50	69.60	93.70	16.10
Cs	ppm	0.10	0.08	0.06	<0.05	0.10	0.08	0.09	0.25	0.09	0.17	1.03	<0.05	10.95
Hf	ppm	1.04	1.52	0.91	0.57	1.26	1.39	0.89	0.37	0.16	0.75	1.24	1.25	6.32
Li	ppm	6.00	32.00	9.00	4.00	4.00	3.00	3.00	4.00	3.00	3.00	109.00	14.00	43.00
Mo	ppm	<3.00	<3.00	<3.00	<3.00	<3.00	<3.00	<3.00	4.00	<3.00	<3.00	<3.00	<3.00	<3.00
Nb	ppm	1.39	2.53	1.48	0.20	2.72	3.51	3.47	1.35	0.35	2.15	3.49	3.37	13.81
Pb	ppm	<8.00	<8.00	<8.00	<8.00	<8.00	<8.00	<8.00	<8.00	<8.00	<8.00	<8.00	<8.00	<8.00
Rb	ppm	1.10	0.50	<0.20	<0.20	0.30	0.30	0.50	0.40	0.20	0.30	16.90	0.20	104.60
Sb	ppm	<10.00	<10.00	<10.00	<10.00	<10.00	<10.00	<10.00	<10.00	<10.00	<10.00	<10.00	<10.00	<10.00
Sc	ppm	51.00	59.00	51.00	53.00	46.00	44.00	34.00	28.00	29.00	10.00	32.00	59.00	6.00
Se	ppm	<20.00	<20.00	<20.00	<20.00	<20.00	<20.00	<20.00	<20.00	<20.00	<20.00	<20.00	<20.00	<20.00
Sn	ppm	<0.30	0.90	<0.30	<0.30	0.50	<0.30	<0.30	<0.30	<0.30	<0.30	<0.30	<0.30	1.6
Sr	ppm	27.00	56.00	33.00	41.00	33.00	101.00	30.00	17.00	27.00	39.00	15.00	16.00	154.00
Ta	ppm	<0.05	<0.05	<0.05	<0.05	<0.05	<0.05	<0.05	<0.05	<0.05	<0.05	<0.05	<0.05	1.21
Tl	ppm	<0.50	<0.50	<0.50	<0.50	0.80	<0.50	0.50	<0.50	<0.50	<0.50	<0.50	<0.50	2.00
W	ppm	2.30	1.40	1.50	1.10	2.40	1.60	1.10	1.70	1.10	1.90	4.20	1.20	2.20
Zn	ppm	62.00	60.00	45.00	49.00	65.00	61.00	83.00	90.00	102.00	104.00	82.00	66.00	70.00
Zr	ppm	17.00	18.00	<3.00	<3.00	<3.00	<3.00	<3.00	<3.00	8.00	11.00	19.00	<3.00	52.00
Hg	ppm	<0.05	<0.05	<0.05	<0.05	<0.05	<0.05	<0.05	<0.05	<0.05	<0.05	<0.05	<0.05	<0.05
Th	ppm	1.90	1.90	0.90	0.50	4.30	0.80	2.70	0.90	0.80	0.80	1.70	3.10	14.60
U	ppm	0.10	0.25	0.11	0.08	0.14	0.15	0.07	0.11	0.07	0.19	0.19	0.20	2.75
Y	ppm	12.06	15.64	10.19	9.17	8.26	6.50	7.13	7.15	5.32	3.53	11.76	12.35	24.34
La	ppm	4.40	11.50	5.80	4.90	6.30	7.00	5.90	7.20	4.60	6.20	11.20	7.60	24.30
Ce	ppm	8.20	18.40	7.90	7.00	8.60	9.70	9.00	9.90	6.80	6.80	18.60	13.70	46.80
Pr	ppm	1.52	2.95	1.35	1.29	1.36	1.38	1.28	1.34	0.94	0.90	2.15	1.84	5.13
Nd	ppm	8.20	15.00	7.90	7.30	7.10	7.00	6.40	7.00	4.70	3.80	8.70	9.50	19.60
Sm	ppm	2.70	4.10	2.50	2.80	2.00	2.10	2.00	2.00	1.30	1.00	1.80	3.10	4.20
Eu	ppm	0.82	1.06	0.70	0.78	0.65	0.40	0.59	0.65	0.40	0.31	0.59	1.12	0.92
Gd	ppm	3.34	4.56	3.06	3.12	2.67	2.28	2.14	2.15	1.44	1.03	2.03	3.71	4.13
Tb	ppm	0.52	0.67	0.44	0.43	0.39	0.33	0.31	0.30	0.22	0.15	0.31	0.54	0.68
Dy	ppm	2.79	3.94	2.44	2.31	2.04	1.88	1.72	1.76	1.20	0.81	2.08	3.05	4.28
Ho	ppm	0.48	0.74	0.44	0.43	0.37	0.32	0.31	0.32	0.21	0.15	0.48	0.62	0.92
Er	ppm	1.20	1.83	1.06	1.14	0.91	0.82	0.76	0.79	0.55	0.36	1.28	1.31	2.73
Tm	ppm	0.17	0.24	0.12	0.13	0.12	0.09	0.09	0.10	0.07	0.05	0.18	0.18	0.39
Yb	ppm	0.90	1.50	0.80	0.80	0.70	0.50	0.60	0.70	0.40	0.20	1.40	1.20	2.50
Lu	ppm	0.13	0.21	0.08	0.08	0.07	0.06	0.07	0.07	0.05	0.05	0.19	0.16	0.36

Cpxt = clinopyroxenite; Ol-Cpxt = olivine clinopyroxenite; Wrlt = wehrlite; Dun = dunite. Chl-Act Schist = chlorite actinolite schist; Qz-Bt Schist = quartz biotite schist.

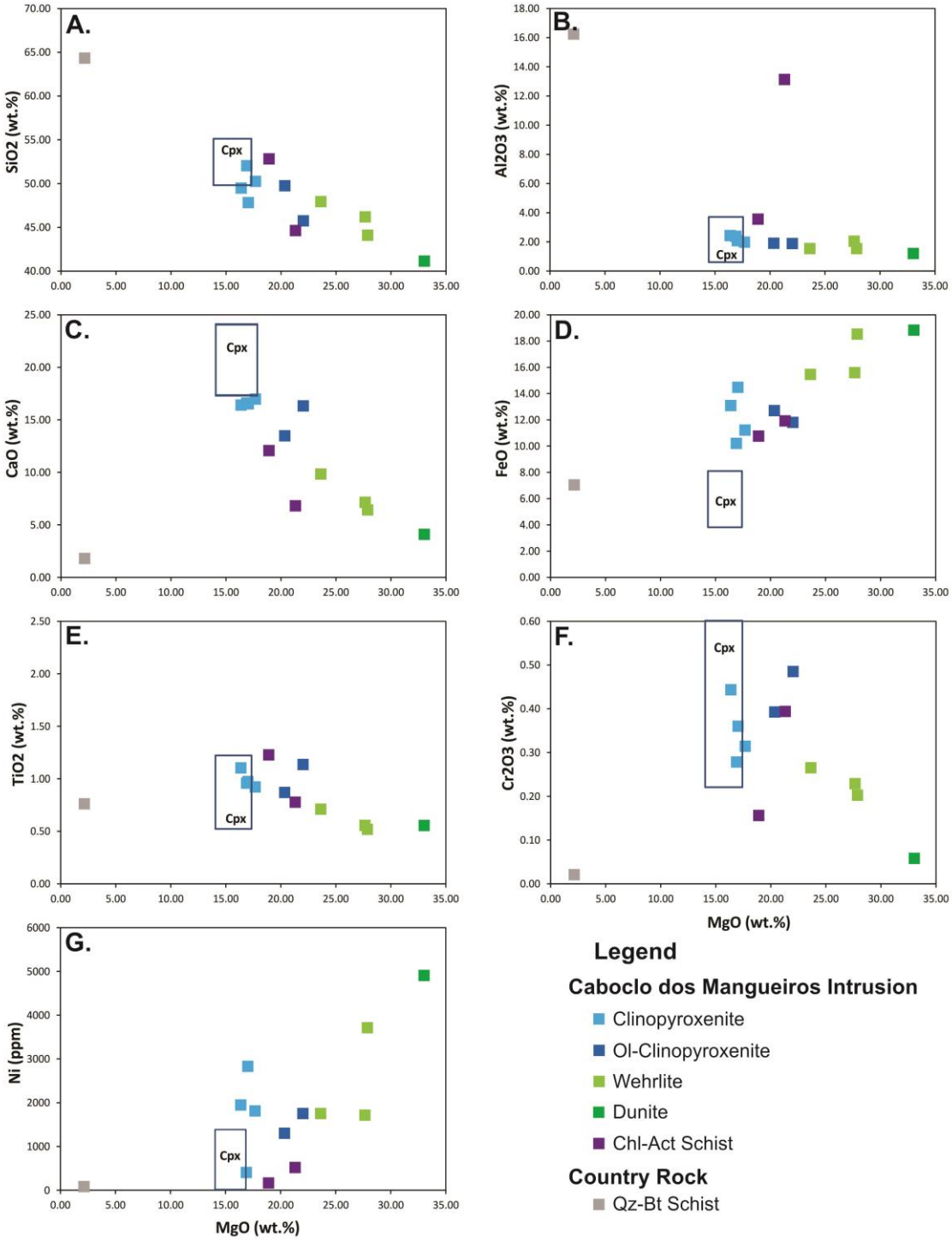

Fig. 9: Plots of MgO versus selected major and minor element contents for rocks of the Caboclo dos Mangueiros intrusion and its country rock. Data from Table 1 normalized to 100% on an anhydrous basis. Compositions of clinopyroxene correspond to microprobe analyses reported in this study (see Appendix 1).

Trace element whole-rock compositions

The incompatible trace elements contents in the ultramafic rocks of the Caboclo dos Mangueiros intrusion are generally low (Table 1), which is expected for cumulates consisting mainly by olivine and clinopyroxene. Variations in contents of incompatible trace elements in mafic-ultramafic cumulates in layered complexes result from the combined effect of variable

assemblages of cumulus minerals, fractionation of the parental magma and variable amounts of trapped intercumulus liquid (e.g., Barnes, 1986; Ferreira Filho et al., 1998; Godel et al., 2011).

Different primitive mantle-normalized rare earth element (REE) patterns characterize different cumulate rocks of the ultramafic intrusion (Fig. 10). REE patterns for dunite and wehrlite have slightly positive slope for both LREE and HREE (Fig. 10A). These olivine cumulates have primitive-mantle normalized Gd/Yb ratios (Gd/Yb_{PM}) and La/Sm_{PM} ranging from 2.66-4.46 and 2.63-3.92, respectively. REE patterns for clinopyroxenite also have slightly positive slope but with lower La/Sm_{PM} ratios. The data reveals that LREE patterns are dependent of the modal proportion of clinopyroxene in the cumulate rocks, as indicated by progressively lower La/Sm_{PM} from dunite (4.01), werhlite (1.91-2.33), olivine-clinopyroxenite (2.04-2.15) and clinopyroxenite (1.05-1.81). This observation is consistent with partition coefficients obtained in experimental studies for clinopyroxene (Hart and Dunn, 1993; Hauri et al., 1994) and several geochemical studies of clinopyroxene-bearing cumulate rocks (e.g., Ferreira Filho et al., 1998; Xue et al., 2016). These studies indicate higher partition coefficients for clinopyroxene compared with olivine, as well as distinctively lower partition coefficients for LREE compared with HREE in clinopyroxene. Contents for several high field strength elements, including Ta, Nb, Th and Hf, in ultramafic rocks of the Caboclo dos Mangueiros intrusion are close to or below their lower detection limits in the analyses (Table 1). To avoid the scattering associated with variable alteration of the cumulate rocks, mantle-normalized trace elements were plot for alteration-resistant elements (Fig. 11A). The mantle-normalized alteration-resistant trace element patterns for peridotites and clinopyroxenites are characterized by relative enrichment in LREE and Th. All these samples have prominent negative Nb-Ta and Zr-Hf anomalies. The composition of the least altered adcumulate clinopyroxenites (samples BM-013 and BM-016) were used as a proxy for the composition of the clinopyroxene. The abundances of the incompatible trace elements in the parental liquid were estimated by their whole-rock concentrations divided by the partition coefficients of these elements between clinopyroxene and basaltic liquids (Hart and Dunn, 1993; Hauri et al., 1994). Results for whole-rock and calculated liquid (Fig. 11B) suggests that the abundance of clinopyroxene in cumulate rocks impact the distribution of trace-elements, an issue to be considered in the following discussions of the composition of the parental magma of the intrusion.

Two samples of chlorite-actinolite schist from the border zone of the intrusion have REE and incompatible trace element patterns similar to those obtained for ultramafic rocks (Fig. 10C and 11A). This result is consistent with the suggestion that the border zone consists of ultramafic rocks compositionally similar to clinopyroxenites and wehrlites, as indicated by major element data. REE pattern for one sample of quartz-biotite schist, a country rock of the ultramafic intrusion, shows positive slope for LREE and almost flat HREE distribution (Fig. 10C). The content of incompatible trace elements in the country rock is greater than those obtained in most of the ultramafic rocks (Fig. 11A).

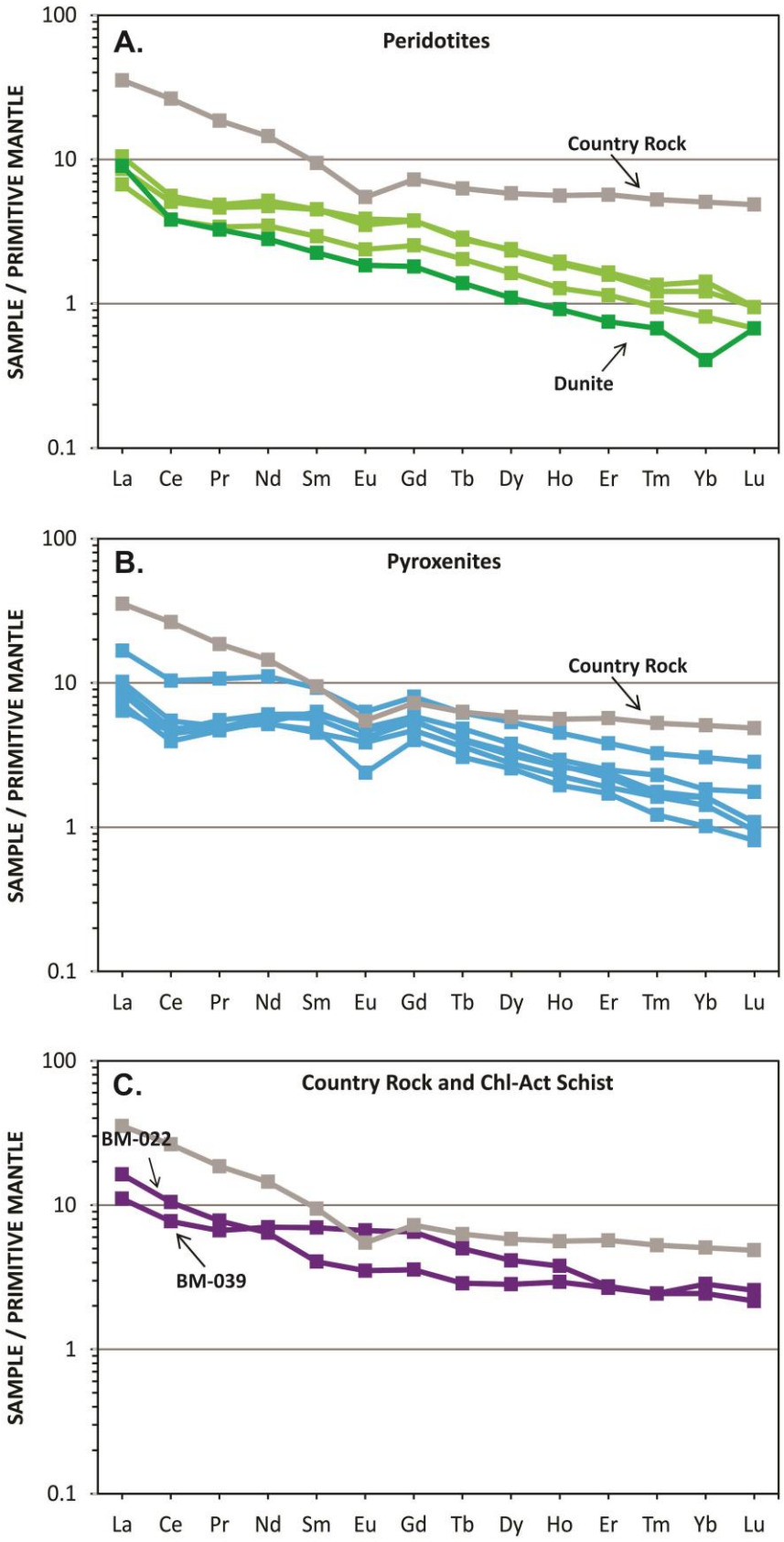

Fig. 10: Primitive mantle-normalized REE patterns for samples of the Caboclo dos Mangueiros intrusion and its country rock. (A) Samples of peridotites. (B) Samples of pyroxenites. (C) Samples of chlorite-actinolite schists of the border zone and one sample of a country rock (quartz-biotite schist). Data from Table 1. Primitive mantle normalization values are from Sun and McDonough (1989). The pattern of the country rock is repeated in (A) and (B) for comparison.

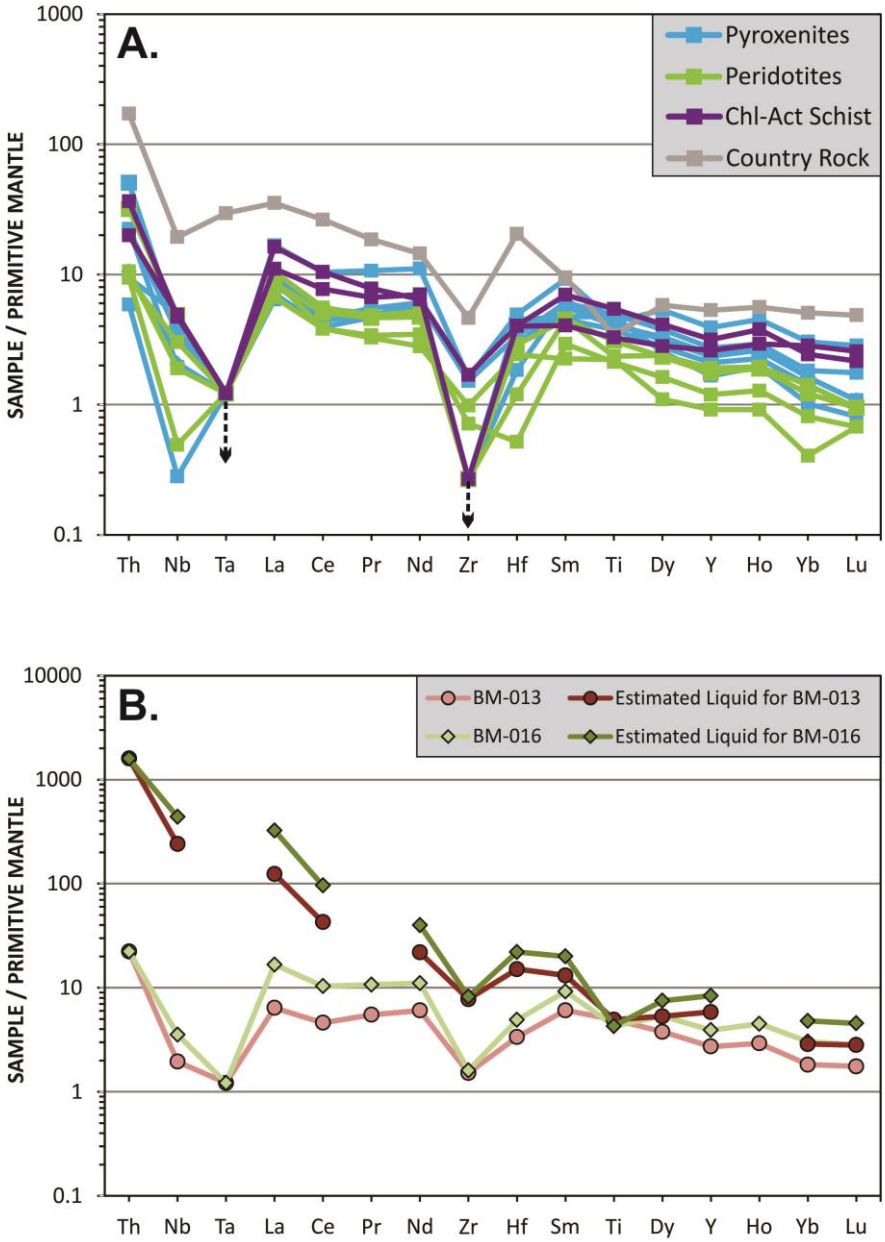

Fig. 11: Primitive mantle-normalized alteration-resistant trace elements patterns for samples of the Caboclo dos Mangueiros intrusion and its country rock. (A) Whole-rock results. (B) Whole-rock and calculated liquid for two samples of adcumulate clinopyroxenite. Black arrow indicates that values are lower than the detection limits of the analytical method. Data from Table 1. Primitive mantle normalization values are from Sun and McDonough (1989).

The Sulfide Mineralization

The Caboclo dos Mangueiros intrusion hosts a large orebody of disseminated Ni-Cu sulfides, as indicated by preliminary resource of ~ 200Mt@0.20%Ni and 0.13%Cu (Projeto Valorização de Alvos Geofísicos; CBPM unpublished internal report). The bulk of sulfide mineralization (~ 99 vol.%) comprises typical disseminated magmatic sulfides associated with ultramafic cumulate rocks, consisting of sulfide blebs (1-5 vol%) within dunite, wehrlite and clinopyroxenite. Disseminated sulfides occur throughout the entire drilled portion of the ultramafic intrusion, suggesting a low-grade orebody coincident with the elongate boat-shaped

intrusion (Fig. 3A). Preliminary estimates by CBPM indicate a 1700x400x200m orebody of consistently low Ni and Cu contents. Remobilized sulfides (~ 1 vol.% of the sulfide resource) are limited to few discrete shear zones (up to 4 m thick) where they occur as irregular strings. Zones of remobilized sulfides have the higher Ni and Cu grades reported in the deposit (up to 4m > 1.0 wt.% Ni). However, their irregular distribution and small size, together with Ni-Cu contents commonly similar to those reported in the disseminated ore, do not indicate any significant high-grade ore zone.

Ore petrography

Ore petrography studies were based upon representative samples of the disseminated (i.e., primary ore) and remobilized sulfide mineralizations. The modal composition of disseminated sulfides in the Caboclo dos Mangueiros deposit is homogeneous with no significant differences throughout the orebody. The sulfide assemblage and textures are typical of magmatic sulfides segregated as immiscible sulfide liquids from mafic-ultramafic magmas (Naldrett, 2004). These primary sulfides consist of pyrrhotite (~80 vol.%), pentlandite (~10 vol.%), chalcopyrite (~8 vol.%) and pyrite / marcasite (~2 vol.%), which occurs as aggregates forming interstitial blebs with up to 3.0 cm diameter (Fig. 12A and 12B). The mineralogy and texture of sulfide blebs are the same for different host rocks (i.e., dunite, wehrlite, clinopyroxenite), with textural differences mainly associated with the grain size of host rocks. Sulfide blebs in coarse-grained rocks may occur included in clinopyroxene or olivine, where sub-spherical morphologies are common. Sulfide aggregates commonly consist of pyrrhotite (<2 mm) containing flames (<20 μm) or inclusions (<300 μm) of pentlandite and chalcopyrite (<600 μm) and/or pyrite (~ 50–500 μm) associated (Fig. 12B and C). Pyrrhotite is eventually be replaced by marcasite, a process that may be limited to fractures in pyrrhotite or pervasive in some samples.

Remobilized sulfides are always closely associated with disseminated ore. They occur in irregular veinlets and breccia that crosscut massive cumulates (Fig. 12D, E and F), as well as sulfide aggregates or stringers concordant with the foliation in discrete shear zones (Fig. 12G and H). The latter are host within fine-grained foliated rocks with abundant amphibole and/or serpentine. Remobilized sulfides consist of pyrrhotite (~50 vol.%) associated with chalcopyrite (~35 vol.%), pyrite / marcasite (~10 vol.%) and minor pentlandite (~5 vol.%). Compared with disseminated sulfides, the aggregates of remobilized sulfides are enriched in chalcopyrite and pyrite/marcasite.

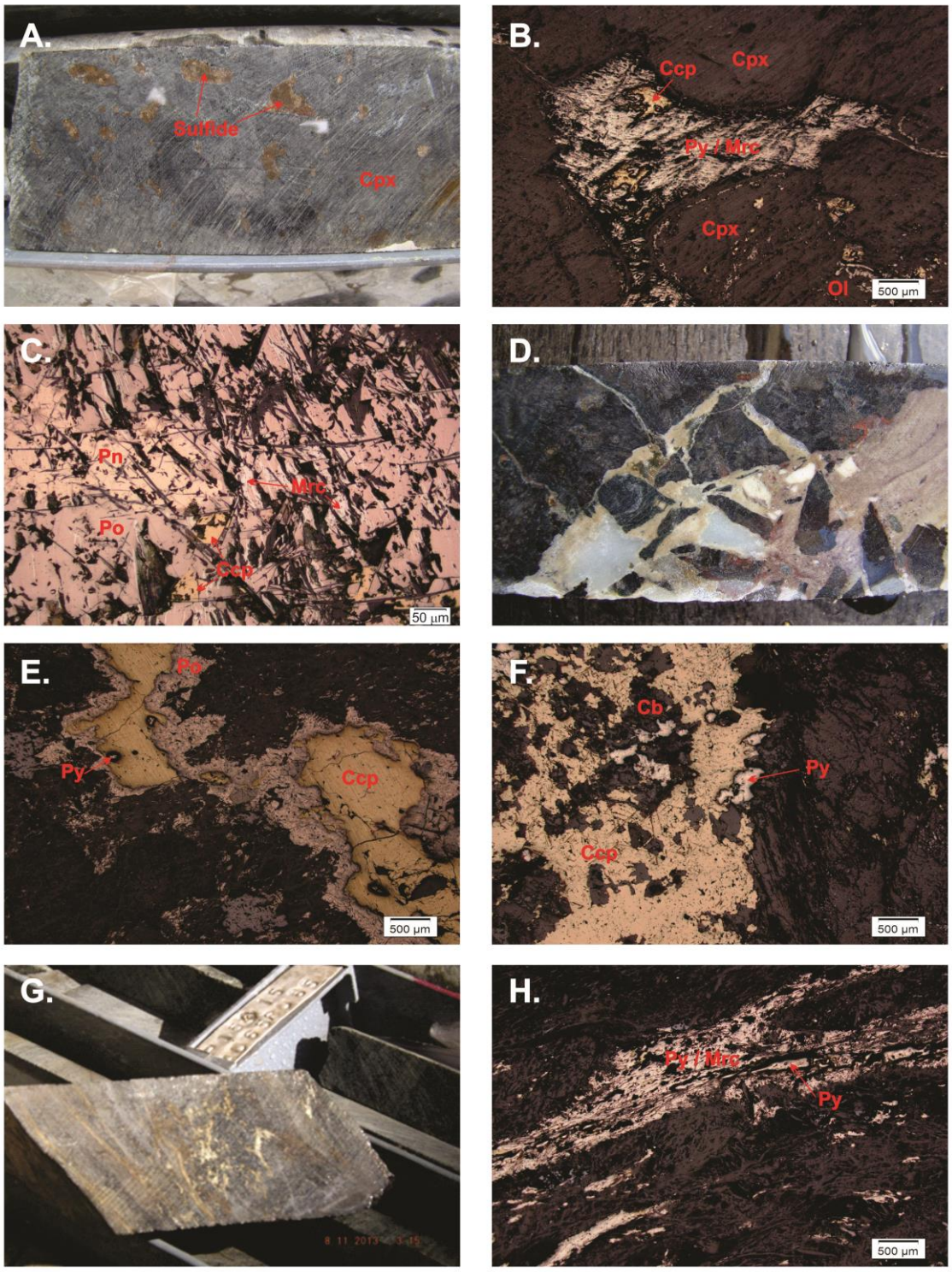

Fig. 12: Types of mineralization in the Caboclo dos Mangueiros deposit. (A) Clinopyroxenite with disseminated primary mineralization. Note the interstitial sulfide blebs texture; (B) Typical interstitial bleb of primary sulfide and sulfide included by silicate crystals (reflected light); (C) An aggregate of primary sulfides comprising pyrrhotite, pentlandite and chalcopyrite. Note replacing of pyrrhotite by marcasite (reflected light); (D) Drill core showing a silico-carbonate alteration zone with breccia and veinlets remobilizing primary sulfides; (E) Veinlet filled out by remobilized pyrrhotite, chalcopyrite and pyrite (reflected light); (F) Breccia zone filled out by remobilized chalcopyrite and pyrite (reflected light); (G) Drill core of a local shear zone. Note the remobilized sulfides throughout the foliation planes; (H) Association of pyrite and marcasite recrystallized throughout the foliation plane in a local shear zone (reflected light). Mineral symbols in accordance with classification of Whitney (2010).

Composition of sulfides

Systematic microprobe analyses were performed on unweathered sulfide minerals to identify their compositions. Results of 169 analyses are provided in Appendix 3. Analyses of pyrrhotite, pentlandite, chalcopyrite and pyrite indicate stoichiometric compositions. Average compositions of pyrrhotite provide a $Fe_{0.81}S$ atomic formula. Ni contents in pyrrhotite are highly scattered but commonly < 0.70 wt.%. Higher Ni contents in pyrrhotite (up to 3 wt.%) result from analyses including tiny pentlandite exsolutions. Pentlandite has Ni contents in the range of 29-40 wt.% (average 35.8 wt.%), Fe contents in the range of 25-31 wt.% (average 27.6 wt.%) and Co contents in the range of 0.5-2.7 wt.% (average 1.7 wt.%). Chalcopyrite has compositions close to the ideal $CuFeS_2$ formula, with average contents of 34.0 wt.% S, 29.9 wt.% Fe and 34.2 wt.% Cu. Pyrite and marcasite have compositions close to the ideal FeS_2 formula, with average contents of 51.8 wt.% S and 45.2 wt.% Fe. Pyrite has low contents of Co (< 0.11 wt.%) and highly scattered Ni contents (up to 1.63 wt.%).

Lithogeochemistry of sulfide ore

The study of chalcophile elements is based upon assays of 10 representative samples of peridotite and clinopyroxenite with disseminated sulfides (Table 1). The plots of S-Ni and and S-Cu are indicated in Figure 13A and 13B, respectively. Positive correlation between S and Ni (0.81) and S and Cu (0.87) indicate that both metals are mainly contained in sulfides. Linear correlations in S-Ni and S-Cu plots indicate moderate tenors for Ni (3.46 wt.% Ni at 35 wt.% S) and Cu (2.93 wt.% Cu at 35 wt.% S). Besides the Ni hosted in sulfides, our whole-rock analyses include an additional amount of Ni hosted in silicates, mainly within olivine pseudomorphs. Because this amount of Ni is not hosted in sulfides, Ni tenor indicated by the S-Ni correlation is overestimated. However, Ni-Cu ratios are not positively correlated to MgO contents (Fig. 13C), suggesting that the amount of Ni hosted in silicates does not significantly impact the indicated Ni tenor. Nevertheless, considering that the indicated Ni tenor is slightly overestimated, the Ni-Cu ratio of the sulfide liquid should be close to 1.

The contents of Pd (< 33 ppb), Pt (< 29 ppb) and Au (< 20 ppb) are distinctively low in the analysed samples (Table 1). These samples have very high Cu/Pd ratios in the range of $0.26x10^5$ to $25x10^5$. These Cu/Pd ratios indicate a depleted sulfide liquid (Fig. 13D).

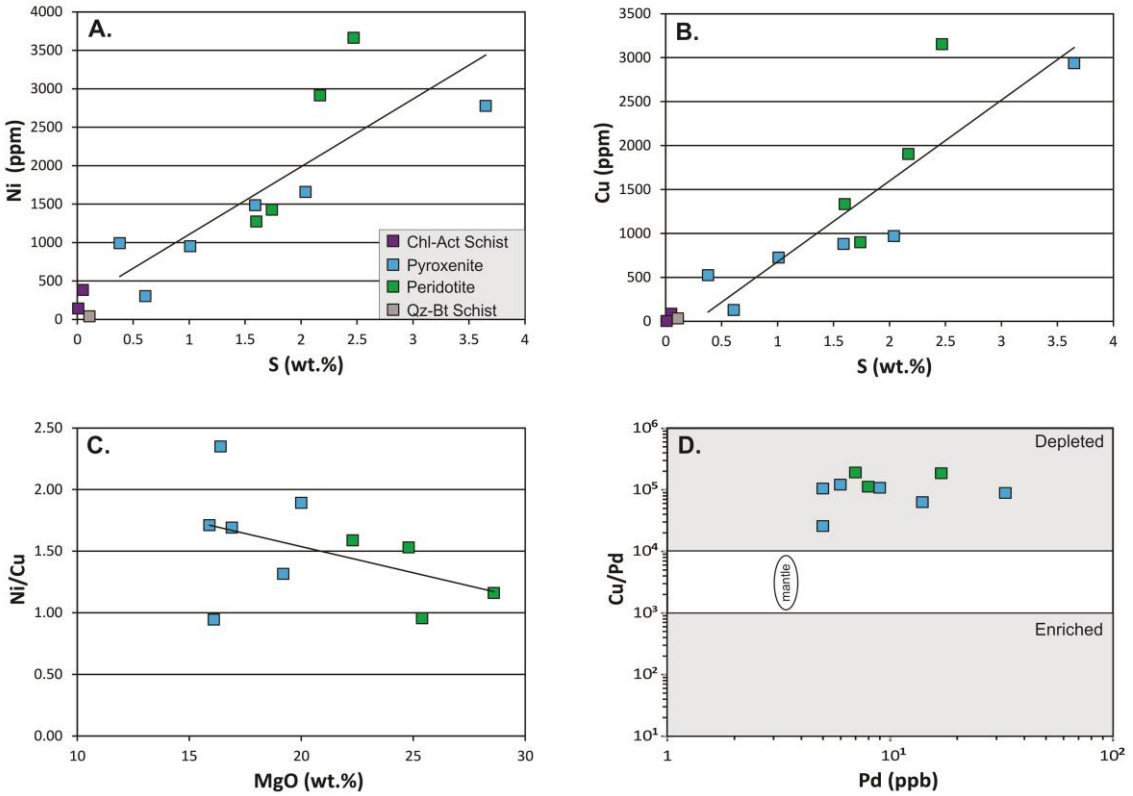

Fig. 13: Lithogeochemistry of sulfide mineralization. (A) Plots of Ni vs S; (B) Plots of Cu vs S; (C) Plots of Ni/Cu vs MgO; (D) Plots of Cu/Pd vs Pd, modified from Barnes and Lightfoot (2005). Data from Table 1.

Sulfur isotopes

The sulfur isotopic composition of six samples representative of disseminated Ni-Cu sulfide ore were analysed in this study. These samples are wehrlite and clinopyroxenite hosting disseminated sulfide blebs consisting of pyrrhotite, pentlandite, chalcopyrite and pyrite. The $\delta 34S$ values for sulfides of these samples are bracketed between -2.19‰ and -1.38‰ (Table 2). Our results indicate isotopic compositions for disseminated sulfides that mainly fit into the mantle range (Fig. 14). Additionally, the narrow compositional range of isotopic compositions in our samples does not suggest differences in isotopic compositions related to different host rocks (i.e., wehrlite or clinopyroxenite) of different location in the ultramafic intrusion.

Table 2: Sulfur isotope analyses of representative samples from the Caboclo dos Mangueiros deposit.

Sample	BM-009	BM-010	BM-013	BM-016	BM-041	BM-042
Drill Hole	FD-3	FD-3	FD-9	FD-9	FD-5	FD-5
Deth (m)	104.1	86.2	258.6	227.2	202.5	132.8
Rock Code	Ol-Cpxt	Wrlt	Cpxt	Cpxt	Wrlt	Cpxt
δ^{34}S ‰	-2.19	-1.60	-1.64	-1.70	-1.38	-1.69

Rock codes in accordance with Table 1.

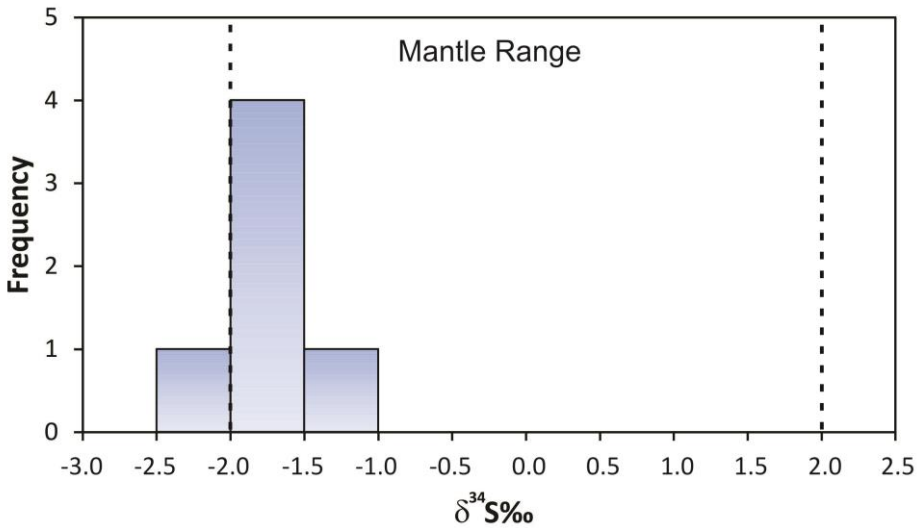

Fig. 14: Sulfur isotope. Histogram for δ^{34}S values of sulfides from the Caboclo dos Mangueiros Deposit. The dashed lines indicate the mantle-deriver sulfur interval. Data from Table 2.

Discussion

The magmatic structure

Ni-Cu-PGE deposits hosted in mafic-ultramafic intrusions are broadly classified into those associated with magma conduits and those associated with layered intrusions (Beresford and Hronsky, 2014). While layered intrusions are best known for hosting reef-type PGE deposits (e.g., Merensky Reef and UG2 in the Bushveld Complex; Cawthorn et al., 2005), Ni-Cu sulfide deposits are commonly hosted within magma conduits (e.g., Noril'sk-Talnakh and Voisey's Bay deposits; Barnes and Lightfoot, 2005). The dynamics of magmatic systems in conduits is relevant to promote the concentration of sulfides and their enrichment in Ni-Cu-PGE through continuous and/or multiple flows of magma (Barnes and Lightfoot, 2005; Barnes et al., 2016). Although typical layered intrusions and conduits have distinct magmatic structures and textures, large Ni-Cu-PGE sulfide deposits are small parts of crustal scale magmatic systems forming a continuous network of highly variable intrusions. Therefore, the characterization of the magmatic structure in a recently discovered Ni-Cu sulfide deposit provides the first clues to guide future investigations of the larger scale magmatic system.

The following summary discusses key features associated with the structure of the ultramafic intrusion and host rocks. It should be considered that different from intrusions with abundant outcrops, the description and interpretation of the magmatic structure of the Caboclo dos Mangueiros intrusion was just based on drill core logging and petrographic studies of core

samples. In addition, the discussion regarding the primary magmatic structure should also evaluate modifications resulting from post-magmatic processes

The elongated boat-shaped intrusion resembles an elongated sill similar to those hosting the Noril'sk-Talnakh Ni-Cu deposit (Naldrett, 2004) or the Ipueira-Medrado chromite deposit (Marques and Ferreira Filho, 2003). Although the upper portions of the ultramafic intrusion were removed at the present erosion surface, a geometry typical of tubular chonoliths (e.g., Nebo-Babel: Seat et al., 2007; Limoeiro: Mota-e-Silva et al., 2013), as well as those typical of pipe- or funnel-like ultramafic intrusion (e.g., Eagle: Ding et al., 2012a; Jinchuan: Song et al., 2012) is not consistent with our results for the Caboclo dos Mangueiros intrusion.

The contact between country rocks and the intrusion consist of thin (up to 4 meters thick) zones of fine-grained chlorite-actinolitite and chlorite-actinolite schist. Although these fine-grained rocks likely represent the border zone of the ultramafic intrusion, their characterization is hampered by limited data from few core intervals where primary textures and minerals are not preserved. The compositions of rocks from the border zone suggest ultramafic rocks variably contaminated with country rocks. Similar trace element distribution for rocks from the border zone and ultramafic cumulates suggests that they originated from compositionally similar parental magmas. Pervasive disseminated sulfides (1-5 vol.%) that occur throughout the ultramafic intrusion sharply disappear in the fine-grained border zone. The abrupt change in sulfide content is possibly related to localized shearing and alteration along the contact zone.

Except for the discrete sheared zones, the degree and intensity of deformation in the country rock is not shown by the intrusion. Country rocks of the Caboclo dos Mangueiros intrusion are foliated and folded graphite-bearing quartz-biotite schists, contrasting with massive cumulates with magmatic textures in the ultramafic rocks. Metamorphic assemblages described in the country rocks (i.e., albite + quartz + biotite + muscovite + epidote), ultramafic cumulates (i.e., tremolite-actinolite + serpentine + magnetite) and rocks from the border zone (i.e., actinolite + chlorite), on the other hand, are all consistent with greenschist facies of regional metamorphism (Bucher and Grapes, 2011). The contrast in deformation between mafic-ultramafic intrusions and metapelitic country rocks are common in metamorphic terrains (e.g., Mota-e-Silva et al., 2013; Teixeira et al., 2015) and result from their distinct rheological properties (e.g., Passchier et al., 1990). This discussion suggests that the ultramafic intrusion and country rocks were subjected to the same event of tectonism and associated greenschist facies metamorphism. However, as no geochronological data is available, the timing of sedimentation, intrusion and tectonic/metamorphic event is unconstrained at the moment.

The internal structure of the ultramafic intrusion lacks well-defined layering characteristic of layered intrusions. The absence of layering together with abrupt changes in textures in scales from centimeters to few meters, common features in magmatic dynamic system, possibly result from magma flowing through and interacting with country rocks as suggested by Barnes et al. (2016).

Constraints for the parental magma of the ultramafic magmatism

The characterization of the parental magmas of mafic-ultramafic intrusions is of great interest because this provides clues on the nature of the mantle source, the assimilation of crustal rocks and their potential to host magmatic mineral deposits. The composition of parental magmas, including those hosting Ni-Cu sulfide mineralization, can be determined directly, from the chilled margins of the magmatic bodies that host the ore deposits, as illustrated by studies of the parental magmas in tube-like conduits of the Limoeiro and Nebo-Babel deposits (Mota-e-Silva, 2014; Seat et al., 2007). The composition of the parental magma of the Caboclo dos Mangueiros deposit is not constrained by this common approach. Hence the nature of the parental magma was inferred from the crystallization sequence and the geochemistry of the cumulate rocks and minerals of the intrusion that host this deposit.

Geological descriptions of drill holes and bulk rock chemical compositions suggest a crystallization sequence consisting of dunite, wehrlite and clinopyroxenite (Fig. 4 and 9). Due to widespread replacement of cumulus minerals, olivine is pervasively altered and compositions were obtained just for clinopyroxene. The cationic Mg# of cumulus clinopyroxene range from 0.78 to 0.94 (Fig. 7), indicating a moderate to primitive composition for the parental magma of the Caboclo dos Mangueiros deposit. The composition of these clinopyroxene crystals is comparable with those reported for wehrlite and clinopyroxenite from the VE3 intrusion in central Brazil (Lima et al., 2008). Clinopyroxene and olivine in wehrlite from the VE3 intrusion have cationic Mg# and Fo content of olivine ranging from 0.85-0.92 and 84-85 mol.% respectively (Lima et al., 2008).

The fractionation of the ultramafic intrusion indicates a crystallization sequence as follow:

Olivine => Olivine + Clinopyroxene => Clinopyroxene

This trend of crystallization is similar to what described for the VE3, Monte do Carmo and São Domingos layered intrusions (Lima et al., 2008), for the Serra do Puma complex (Rosa, 2014) and for the paleoproterozoic Ni-bearing intrusions in the Pechenga Ore Field in Russia (Latypov et al., 2001; Naldrett, 2004). This fractionation characterizes silica undersaturated parental magmas. In addition, the early crystallization of cumulus clinopyroxene rather than orthopyroxene, leads to progressive depletion of chromium in the magma, thus providing an explanation for the lack of chromite in the crystallization sequence of the Caboclo dos Mangueiros intrusion. The same explanation is commonly used to justify the absence of significant chromium deposits associated with silica undersaturated magmas (Cawthorn, 1996; Ferreira Filho and Araújo, 2009).

The lack of mafic rocks in the intrusion could suggest an ultramafic parental magma. However, clinopyroxene and whole-rock compositions are consistent with a basic parental magma. In addition, the contents of Ni/Cu ratios of the deposit, a subject discussed hereinafter, are distinctively low (~1 to 2) and indicative of basic compositions (Barnes and Lightfoot, 2005). Therefore, our results indicate that the ultramafic intrusion result from the crystallization of a basic parental magma with moderate to primitive composition.

REE and primitive mantle-normalized patterns for the ultramafic cumulates vary from different types of cumulates. Our results indicate progressively lower La/Sm_{PM} from dunite (4.01), werhlite (1.91-2.33), olivine-clinopyroxenite (2.04-2.15) and clinopyroxenite (1.05-1.81), suggesting that the distribution of LREE is partially controlled by the modal proportion of clinopyroxene (Fig. 10A and 10B). This observation is consistent with partition coefficients obtained in experimental studies for clinopyroxene (Hart and Dunn, 1993; Hauri et al., 1994) and several geochemical studies of clinopyroxene-bearing cumulate rocks (e.g., Ferreira Filho et al., 1998; Xue et al., 2016). The content of trace elements in cumulate rocks are modeled as the result of combined content of cumulate minerals and trapped intercumulus liquid (Barnes, 1986). Due to low partition coefficient for incompatible trace elements (<< 1) for common cumulus minerals in primitive mafic-ultramafic rocks (e.g., olivine, orthopyroxene, clinopyroxene), the contribution of the amount of these elements contained in cumulate minerals become significant just in whole-rock compositions of adcumulate rocks (Barnes, 1986). However, clinopyroxene has higher partition coefficients for LREE, as well as some other incompatible trace elements, than olivine and orthopyroxene (Hart and Dunn, 1993; Hauri et al., 1994). Therefore, the contribution of trace elements contained in cumulate minerals should be particularly relevant for adcumulate clinopyroxenite. Based upon this reasoning, the composition of the least altered adcumulate clinopyroxenites were used as a proxy for the composition of the clinopyroxene. The abundances of the incompatible trace elements in the liquid were then estimated considering the partition coefficients of these elements between clinopyroxene and basaltic liquids (Hart and Dunn, 1993; Hauri et al., 1994). Although the composition calculated for the parental liquid (Fig. 11B) may be overestimated (i.e., indicate higher contents of incompatible elements than the actual magma) due to the re-equilibrium of clinopyroxene and trapped liquid (Barnes, 1986; Godel et al., 2011), the calculated liquid largely reduce the effect of cumulus minerals in trace element patterns. Primitive mantle-normalized alteration-resistant trace elements patterns for the calculated parental liquid are fractionated, as indicated by enrichment in LREE and Th (Fig. 11B). The strong Nb-Ta anomalies indicated in whole-rock analyses of ultramafic cumulates (Fig. 11A) does not occur in the calculated parental liquid (Fig. 11B). Although the lack of isotopic results for the ultramafic intrusion largely limit the discussion of mantle and crustal processes associated with the composition of the parental magma, the fractionated pattern of the calculated parental liquid, together with primitive compositions indicated by whole-rock and mineral compositions, provide some constraints for these processes. Significant assimilation of crustal rocks during ascent and emplacement of the magma is not supported by the crystallization sequence typical of silica undersaturated magmas, as well as by the absence of Nb-Ta anomalies. The composition of the biotite-quartz schist (Fig. 11A), the country rock of the ultramafic intrusion, does not provide an appropriate contaminant to promote the trace elements patterns of the calculated parental liquid (Fig. 11B).

Implications of the sulfide textures and compositions

The Caboclo dos Mangueiros deposit consists mainly of disseminated sulfide as interstitial blebs (Fig. 12), comprising an association of pyrrhotite, pentlandite, chalcopyrite and minor pyrite. Textures and mineralogical composition of sulfides indicate that they originated from immiscible sulfide liquids segregated from mafic-ultramafic magmas (Naldrett, 2004). Whole-rock compositions indicate low Ni/Cu ratios (between 0.95 and 2.35) consistent with the segregation of the sulfide liquid from a mafic parental magma. The remarkably low content of precious metals (i.e., Pt, Pd, and Au) and Cu/Pd (Fig. 13D) ratios indicates that the parental magma is depleted in PGE-Au. Mantle-derived magmas with low MgO contents are commonly PGE depleted owing to the retention of sulfides in the mantle (Barnes and Lightfoot, 2005). These magmas give rise to ores with normal Ni and Cu contents but relatively depleted in PGE contents (Barnes and Lightfoot, 2005). Given the moderate to primitive composition of the suggested parental magma of the Caboclo dos Mangueiros intrusion, the degree of partial melting was sufficient to originate a sulfide fertile parental magma that removed all sulfides from the mantle source. Therefore, the depletion of PGE in the deposit is most likely due to previous sulfide segregation. Current models for a number of important deposits attribute the initial segregation of sulfide liquid to deep seated processes, occurring in the lower crust well below the eventual level of formation of the actual deposits, followed by entrainment, upward transport and mechanical deposition (Barnes et al., 2016).

The attainment of sulfide saturation in a determinate magma and the segregation of an immiscible sulfide liquid, coupled with the presence of physical environment appropriated to the collect and concentration of metal-rich sulfide liquid are key factors to the formation of magmatic Ni-Cu-PGE deposits (Naldrett, 1999b; Barnes and Lightfoot, 2005; Ripley and Li, 2013). Although sulfide saturation in mafic magmas may be attained just by the decrease of temperature and hence fractional crystallization, it may be accelerated by contamination processes, such as assimilation of volatiles, assimilation of siliceous country rocks, mixing of magmas and/or addition of crustal-derived sulfur (Ripley and Li, 2013).

The amount of sulfide through the relatively small-sized intrusion, with average of 3-5 vol.%, lead to the discussion about the cotectic proportion of sulfide in an ultramafic intrusion. The increase in sulfur concentration of a melt as a result of crystallization of olivine and pyroxene by fractional crystallization, may lead to the separation of what is known as cotectic proportions of sulfide liquid (Barnes, 2007; Li and Ripley, 2009). The amount of sulfide liquid produced per crystallization increment is small and very efficient collection is required to produce horizons with more than ~2 vol.% sulfide (Ripley and Li, 2013). In closed systems, even if the sulfide saturation had been attained by contamination processes, excepting the addition of crustal-derived sulfur, the content of sulfide produced is very close to the cotectic proportions produced only by fractional crystallization. Furthermore, although rare, it can form economic sulfide deposits as illustrated by the Santa Rita Ni-Cu deposit hosted in the Fazenda Mirabela intrusion (Barnes et al., 2011; Lazarin, 2011, Ferreira Filho et al., 2013) with resources of ~ 236Mt@0.60%Ni and 0.16%Cu (Mirabela Nickel Ltd, 2012, Annual Report).

The amount of sulfides in the Caboclo dos Mangueiros deposit, together with the structure and composition of the host ultramafic rocks, suggest an open dynamic flow system with constant passage of magma containing sulfides. This scenario is consistent with sulfide contents above the cotectic proportion in the deposit. Conduits provide a physical environment where sulfide collection and upgrading may occur, related in part to the passage of multiple pulses of magma (Ripley and Li, 2013), then providing accumulating of Ni-Cu sulfides well above the cotectic proportion. Although no evidences of the direction of magma flow, the structure of the intrusion that hosts the Caboclo dos Mangueiros deposit, thicker in the central portion and progressively thinner toward the extremities, probably was a favorable physical environment that provided changes in the flow dynamics of the magma leading to sulfide mechanical deposition. This process is similar to that proposed for several Ni-Cu sulfide deposits (Barnes and Lightfoot, 2005; Barnes et al., 1016), as illustrated by the Limoeiro Ni-Cu deposit (Mota-e-Silva et al., 2013) and Ni-Cu deposits in the Voisey's Bay area (Li and Naldrett, 1999).

Sulfur source

In several world-class Ni-Cu sulfide deposits the sulfur isotopic compositions indicate the importance of assimilated crustal sulfur for their origin (e.g., Ripley and Li, 2003, 2013; Keays and Lightfoot, 2010). However, isotopic results have also indicated that Ni-Cu deposits may originate without an external source of sulfur (e.g., Seat et al., 2009; Ferreira Filho et al., 2013).

The sulfides of the Caboclo dos Mangueiros deposit show homogeneous isotopic compositions with short range of values, from -2.19 to -1.38 δ^{34}S ‰ (Fig. 14). These homogeneous results correspond to analyses of sulfide fractions with variable proportions of sulfide minerals (i.e., pyrrhotite, pentlandite, chalcopyrite and pyrite). The sulfur isotopic compositions of sulfides from the Caboclo dos Mangueiros deposit are consistent with mantle-derived sulfides (Fig. 14). Isotopic compositions of Ni-Cu sulfide deposits have highly variable compositions (Fig. 15). These results are consistent with the existence of deposit with significant contribution of crustal-derived sulfur (e.g., Noril'sk-Talnakh), as well as deposits where sulfur is mainly mantle-derived (e.g., Santa Rita). Therefore the sulfur isotopic compositional characteristics of the Caboclo dos Mangueiros deposit reflect the mantle source of sulfides with no significant addition of crustal-derived sulfur.

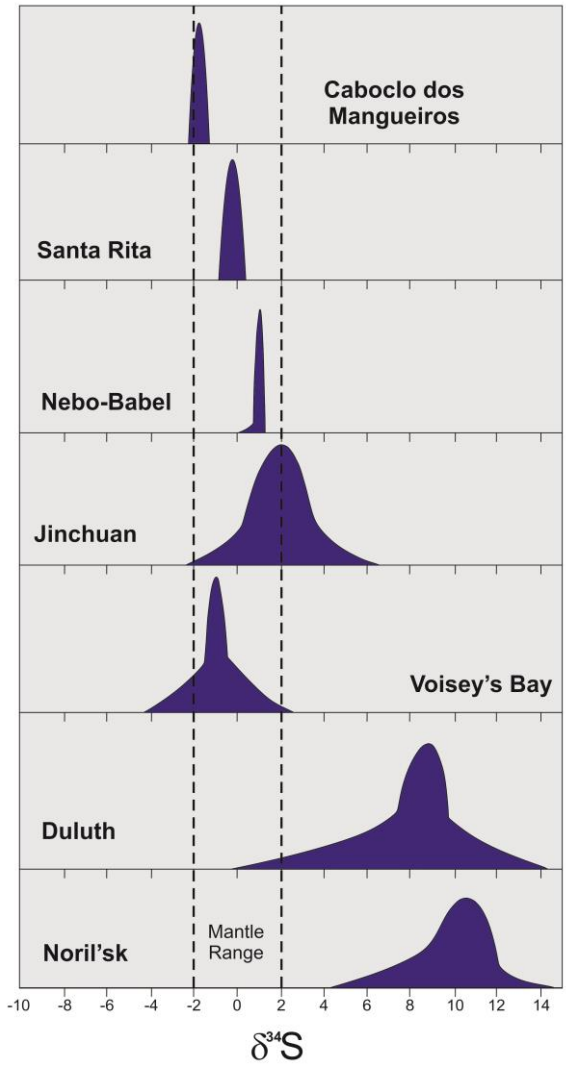

Fig. 15: Sulfur isotope. Histogram for representative $\delta^{34}S$ values of magmatic Ni-Cu deposits worldwide. The dashed lines indicate the mantle-deriver sulfur interval. References - Noril'sk, Duluth, Voisey's Bay, Jinchuan and Nebo-Babel: Seat et al. (2009) and references therein; Santa Rita: Lazarin (2011). Partially modified from Seat et al. (2009) and Lazarin (2011).

Tectonic setting

The intrusion that hosts the Caboclo dos Mangueiros Ni-Cu sulfide deposit consist of an ultramafic body located in the northwestern edge of the São Francisco Craton (Fig. 1). Several world-class Ni-Cu-PGE sulfide deposits are located close to cratonic borders, such as Noril'sk (e.g., Naldrett, 1992, 1999b) located on the northwest margin of the Siberia craton, Voisey's Bay (e.g., Li and Naldrett, 1999) located on the Nain craton margin, and Jinchuan located on the margin of North China craton (e.g, Song et al., 2012). The common association of Ni-Cu sulfide deposits and cratonic margins support geodynamic models connecting the origin of Ni-Cu-PGE fertile mafic magmas in the mantle and their final emplacement in the crust (Begg et al. 2010; Barnes et al., 2016). This association is thought to be related to deflection of the heads of mantle plumes, or melts from the plume, towards zones of thin lithosphere at craton margins (Barnes et al., 2016). The transport of these upwelling magmas to the crust is interpreted to occur through large systems of translithospheric faults in craton margins (Begg et al., 2010). The architecture of the crust controls the development of variable conduit systems and

favorable or unfavorable environments for mineralization, as illustrated by Barnes et al. (2016). In addition, these favorable environments may develop small structures (e.g., small conduits) through which large volumes of magma may pass and deposit large amounts of sulfide. Such conduits may facilitate the reaction of transported sulfide with large volumes of magma giving rise to high volume ratio of sulfide to silicate and hence high ore tenors in intrusions with relatively small size (Barnes et al., 2016). These small structures or conduits are recognized in several deposits, as exemplified by the intrusions hosting the Ni-Cu-PGE Yangliuping deposit (Song et al., 2003) located on the margin of the South China craton.

Significant importance has been given to this tectonic setting, associated to a magmatic system through which large volume of magma passed, as promising mineral exploration target for Ni-Cu-PGE sulfide deposits. In fact, the Caboclo dos Mangueiros deposit is located in a promising tectonic setting for the development of these base metals sulfide deposits. Despite the lack of integrated studies, it is suggestive that this magmatic system may be represented by other mineralized intrusions occurring in that region, suggesting a cluster of mafic-ultramafic complexes (Fig. 2A).

The lack of an absolute age for the ultramafic rocks that host the Caboclo dos Mangueiros deposit is a limiting factor to positioning this one in the tectonic evolution of the São Francisco Craton. Robust geochronological results in the regional setting of the deposit is available only to the Angico dos Dias carbonatite complex (Silva et al., 1987). U-Pb zircon and baddeleyite 2010±6 Ma age was obtained for the Angico dos Dias carbonatite complex (Silva et al., 1987). This complex is intruded within deep faults NE-SW trending of the Archean Sobradinho-Remanso complex located in northern edge of the São Francisco Craton, close to the contact with the Riacho do Pontal fold belt (Uhlein et al., 2011) (Fig. 1). Geochronological studies of the Caboclo dos Mangueiros intrusion and country-rocks are currently being developed. These results will better constraint the geotectonic setting of the Caboclo dos Mangueiros deposit.

Descriptive Model

The proposed descriptive model for the evolution and emplacement of the intrusive ultramafic body that host the Caboclo dos Mangueiros deposit is presented on Figures 16 and 17. This model is based on geological features, whole-rock and mineral compositions and sulfur isotopic results.

The cratonic margin setting which the Caboclo dos Mangueiros deposit is located, coupled with the presence of several mafic-ultramafic intrusions in that region, leads to suggest a similar model proposed by Begg et al. (2010) and Barnes et al. (2016) for the origin of the parental magma. A plume originated by mantle melting that impinged beneath thick lithosphere and was deflected to a thinner lithosphere zone adjacent to the São Francisco Craton margin (Fig. 16A), where the plume undergone decompression-related medium-to high degree partial melting at shallower depths (Fig. 16B). Due to the lack of the absolute age of the intrusion the positioning of this one in the tectonic evolution of the São Francisco Craton remains uncertain.

The moderate to primitive composition of the parental magma suggests that the degree of partial melting was sufficient to originate a fertile mafic magma. Decrease in temperature may have been the main mechanism to the attainment of sulfide saturation throughout the upward migration of the mafic parental magma and hence to the segregation of an immiscible sulfide liquid with no significant addition of crustal-derived sulfur. The depleted composition of the sulfide liquid in the Caboclo dos Mangueiros deposit suggests that a prior segregation of immiscible sulfide liquid occurred, thus leading to low PGE contents and high Cu/Pd ratios in the deposit.

The migration of the mafic parental magma upward within the crust carrying sulfide droplets probably was favored by the buoyancy of the magma column (Barnes et al., 2016). This migration probably was also favored by active, steeply-dipping, translithospheric faults. Such faults are likely to be a feature of craton margins, particularly during periods of transcurrent movement, and are likely to have good vertical connectivity (Begg et al., 2010). These faults would have formed wide range conduit systems, where large volumes of magma have passed and precipitated or not significant contents of Ni-Cu sulfides within favorable sites of the crust.

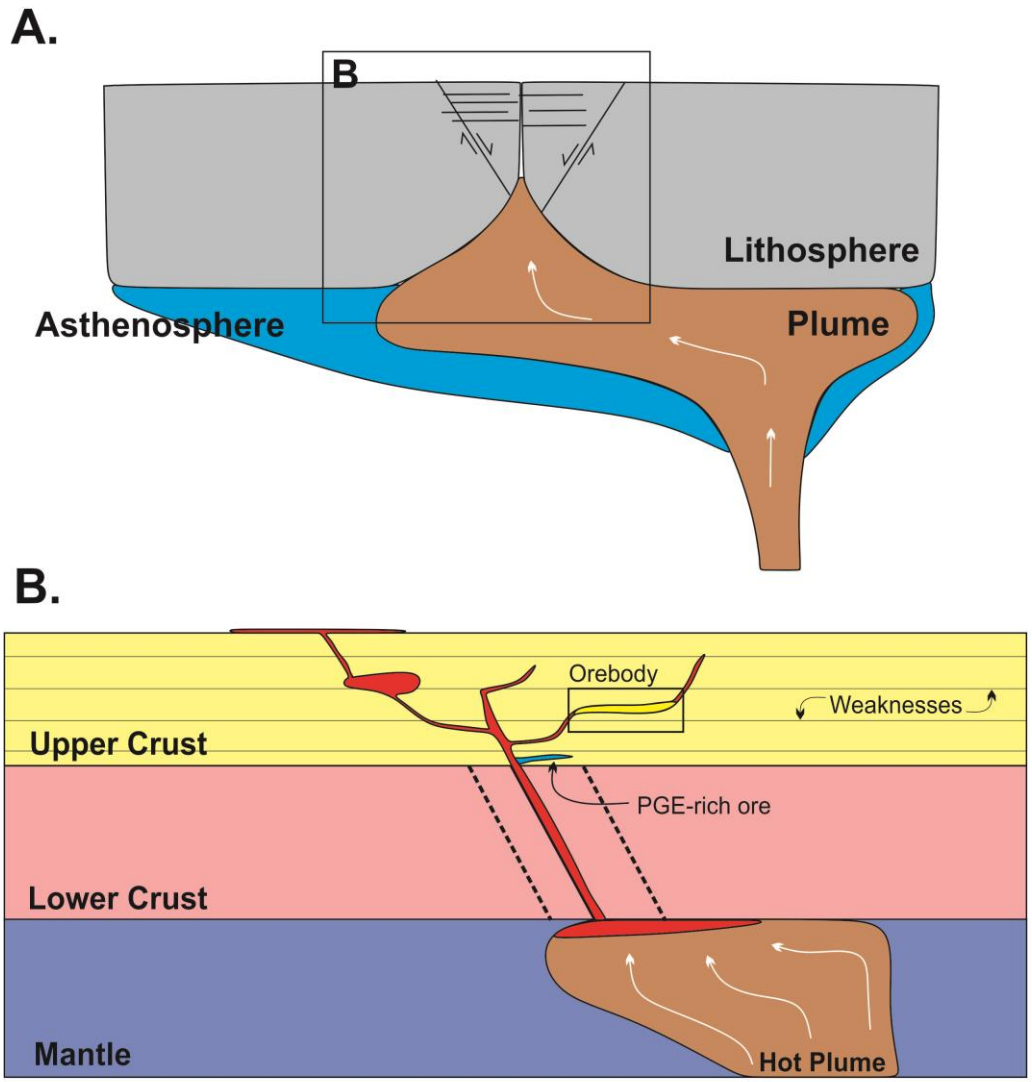

Fig. 16: Schematic model for parental magma origin. (A) Deflection of the head mantle plume toward zones of thin lithosphere adjacent to craton margins. Partially modified from Begg et al. (2010); (B) Decompression-related partial melting of the plume heads and migration of magma upward within the crust through traslithopheric faults. The two black dashed lines indicate predominating of faults, where conduit systems are formed. The black square suggests the formation of the Caboclo dos Mangueiros deposit. Partially modified from Barnes et al. (2016).

The architecture of the crust, locally comprising stratified pelitic sediments, probably provided the favorable environment for the emplacement of the primary structure of the Caboclo dos Mangueiros deposit (Fig. 17A). Linear weaknesses in the country rocks such as sedimentary layers probably facilitated the flowing of the mafic parental magma. The enlargement in the central portions of the conduit structure that host the Caboclo dos Mangueiros deposit may have provided changes in the flow dynamics of the magma, leading to precipitation of the sulfide droplets. When the magma that flows through a narrow chamber reaches a more enlarged space it will slow down and will be less capable of carrying the sulfide blebs (Maier et al., 2001; Mota-e-Silva et al., 2013).

The actual basculated disposition of the rocks that hosts this Ni-Cu sulfide deposit (Fig. 17B), as well as the metamorphic parageneses in greenschist facies affecting cumulate

ultramafic rocks and sedimentary country rocks, indicate that the intrusion and country rocks were submitted to tectonism and associated metamorphism. Due to the lack of the absolute age of the intrusion and detailed studies of the country rocks, the correlation of these events to the evolution of the northern portion of the São Francisco Craton remains uncertain.

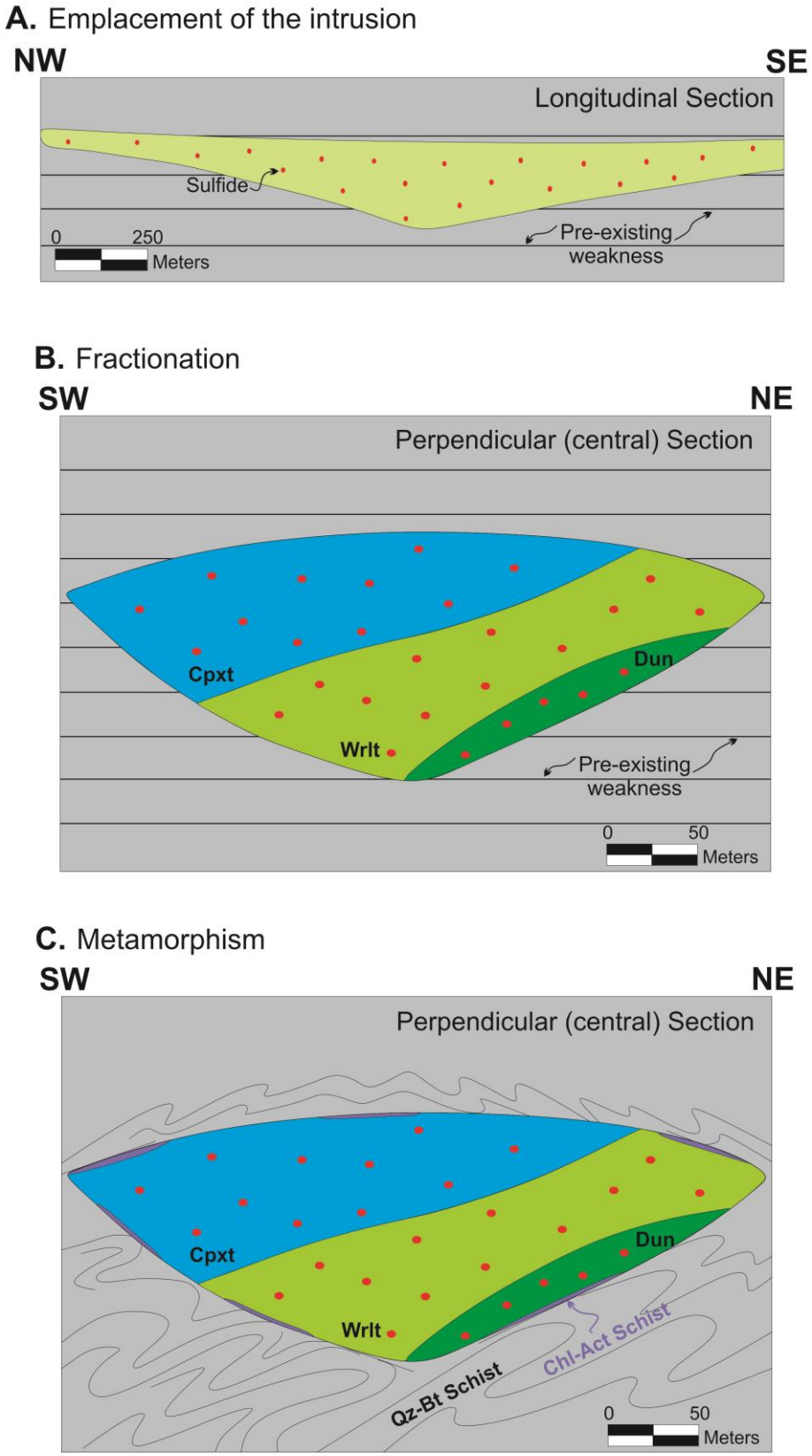

Fig. 17: Schematic model for the Caboclo dos Mangueiros deposit. (A) Longitudinal section showing the emplacement of the intrusion through pre-existing weak layers of the sedimentary rocks. Emplacement of magma carrying sulfide droplets through the conduit structure that later solidified as an elongated sill boat-shaped; (B) Perpendicular central SW-NE section showing the fractionation of the mafic parental magma; (C) Perpendicular central SW-NE section after the tectonics and regional metamorphism. Rock codes in accordance with Table 1.

Implication for exploration

The extreme northwestern portion of the São Francisco Craton has significant potential to host magmatic deposits, as illustrated by the presence of different types of mineralization. These can be exemplified by the Fe-Ti-V magmatic deposit of the Campo Alegre de Lourdes mafic-ultramafic Complex (Sampaio et al., 1986), the P_2O_5 deposit of the Angico dos Dias Carbonatite Complex (Silva et al., 1988; 1997; Antonini et al., 2003), as well as by the Ni-Cu magmatic sulfide deposit here studied. In addition, several magnetic anomalies (Fig. 2B) that are widely covered by tertiary-quaternary sediments remain unexplained and provide additional targets.

The Ni-Cu sulfide mineralization in the Caboclo dos Mangueiros deposit implies that a large volume of sulfide droplets have been transported and concentrated in the ultramafic intrusion in proportion above the cotectic proportions. Therefore, in the proposed model the Caboclo dos Mangueiros deposit represents a small part of a large magmatic system (Fig. 16), suggesting a scenario with high potential for new discoveries. The results presented in this study indicate that the northwestern margin of the São Francisco Craton should be looked as a potential new metallogenetic province.

Conclusions

The conclusions of this study are as follow:

1. The Caboclo dos Mangueiros magmatic Ni-Cu sulfide deposit is a recent discovery situated in the northwestern edge of the São Francisco craton, a tectonic setting broadly recognized for Ni-Cu-PGE deposits worldwide;
2. The orebody is hosted in a relatively small-sized intrusion consisting an elongated boat-shaped sill WNW-ESE trending, with cross sections a few hundreds of meters depth, ~2 km long and ~500 m wide;
3. The ultramafic intrusion that hosts the Caboclo dos Mangueiros deposit is fractionated from the northern portion, where dunite and wehrlite prevail, to the southern portion where clinopyroxenite is abundant;
4. The major element compositions of the ultramafic rocks are controlled by the ratios of olivine to clinopyroxene, which follows a crystallization sequence consisting of Ol => Ol + Cpx => Cpx;
5. The abundance of ultramafic rocks and the compositional range of cationic Mg# of cumulus clinopyroxene, from 0.78 to 0.94, support a moderate to primitive composition for the parental magma;
6. The crystallization sequence of the intrusion indicates a silica undersaturated composition for the parental magma and the absence of cumulus orthopyroxene suggests that the parental magma remained with this compositional characteristic, with no significant assimilation of siliceous crustal rocks during ascent and emplacement;
7. Primitive mantle-normalized alteration-resistant trace elements profile estimated for the parental magma indicates an enriched composition in LREE, which is reflected on

primitive mantle-normalized alteration-resistant trace element profiles for ultramafic cumulate rocks coupled with significant negative Nb and Ta anomalies;

8. The distribution of primitive mantle-normalized LREE in cumulate ultramafic rocks is partially controlled by the modal proportion of clinopyroxene;
9. The textures and the amounts of sulfide, well above the cotectic proportion, in the Caboclo dos Mangueiros magmatic sulfide Ni-Cu deposit suggest emplacement of sulfide droplets-charged magma through a conduit structure that later solidified as an elongated boat-shaped sill;
10. The contents of sulfides above the cotectic proportion also suggest that large volumes of sulfide droplets have been transported by the magmatic system;
11. The depletion of PGE in the composition of sulfide from a parental magma with moderate to primitive composition is suggestive that has been occurred previous sulfide segregation at depth;
12. Sulfur isotope compositional characteristics of the deposit reflect the mantle source of sulfides with no significant addition of crustal-derived sulfur;
13. Metamorphic assemblages described for country rocks, ultramafic cumulates and rocks from the border zone suggest that the ultramafic intrusion and country rocks were subjected to the same event of tectonism and associated greenschist facies metamorphism. Nevertheless the primary magmatic structure of the intrusion remained preserved;
14. Although similar trace element distribution for rocks from the border zone and ultramafic cumulates suggests that they originated from compositionally similar parental magmas, additional data are required to feature this zone of the intrusion;
15. The positioning of the Caboclo dos Mangueiros deposit in the tectonic evolution of the São Francisco craton is not even constrained because the lack of an absolute age for the ultramafic intrusion; and
16. The abundance of unexplained magnetic anomalies in the regional setting of the Caboclo dos Mangueiros deposit, coupled with the tectonic setting that the deposit is situated indicate a high potential for Ni-Cu-PGE deposits in this region.

Acknowledgements

This study was supported by Universidade de Brasília (UnB), Companhia Baiana de Pesquisa Mineral (CBPM) and Coordenação de Aperfeiçoamento de Pessoal de Nível Superior (CAPES). The authors acknowledge Prof. Dr. Haroldo Sá and Prof. Dr. Johildo Barbosa from the University of Bahia (UFBA) for contacts with CBPM during all phases of this project. The authors also acknowledge fruitful geological discussions with Prof. Haroldo Sá and Prof. Johildo Barbosa. We thank CBPM's Director (Dr. Rafael Avena Neto) for supporting field and laboratory activities, and access to exploration data. We thank the Geochronology and Microprobe Laboratories of the University of Brasília for sulfur isotope and microprobe analyses, respectively. Vitor B. M. Matos holds a scholarship from CAPES and this study is part of his M.Sc dissertation at the Instituto de Geociências (University of Brasília). Cesar F. Ferreira Filho

is a Research Fellow of Conselho Nacional de Desenvolvimento Científico e Tecnológico since 1996, and acknowledges the continuous support through research grants and scholarships for the **"**Metalogenênese de Depósitos Associados ao Magmatismo Máfico-Ultramáfico**"** Research Group.

References

Alkmim, F.F., Brito Neves, B.B., and Castro Alves, J.A., 1993, Arcabouço tectônico do Cráton do São Francisco: uma revisão, in Dominguez, J.M.L., Misi, A., eds., O Cráton do São Francisco, SBG/SGM/CNPq, Salvador, p. 45–62.

Almeida, F.F.M., 1977, O Cráton do São Francisco: Revista Brasileira Geociências, v. 7, n. 4, p. 349–364.

Antonini, P., Comin-Chiaramonti, P., Gomes, C.B., Censi, P., Riffel, B.F., and Yamamoto, E., 2003, The Early Proterozoic carbonatite complex of Angico dos Dias, Bahia State, Brazil: geochemical and Sr-Nd isotopic evidence for an enriched mantle origin: Mineralogical Magazine, v. 67, n. 5, p. 1039–1057.

Barbosa, J.S.F., and Sabaté, P., 2004, Archean and Paleoproterozoic crust of the São Francisco Craton, Bahia, Brazil: geodynamic features: Precambrian Research, v. 133, p. 1–27.

Barbosa, J.S.F., Cruz, S.C.P., and Souza, J.S., 2012, Terrenos Metamórficos do Embasamento, *in:* Barbosa, J.S.F. et al., eds., Geologia da Bahia – Pesquisa e Atualização, Salvador, UFBA-CBPM Publishing, p. 101–202.

Barnes, S.J., 1986, The effect of trapped liquid crystallization on cumulus mineral 59 compositions in layered intrusions: Contributions to Mineralogy and Petrology, v. 93, p. 524–531.

Barnes, S.J., 2007, Cotectic precipitation of olivine and sulfide liquid from komatiite magma and the origin of komatiite-hosted disseminated nickel sulfide mineralization at Mount Keith and Yakabindie, Western Australia: Economic Geology, v. 102, p. 299–304.

Barnes, S.J., Osborne, G.A., Cook, D., Barnes, L., Maier, W.D., and Godel, B., 2011, The Santa Rita Nickel Sulfide Deposit in the Fazenda Mirabela Intrusion, Bahia, Brazil: Geology, Sulfide Geochemistry, and Genesis: Economic Geology, v. 106, p. 1083–1110.

Barnes, S.J., Cruden, A.R., Arndt, N.T., and Saumur, B.M., 2016, The mineral system approach applied to magmatic Ni-Cu-PGE sulphide deposits: Ore Geology Reviews**,** v. 76, p. 296–316.

Barnes, S.-J., and Lightfoot, P.C., 2005, Formation of magmatic nickel sulfide ore deposits and processes affecting their copper and platinum group element contents: Economic Geology 100th Anniversary Volume, p. 179–213.

Begg, G.C., Hronsky, J.A.M., Arndt, N.T., Griffin, W.L., O'Reilly, S.Y., and Hayward, N., 2010, Lithospheric, cratonic and geodynamic setting of Ni–Cu–PGE sulfide deposits: Economic Geology, v. 105, p. 1057–1070.

Beresford, S.W., and Hronsky, J.M.A., 2014, The chonolith Ni–Cu model: expanding the footprint of Ni–Cu deposits [ext. abs.]: International Platinum Symposium, 12th, Yekaterinburg, Russia, 2014, Extended Abstracts, p. 102–103.

Bucher, K., and Grapes, R., 2011, Petrogenesis of Metamorphic Rocks - 8th Edition: Berlin, Springer, 428 p.

Cawthorn, R.G., 1996, Layered intrusions, Amsterdam, Elsevier, 531 p.

Cawthorn, R.G., Barnes, S.J., Ballhaus, C., and Malitch, K.N., 2005, Platinum Group Element, Chromium, and Vanadium Deposits in Mafic and Ultramafic Rocks: Economic Geology 100th Anniversary Volume, p. 215–249.

Dantas, E.L., Neves, B. B., and Fuck, R. A., 2010, Looking for the oldest rocks of South America: Paleoarchean orthogneiss of the Sobradinho Block, northernmost foreland of the São Francisco Craton, Petrolina, Pernambuco, Brazil, *in*: South American Symposium on Isotope Geology, 7, Anais, Brasília, p. 137–140.

Ding, X., Ripley, E.M., and Li, C.S., 2012a, PGE geochemistry of the Eagle Ni–Cu–(PGE) deposit, Upper Michigan: constraints on ore genesis in a dynamic magma conduit: Mineralium Deposita, v. 47, p. 89–104.

Ferreira Filho, C.F., and Araújo, S.M., 2009, Review of Brazilian chromite deposits associated with layered intrusions: geological and petrological constraints for the origin of stratiform chromitites: Applied Earth Sciences (Transactions of the Institution of Mining and Metallurgy), v. 118, p. 86–100.

Ferreira Filho, C.F., Naldrett, A.J. and Gorton, M.P., 1998, REE and pyroxene compositional variation across the Niquelândia layered intrusion, Brazil: petrological and metallogenetic implications: Applied Earth Sciences (Transactions of the Institution of Mining and Metallurgy), v. 107, p. 1–22.

Ferreira Filho, C.F., Cunha, E.M., Lima, A.C., and Cunha, J.C., 2013, Depósito de Níquel-Cobre Sulfetado de Santa Rita, Itagibá, Bahia, Brasil: Salvador, Companhia Baiana de Pesquisa Mineral, 64 p.

Godel, B., Barnes, S.-J., and Maier, W.D., 2011, Parental magma composition inferred from trace element in cumulus and intercumulus silicate minerals: An example from the Lower and Lower Critical zones of the Bushveld Complex, South-Africa: Lithos, v. 125, p. 537–552.

Hart, S.R., and Dunn, T., 1993, Experimental cpx/melt partitioning of 24 trace elements: Contributions to Mineralogy and Petrology, v. 113, p. 1–8.

Hauri, E.H., Wagner, T.P., and Grove, T.L., 1994, Experimental and natural partitioning of Th, U, Pb and other trace elements between garnet, clinopyroxene and basaltic melts: Chemical Geology, v. 117, p. 149–166.

Keays, R.R., and Lightfoot, P.C., 2010, Crustal sulfur is required to form magmatic Ni-Cu sulfide deposits: Evidence from chalcophile element signatures of Siberian and Deccan Trap basalts: Mineralium Deposita, v. 45, p. 241–257.

LASA Engenharia e Prospecção S. A., 2006, Projeto Levantamento Aerogeofísico da área Campo Alegre de Lourdes / Mortugaba: relatório final de aquisição e processamento de dados, Rio de Janeiro, v. 27. Convênio de Cooperação Técnica com a CBPM e CPRM.

Latypov, R.M., Smolkin, V.F., and Alapieti, T.T., 2001, Differentiation trend and parental melt composition of Ni-bearing gabbro-wehrlite Pechenga intrusions, Kola Peninsula: Petrology, v. 9, p. 329–344.

Lazarin, F.A., 2011, Geologia, petrologia e estudos isotópicos dos depósitos de níquel-cobre sulfetados Santa Rita e Peri-Peri, nordeste do Brasil: Unpublished M.Sc. thesis, Brasília, Brazil, University of Brasília, 109 p.

Leite, C.M.M. (Org.), 1997, Campo Alegre de Lourdes, folha SC.23-X-DIV, Peixe, folha SC.23-X-D-I: Estado da Bahia. Brasília, DF: CPRM, Programa Levantamentos Geológicos Básicos do Brasil.

Leite, C.M.M., Santos, R.A., and Conceição, H., 1993, A província toleítica-alcalina de Campo Alegre de Lourdes: geologia e evolução tectônica, *in:* Simpósio Sobre o Cráton São Francisco, 2, Anais, Salvador: SBG, SGM, v. 1, p. 56–59.

Li, C., and Naldrett, A.J., 1999, Geology and petrology of the Voisey's Bay intrusion: Reaction of olivine with sulfide and silicate liquids: Lithos, v. 47, p. 1–31.

Li, C., and Ripley, E.M., 2009, Sulfur contents at sulfide-liquid or anhydrite saturation in silicate melts: Empirical equations and example applications: Economic Geology, v. 104, p. 405–412.

Lima, H.A.F., Ferreira Filho, C.F., Pimentel, M.M., Dantas, E.L., and Araújo, S.M., 2008, Geology, petrology and geochronology of the layered mafic-ultramafic intrusions in the Porto Nacional area, central Brazil: Journal of South American Earth Sciences, v. 26, p. 300–317.

Maier, W., Li, C., and De Waal, S.A., 2001, Why are there no major Ni-Cu sulfide deposits in large layered mafic-ultramafic intrusions?: The Canadian Mineralogist, v. 39, p. 547–556.

Marques, J.C., and Ferreira Filho, C.F., 2003, The Chromite Deposit of the Ipueira-Medrado Sill, São Francisco Craton, Bahia State, Brazil: Economic Geology, v. 98, p. 87–108.

Mota-e-Silva, J., 2014, O depósito sulfetado Ni-Cu-(PGE) de Limoeiro: metalogênese, magmatismo máfico e metamorfismo no leste da Província Borborema: Unpublished PhD thesis, Brasília, Brazil, University of Brasília, 304 p.

Mota-e-Silva, J., Ferreira Filho, C.F., Della Giustina, M.E.S., 2013, The Limoeiro Deposit: Ni-Cu-PGE Sulfide mineralization hosted within an ultramafic tubular magma conduit in the Borborema Province, Northeastern Brazil: Economic Geology, v. 108, n. 7, p. 1753–1771.

Naldrett, A.J., 1992, A model for the Ni-Cu-PGE ores of the Noril'sk region and its application to other areas of flood basalts: Economic Geology, v. 87, p. 1945−1962.

Naldrett, A.J., 1999b, World-class Ni-Cu-PGE deposits: key factors in their genesis: Mineralium Deposita, v. 34, p. 227–240.

Naldrett, A.J., 2004, Magmatic sulfide deposits – geology, geochemistry and exploration: Berlin, Springer, 724 p.

Passchier, C.W., Myers, J.S., and Kroner, A., 1990, Field geology of high-grade gneiss terrains: Berlin, Springer, 150 p.

Peucat, J.J., Barbosa, J.S.F., Pinho, I.C.A., Paquette, J.L., Martin, H., Fanning, C.M., Leal, A.B.M., and Cruz, S., 2011, Geochronology of granulites from the south Itabuna-Salvador-Curaçá Block, São Francisco Craton (Brazil): Nd isotopes and U/Pb zircon ages: Journal of South American Earth Sciences, v. 31, p. 397–413.

Plá Cid, J., 1994, Granitogênese Alcalina de Campo Alegre de Lourdes (Norte da Bahia): petrografia, mineraloquímicagia e geoquímica: Unpublished M.Sc. thesis, Salvador, Brazil, Federal University of Bahia, 232 p.

Ripley, E.M., and Li, C., 2003, Sulfur isotope exchange and metal enrichment in the formation of magmatic Cu-Ni-(PGE) deposits: Economic Geology, v. 98, p. 635–641.

Ripley, E.M., and Li, C., 2013, Sulfide saturation in mafic magmas: is external sulfur required for magmatic Ni–Cu–(PGE) ore genesis?: Economic Geology, v. 108, p. 45–58.

Rosa, W.D., 2014, Complexos acamadados Serra do Onça e Serra do Puma: geologia e petrologia de duas intrusões máfico-ultramáficas com sequência de cristalização distinta na província arqueana de Carajás, Brasil: Unpublished M.Sc. thesis, Brasília, Brazil, University of Brasília, 87 p.

Sampaio, D.R., Lima, R.F.F.F., and Moreira, J.F.C., 1986, Os depósitos de ferro, titânio e vanádio de Campo Alegre de Lourdes, Bahia, *in*: Schobbenhaus, C.; and Coelho, C.E.S. (Coords.), Principais Depósitos Minerais do Brasil, Brasília, DNPM-CVRD, v. II, p. 481–491.

Seat, Z., Beresford, S.W., Grguric, B.A., Waugh, R.S., Hronsky, J.M.A., Gee, M.A.M., Groves, D.I., and Mathison, C.I., 2007, Architecture and emplacement of the Nebo-Babel gabbronorite-hosted magmatic Ni-Cu-PGE sulphide deposit, West Musgrave, Western Australia: Mineralium Deposita, v. 42, p. 551–581.

Seat, Z., Beresford, S.W., Grguric, B.A., Gee, M.A.M., and Grassineau, N.V., 2009, Reevaluation of the role of external sulfur addition in the genesis of Ni-Cu-PGE deposits: Evidence from the Nebo-Babel Ni-Cu-PGE deposit, West Musgrave, Western Australia: Economic Geology, v. 104, p. 521–538.

Silva, A.B., Liberal, G.S., Issa Filho, A., Rodrigues, C.S., and Riffel B.F., 1987, Depósito de fosfato em carbonatito pré-cambriano, Angico dos Dias-Ba: Soc. Bras. Geol., Núcleo da Bahia, Salvador, 15 p.

Silva, A.B., Liberal, G.S., Grossi Sad, J.H., Issa Filho, A., Rodrigues, C.S., and Riffel, B.F., 1988, Geologia e petrologia do Complexo Angico dos Dias (Bahia, Brasil), uma associação metacarbonatítica pré-cambriana: Geochimica Brasiliensis, v.2, n. 1, p. 81–108.

Silva, A.B., Liberal, G.S., Riffel, B.F., and Issa Filho, A., 1997, Depósito de fosfato de Angico dos Dias, Campo Alegre de Lourdes, Bahia, *in*: Schobbenhaus, C., and Coelho, C.E.S. (Coords.), Principais Depósitos Minerais do Brasil, Brasília, DNPM-CPRM, v. IV-C, p. 123–130.

Song, X-Y., Zhou, M-F., Cao, Z-M., Sun, M., and Wang, Y-L., 2003, The Ni-Cu-(PGE) magmatic sulfide deposits in the Yangliuping area within the Permian Emeishan large igneous province, SW China: Mineralium Deposita, v. 38, p. 831–843.

Song, X-Y., Danyushevsky, L.V., Keays, R.R., Chen, L-M., Wang, Y-S., Tian, Y-L., and Xiao. J-F., 2012, Structural, lithological, and geochemical constraints on the dynamic magma plumbing system of the Jinchuan Ni-Cu sulfide deposit, NW China: Mineralium Deposita, v. 47, p. 277–297.

Sun, S.S., McDonough, W.F., 1989, Chemical and isotopic systematics of oceanic basalts: implications for mantle composition and processes, in Saunders, A.D., Norry, M.J. (eds), Magmatism in the Ocean Basins, Geological Society Special Publication, v. 42, p. 313–345.

Teixeira, A.S., Ferreira Filho, C.F., Della Giustina, M.E.S., Araujo, S.M., and Silva, H.H.A.B., 2015, Geology, petrology and geochronology of the Lago Grande layered complex: Evidence for a PGE-mineralized magmatic suite in the Carajas Mineral Province, Brazil: Journal of South American Earth Sciences, v. 64, p. 116–138.

Uhlein, A., Caxito, F.A., Sanglard, J.C.D., Uhlein, G.J., and Suckau, G.L., 2011, Estratigrafia e tectônica das faixas neoproterozoicas da porção norte do Cráton do São Francisco: Geonomos, v. 19, n. 2, p. 8–31.

Vasconcelos, A.M., Kosin, M., Souza, J.D., Valente, C.R., Neves, J.P., Heineck, C.A.,Lacerda Filho, J.V., Teixeira, L.R., Borges, V.P., Bento, R.V., Guimarães, J.T., Neves, J.P., Oliveira, I.W.B., Gomes, I.P., Malouf, R.F., Carvalho, L.M. de, and Abreu Filho, W., 2004, Folha SC.23 - Rio São Francisco, *in*: Schobbenhaus, C., Gonçalves, J.H., Santos, J.O.S., Abram, M.B., Leão Neto, R., Matos, G.M.M., Vidotti, R.M., Ramos, M.A.B., and Jesus, J.D.A. (eds.), Carta Geológica do Brasil ao Milionésimo, Sistema de Informações Geográficas. Programa Geologia do Brasil, CPRM, Brasília. CD-ROM.

Whitney, D.L., and Evans, B.W., 2010, Abbreviations for names of rock-forming minerals: American Mineralogist, v. 95, p. 185–187.

Xue, S., Qin, K., Li, C., Tang, D., Mao, Y., Qi, L., and Ripley, E.M., 2016, Geochronological, petrological, and geochemical constraints on Ni-Cu sulfide mineralization in the Poyi ultramafic-troctolitic intrusion in the northeast rim of the Tarim craton, western China: Economic Geology, v. 111, p. 1465–1484.

APPENDIXES

1. Clinopyroxene compositions;
2. Amphibole compositions; and
3. Sulfide compositions.

Appendix 1: Clinopyroxene compositions.

Sample		BM-016	BM-016	BM-016	BM-016	BM-042	BM-042	BM-042	BM-042	BM-042	BM-013	BM-013	BM-013	BM-013	BM-013	BM-013
Drill Hole		FD-9	FD-9	FD-9	FD-9	FD-5	FD-5	FD-5	FD-5	FD-5	FD-9	FD-9	FD-9	FD-9	FD-9	FD-9
Rock Code		Cpxt	Cpxt	Cpxt	Cpxt	Cpxt	Cpxt	Cpxt	Cpxt	Cpxt	Cpxt	Cpxt	Cpxt	Cpxt	Cpxt	Cpxt
SiO2	wt.%	53.24	53.63	52.16	52.18	51.07	51.58	50.20	54.17	51.35	51.42	51.99	51.61	51.60	53.02	53.20
TiO2	wt.%	0.54	0.58	1.05	0.83	0.92	1.16	0.79	0.40	1.08	1.25	0.97	1.05	0.99	0.60	0.51
Al2O3	wt.%	1.40	1.87	2.25	2.18	2.75	2.15	3.06	0.42	2.26	2.77	2.52	2.60	2.69	1.79	1.29
FeO	wt.%	5.77	7.14	6.13	6.45	5.76	6.12	6.85	4.49	8.24	6.68	6.65	6.21	7.26	7.03	6.73
MnO	wt.%	0.09	0.23	0.15	0.23	0.21	0.26	0.18	0.16	0.25	0.11	0.08	0.13	0.08	0.15	0.10
MgO	wt.%	15.55	16.21	14.68	14.46	15.39	15.02	15.97	16.15	15.53	15.15	14.90	14.66	14.45	14.90	14.92
CaO	wt.%	22.52	18.85	21.50	22.02	21.95	22.23	19.96	23.66	19.89	21.37	22.14	21.69	21.11	21.63	22.13
Na2O	wt.%	0.29	0.40	0.46	0.37	0.36	0.34	0.33	0.04	0.28	0.38	0.38	0.45	0.41	0.46	0.27
Cr2O3	wt.%	0.34	0.42	0.43	0.31	0.44	0.38	0.55	0.22	0.47	0.62	0.44	0.60	0.25	0.32	0.31
V2O3	wt.%	0.05	0.03	0.09	0.06	0.08	0.12	0.06	0.03	0.06	0.06	0.02	0.13	<0.01	<0.01	0.02
NiO	wt.%	0.07	0.03	<0.01	0.13	0.04	0.05	0.14	<0.01	0.01	<0.01	0.03	<0.01	<0.01	<0.01	<0.01
Total	wt.%	99.87	99.38	98.90	99.21	98.95	99.41	98.10	99.74	99.42	99.80	100.11	99.14	98.84	99.90	99.49
Na	ppm	0.02	0.03	0.03	0.03	0.03	0.02	0.02	<0.01	0.02	0.03	0.03	0.03	0.03	0.03	0.02
Al	ppm	0.06	0.08	0.10	0.10	0.12	0.09	0.14	0.02	0.10	0.12	0.11	0.11	0.12	0.08	0.06
Mg	ppm	0.86	0.90	0.82	0.80	0.85	0.83	0.89	0.89	0.86	0.84	0.82	0.81	0.81	0.82	0.83
Si	ppm	1.96	1.99	1.95	1.95	1.90	1.92	1.88	2.00	1.91	1.90	1.92	1.92	1.93	1.96	1.98
Ca	ppm	0.89	0.75	0.86	0.88	0.87	0.89	0.80	0.93	0.79	0.85	0.88	0.87	0.85	0.86	0.88
Mn	ppm	<0.01	0.01	<0.01	0.01	0.01	0.01	0.01	<0.01	0.01	<0.01	<0.01	<0.01	<0.01	<0.01	<0.01
Ti	ppm	0.01	0.02	0.03	0.02	0.03	0.03	0.02	0.01	0.03	0.03	0.03	0.03	0.03	0.02	0.01
Fe2+	ppm	0.18	0.22	0.19	0.20	0.14	0.17	0.15	0.14	0.24	0.20	0.19	0.19	0.23	0.22	0.21
Fe3+	ppm	<0.01	<0.01	<0.01	<0.01	0.04	0.02	0.06	<0.01	0.02	0.01	0.01	<0.01	<0.01	<0.01	<0.01
Ni	ppm	<0.01	<0.01	<0.01	<0.01	<0.01	<0.01	<0.01	<0.01	<0.01	<0.01	<0.01	<0.01	<0.01	<0.01	<0.01
Cr	ppm	0.01	0.01	0.01	0.01	0.01	0.01	0.02	0.01	0.01	0.02	0.01	0.02	0.01	0.01	0.01
Li	ppm	<0.01	<0.01	<0.01	<0.01	<0.01	<0.01	<0.01	<0.01	<0.01	<0.01	<0.01	<0.01	<0.01	<0.01	<0.01
Sc	ppm	<0.01	<0.01	<0.01	<0.01	<0.01	<0.01	<0.01	<0.01	<0.01	<0.01	<0.01	<0.01	<0.01	<0.01	<0.01
V	ppm	<0.01	<0.01	<0.01	<0.01	<0.01	<0.01	<0.01	<0.01	<0.01	<0.01	<0.01	<0.01	<0.01	<0.01	<0.01
Zn	ppm	<0.01	<0.01	<0.01	<0.01	<0.01	<0.01	<0.01	<0.01	<0.01	<0.01	<0.01	<0.01	<0.01	<0.01	<0.01
Zr	ppm	<0.01	<0.01	<0.01	<0.01	<0.01	<0.01	<0.01	<0.01	<0.01	<0.01	<0.01	<0.01	<0.01	<0.01	<0.01
Mg#		0.83	0.80	0.81	0.80	0.86	0.83	0.85	0.87	0.78	0.81	0.81	0.81	0.78	0.79	0.80

Sample		BM-027	BM-027	BM-027	BM-027	BM-011	BM-011	BM-011	BM-011	BM-011	BM-011	BM-011	BM-011	BM-011	BM-011	BM-011
Drill Hole		FD-6	FD-6	FD-6	FD-6	FD-3	FD-3	FD-3	FD-3	FD-3	FD-3	FD-3	FD-3	FD-3	FD-3	FD-3
Rock Code		Cpxt	Cpxt	Cpxt	Cpxt	Cpxt	Cpxt	Cpxt	Cpxt	Cpxt	Cpxt	Cpxt	Cpxt	Cpxt	Cpxt	Cpxt
SiO2	wt.%	52.48	52.89	52.06	51.87	52.03	52.34	52.24	49.50	52.32	52.40	51.70	52.71	51.85	51.61	52.09
TiO2	wt.%	0.87	1.12	1.21	0.99	1.03	0.97	0.80	1.05	0.84	0.96	0.96	0.95	0.59	0.78	0.84
Al2O3	wt.%	2.20	2.35	2.27	2.32	2.56	2.90	2.32	6.37	2.15	2.70	2.93	2.67	2.17	2.64	1.91
FeO	wt.%	5.70	5.81	6.13	6.09	6.31	6.30	6.08	6.22	5.92	5.79	5.89	5.56	6.32	6.23	6.12
MnO	wt.%	0.21	0.13	0.19	0.04	0.16	0.17	0.14	0.24	0.10	0.19	0.17	0.20	0.20	0.24	0.22
MgO	wt.%	15.64	15.56	15.23	16.85	15.84	15.81	16.74	15.42	16.00	15.77	16.15	15.46	16.61	16.47	15.35
CaO	wt.%	22.11	22.27	22.67	20.90	21.89	21.99	20.95	20.13	22.26	21.71	21.81	22.21	20.90	21.42	21.96
Na2O	wt.%	0.28	0.29	0.35	0.27	0.34	0.30	0.32	0.33	0.36	0.39	0.36	0.44	0.36	0.37	0.38
Cr2O3	wt.%	0.38	0.33	0.22	0.31	N.A.	N.A.	N.A.	N.A.	N.A.	N.A.	N.A.	N.A.	N.A.	N.A.	N.A.
V2O3	wt.%	0.08	0.05	0.05	0.01	0.09	0.07	0.04	0.13	0.05	<0.01	0.09	0.05	0.07	0.06	0.07
NiO	wt.%	<0.01	<0.01	0.10	0.10	<0.01	<0.01	<0.01	0.04	0.06	<0.01	0.05	<0.01	0.05	<0.01	0.04
Total	wt.%	99.93	100.80	100.47	99.75	100.25	100.86	99.63	99.43	100.05	99.91	100.11	100.25	99.12	99.83	98.96
Na	ppm	0.02	0.02	0.03	0.02	0.02	0.02	0.02	0.02	0.03	0.03	0.03	0.03	0.03	0.03	0.03
Al	ppm	0.10	0.10	0.10	0.10	0.11	0.12	0.10	0.28	0.09	0.12	0.13	0.12	0.09	0.11	0.08
Mg	ppm	0.86	0.85	0.83	0.92	0.87	0.86	0.92	0.85	0.88	0.86	0.88	0.84	0.91	0.90	0.85
Si	ppm	1.93	1.93	1.91	1.91	1.91	1.91	1.92	1.82	1.92	1.93	1.89	1.93	1.92	1.89	1.94
Ca	ppm	0.87	0.87	0.89	0.82	0.86	0.86	0.83	0.79	0.88	0.85	0.86	0.87	0.83	0.84	0.88
Mn	ppm	0.01	<0.01	0.01	<0.01	<0.01	0.01	<0.01	0.01	<0.01	0.01	0.01	0.01	0.01	0.01	0.01
Ti	ppm	0.02	0.03	0.03	0.03	0.03	0.03	0.02	0.03	0.02	0.03	0.03	0.03	0.02	0.02	0.02
Fe2+	ppm	0.18	0.18	0.16	0.14	0.16	0.17	0.15	0.16	0.14	0.17	0.12	0.17	0.13	0.11	0.17
Fe3+	ppm	<0.01	<0.01	0.03	0.04	0.04	0.02	0.04	0.04	0.05	0.01	0.06	<0.01	0.06	0.08	0.02
Ni	ppm	<0.01	<0.01	<0.01	<0.01	<0.01	<0.01	<0.01	<0.01	<0.01	<0.01	<0.01	<0.01	<0.01	<0.01	<0.01
Cr	ppm	0.01	0.01	0.01	0.01	N.A.	N.A.	N.A.	N.A.	N.A.	N.A.	N.A.	N.A.	N.A.	N.A.	N.A.
Li	ppm	<0.01	<0.01	<0.01	<0.01	<0.01	<0.01	<0.01	<0.01	<0.01	<0.01	<0.01	<0.01	<0.01	<0.01	<0.01
Sc	ppm	<0.01	<0.01	<0.01	<0.01	<0.01	<0.01	<0.01	<0.01	<0.01	<0.01	<0.01	<0.01	<0.01	<0.01	<0.01
V	ppm	<0.01	<0.01	<0.01	<0.01	<0.01	<0.01	<0.01	<0.01	<0.01	<0.01	<0.01	<0.01	<0.01	<0.01	<0.01
Zn	ppm	<0.01	<0.01	<0.01	<0.01	<0.01	<0.01	<0.01	<0.01	<0.01	<0.01	<0.01	<0.01	<0.01	<0.01	<0.01
Zr	ppm	<0.01	<0.01	<0.01	<0.01	<0.01	<0.01	<0.01	<0.01	<0.01	<0.01	<0.01	<0.01	<0.01	<0.01	<0.01
Mg#		0.83	0.83	0.84	0.86	0.85	0.84	0.86	0.84	0.87	0.83	0.88	0.83	0.88	0.89	0.83

Sample		BM-011	BM-011	BM-013	BM-013	BM-013	BM-013	BM-013	BM-013	BM-013	BM-013	BM-013	BM-013	BM-013	BM-013	BM-013
Drill Hole		FD-3	FD-3	FD-9	FD-9	FD-9	FD-9	FD-9	FD-9	FD-9	FD-9	FD-9	FD-9	FD-9	FD-9	FD-9
Rock Code		Cpxt	Cpxt	Cpxt	Cpxt	Cpxt	Cpxt	Cpxt	Cpxt	Cpxt	Cpxt	Cpxt	Cpxt	Cpxt	Cpxt	Cpxt
SiO2	wt.%	52.34	51.23	52.93	52.74	52.20	52.27	52.18	51.83	51.83	51.59	51.32	51.38	50.56	52.37	51.89
TiO2	wt.%	0.62	0.97	1.05	0.84	0.92	0.34	0.94	1.05	1.43	0.99	1.16	0.84	0.70	0.97	1.20
Al2O3	wt.%	1.85	2.35	2.52	2.17	2.39	1.95	2.30	2.71	2.52	2.68	2.87	2.46	1.59	2.05	2.56
FeO	wt.%	5.90	6.09	6.27	6.26	6.70	7.07	6.60	7.15	6.89	7.13	7.38	6.48	9.30	6.16	6.91
MnO	wt.%	0.25	0.24	0.13	0.15	0.09	0.16	0.17	0.14	0.20	0.15	0.18	0.15	0.17	0.25	0.17
MgO	wt.%	16.53	16.22	14.93	15.32	14.76	15.03	14.80	15.37	15.11	15.55	15.78	15.36	14.80	15.48	15.02
CaO	wt.%	21.91	21.46	22.58	22.35	22.25	22.23	22.50	20.96	21.25	20.98	20.60	21.83	21.82	21.26	21.05
Na2O	wt.%	0.31	0.41	0.34	0.38	0.37	0.19	0.29	0.46	0.36	0.39	0.31	0.32	0.43	0.40	0.33
Cr2O3	wt.%	N.A.	N.A.	N.A.	N.A.	N.A.	N.A.	N.A.	N.A.	N.A.	N.A.	N.A.	N.A.	N.A.	N.A.	N.A.
V2O3	wt.%	0.10	0.02	0.03	0.01	0.06	0.05	<0.01	0.04	0.11	0.03	0.05	0.08	0.07	0.01	0.05
NiO	wt.%	0.04	0.06	<0.01	0.14	0.01	<0.01	0.09	0.01	0.11	0.12	<0.01	<0.01	<0.01	<0.01	<0.01
Total	wt.%	99.85	99.04	100.78	100.35	99.75	99.30	99.85	99.72	99.80	99.59	99.64	98.91	99.44	98.93	99.19
Na	ppm	0.02	0.03	0.02	0.03	0.03	0.01	0.02	0.03	0.03	0.03	0.02	0.02	0.03	0.03	0.02
Al	ppm	0.08	0.10	0.11	0.09	0.10	0.09	0.10	0.12	0.11	0.12	0.13	0.11	0.07	0.09	0.11
Mg	ppm	0.90	0.90	0.82	0.84	0.82	0.83	0.82	0.85	0.83	0.86	0.87	0.85	0.82	0.86	0.83
Si	ppm	1.92	1.90	1.94	1.94	1.93	1.94	1.93	1.92	1.92	1.91	1.90	1.91	1.89	1.95	1.93
Ca	ppm	0.86	0.85	0.89	0.88	0.88	0.89	0.89	0.83	0.84	0.83	0.82	0.87	0.87	0.85	0.84
Mn	ppm	0.01	0.01	<0.01	<0.01	<0.01	0.01	0.01	<0.01	0.01	<0.01	0.01	<0.01	0.01	0.01	0.01
Ti	ppm	0.02	0.03	0.03	0.02	0.03	0.01	0.03	0.03	0.04	0.03	0.03	0.02	0.02	0.03	0.03
Fe2+	ppm	0.12	0.11	0.19	0.18	0.21	0.20	0.20	0.20	0.21	0.18	0.19	0.16	0.14	0.19	0.22
Fe3+	ppm	0.06	0.08	<0.01	0.01	<0.01	0.02	<0.01	0.02	<0.01	0.04	0.03	0.04	0.15	<0.01	<0.01
Ni	ppm	<0.01	<0.01	<0.01	<0.01	<0.01	<0.01	<0.01	<0.01	<0.01	<0.01	<0.01	<0.01	<0.01	<0.01	<0.01
Cr	ppm	N.A.	N.A.	N.A.	N.A.	N.A.	N.A.	N.A.	N.A.	N.A.	N.A.	N.A.	N.A.	N.A.	N.A.	N.A.
Li	ppm	<0.01	<0.01	<0.01	<0.01	<0.01	<0.01	<0.01	<0.01	<0.01	<0.01	<0.01	<0.01	<0.01	<0.01	<0.01
Sc	ppm	<0.01	<0.01	<0.01	<0.01	<0.01	<0.01	<0.01	<0.01	<0.01	<0.01	<0.01	<0.01	<0.01	<0.01	<0.01
V	ppm	<0.01	<0.01	<0.01	<0.01	<0.01	<0.01	<0.01	<0.01	<0.01	<0.01	<0.01	<0.01	<0.01	<0.01	<0.01
Zn	ppm	<0.01	<0.01	<0.01	<0.01	<0.01	<0.01	<0.01	<0.01	<0.01	<0.01	<0.01	<0.01	<0.01	<0.01	<0.01
Zr	ppm	<0.01	<0.01	<0.01	<0.01	<0.01	<0.01	<0.01	<0.01	<0.01	<0.01	<0.01	<0.01	<0.01	<0.01	<0.01
Mg#		0.88	0.89	0.81	0.82	0.80	0.80	0.80	0.81	0.80	0.82	0.82	0.84	0.85	0.82	0.79

Sample		BM-013	BM-013	BM-013	BM-013	BM-016	BM-016	BM-016	BM-016	BM-016	BM-016	BM-016	BM-016	BM-016	BM-016	BM-016
Drill Hole		FD-9	FD-9	FD-9	FD-9	FD-9	FD-9	FD-9	FD-9	FD-9	FD-9	FD-9	FD-9	FD-9	FD-9	FD-9
Rock Code		Cpxt	Cpxt	Cpxt	Cpxt	Cpxt	Cpxt	Cpxt	Cpxt	Cpxt	Cpxt	Cpxt	Cpxt	Cpxt	Cpxt	Cpxt
SiO2	wt.%	51.69	52.75	51.93	51.89	52.69	52.74	53.12	53.56	52.65	52.10	51.85	52.49	52.16	51.55	51.60
TiO2	wt.%	1.00	0.70	0.87	1.13	1.04	1.07	0.92	0.84	1.09	1.10	1.13	0.90	0.80	0.94	0.91
Al2O3	wt.%	2.60	2.00	2.14	2.53	2.45	2.11	2.06	2.20	2.28	2.49	2.44	2.59	2.53	3.00	2.54
FeO	wt.%	6.07	6.01	6.93	6.45	6.98	5.95	6.50	5.92	5.92	6.18	6.93	6.79	6.95	7.02	7.33
MnO	wt.%	0.25	0.11	0.15	0.20	0.15	0.27	0.08	0.13	0.09	0.14	0.17	0.21	0.18	0.15	0.19
MgO	wt.%	15.39	15.38	15.17	15.59	16.24	14.51	15.20	15.20	15.37	16.02	15.79	15.52	16.36	14.89	15.31
CaO	wt.%	21.63	22.10	21.95	20.92	19.52	22.76	22.65	21.94	21.62	20.52	20.59	21.98	20.10	21.59	21.52
Na2O	wt.%	0.33	0.34	0.32	0.45	0.32	0.50	0.50	0.40	0.66	0.51	0.64	0.36	0.32	0.46	0.33
Cr2O3	wt.%	N.A.	N.A.	N.A.	N.A.	N.A.	N.A.	N.A.	N.A.	N.A.	N.A.	N.A.	N.A.	N.A.	N.A.	N.A.
V2O3	wt.%	0.10	0.04	0.05	0.03	<0.01	0.03	<0.01	0.08	0.06	0.01	0.04	0.07	0.05	0.04	0.10
NiO	wt.%	<0.01	<0.01	0.04	<0.01	<0.01	0.03	<0.01	<0.01	0.02	<0.01	0.01	0.02	0.02	<0.01	0.02
Total	wt.%	99.06	99.44	99.53	99.18	99.39	99.97	101.03	100.28	99.75	99.06	99.56	100.92	99.46	99.63	99.85
Na	ppm	0.02	0.02	0.02	0.03	0.02	0.04	0.04	0.03	0.05	0.04	0.05	0.03	0.02	0.03	0.02
Al	ppm	0.11	0.09	0.09	0.11	0.11	0.09	0.09	0.10	0.10	0.11	0.11	0.11	0.11	0.13	0.11
Mg	ppm	0.85	0.85	0.84	0.86	0.90	0.80	0.83	0.83	0.84	0.88	0.87	0.84	0.90	0.82	0.84
Si	ppm	1.92	1.95	1.93	1.92	1.95	1.95	1.94	1.97	1.94	1.93	1.91	1.92	1.93	1.91	1.91
Ca	ppm	0.86	0.88	0.87	0.83	0.77	0.90	0.89	0.86	0.85	0.81	0.81	0.86	0.80	0.86	0.85
Mn	ppm	0.01	<0.01	<0.01	0.01	<0.01	0.01	<0.01	<0.01	<0.01	<0.01	0.01	0.01	0.01	<0.01	0.01
Ti	ppm	0.03	0.02	0.02	0.03	0.03	0.03	0.03	0.02	0.03	0.03	0.03	0.02	0.02	0.03	0.03
Fe2+	ppm	0.18	0.19	0.19	0.19	0.22	0.18	0.18	0.18	0.17	0.18	0.17	0.18	0.20	0.19	0.18
Fe3+	ppm	0.01	<0.01	0.03	0.01	<0.01	<0.01	0.02	<0.01	0.01	0.01	0.05	0.03	0.01	0.03	0.04
Ni	ppm	<0.01	<0.01	<0.01	<0.01	<0.01	<0.01	<0.01	<0.01	<0.01	<0.01	<0.01	<0.01	<0.01	<0.01	<0.01
Cr	ppm	N.A.	N.A.	N.A.	N.A.	N.A.	N.A.	N.A.	N.A.	N.A.	N.A.	N.A.	N.A.	N.A.	N.A.	N.A.
Li	ppm	<0.01	<0.01	<0.01	<0.01	<0.01	<0.01	<0.01	<0.01	<0.01	<0.01	<0.01	<0.01	<0.01	<0.01	<0.01
Sc	ppm	<0.01	<0.01	<0.01	<0.01	<0.01	<0.01	<0.01	<0.01	<0.01	<0.01	<0.01	<0.01	<0.01	<0.01	<0.01
V	ppm	<0.01	<0.01	<0.01	<0.01	<0.01	<0.01	<0.01	<0.01	<0.01	<0.01	<0.01	<0.01	<0.01	<0.01	<0.01
Zn	ppm	<0.01	<0.01	<0.01	<0.01	<0.01	<0.01	<0.01	<0.01	<0.01	<0.01	<0.01	<0.01	<0.01	<0.01	<0.01
Zr	ppm	<0.01	<0.01	<0.01	<0.01	<0.01	<0.01	<0.01	<0.01	<0.01	<0.01	<0.01	<0.01	<0.01	<0.01	<0.01
Mg#		0.83	0.82	0.82	0.82	0.81	0.81	0.82	0.82	0.83	0.83	0.84	0.83	0.82	0.82	0.82

Sample		BM-016	BM-016	BM-016	BM-016	BM-027	BM-027	BM-027	BM-027	BM-027	BM-027	BM-027	BM-027	BM-027	BM-027	BM-027
Drill Hole		FD-9	FD-9	FD-9	FD-9	FD-6	FD-6	FD-6	FD-6	FD-6	FD-6	FD-6	FD-6	FD-6	FD-6	FD-6
Rock Code		Cpxt	Cpxt	Cpxt	Cpxt	Cpxt	Cpxt	Cpxt	Cpxt	Cpxt	Cpxt	Cpxt	Cpxt	Cpxt	Cpxt	Cpxt
SiO2	wt.%	52.70	52.76	52.58	52.50	52.55	51.06	51.94	52.33	51.46	51.81	52.25	52.46	51.07	53.17	53.88
TiO2	wt.%	0.87	1.00	1.00	0.82	0.80	0.87	1.08	0.75	1.05	1.26	0.79	0.84	0.70	0.82	0.81
Al2O3	wt.%	2.36	2.37	2.67	2.54	2.00	2.91	2.34	2.21	2.45	2.22	1.65	1.91	2.59	1.71	1.77
FeO	wt.%	6.95	6.68	6.81	6.37	5.02	5.63	5.52	5.92	7.89	6.68	6.30	5.40	5.62	5.53	5.70
MnO	wt.%	0.29	0.18	0.19	0.24	0.14	0.15	0.08	0.28	0.20	0.20	0.20	0.20	0.16	0.17	0.15
MgO	wt.%	15.51	15.16	15.30	15.55	16.00	16.14	15.28	14.35	15.51	15.53	15.62	15.20	15.32	15.44	15.86
CaO	wt.%	21.57	21.40	21.43	21.95	22.87	21.49	22.71	22.99	19.78	21.19	21.60	23.17	21.25	22.86	21.78
Na2O	wt.%	0.50	0.43	0.41	0.38	0.30	0.38	0.29	0.33	0.27	0.27	0.31	0.30	0.32	0.25	0.34
Cr2O3	wt.%	N.A.	N.A.	N.A.	N.A.	N.A.	N.A.	N.A.	N.A.	N.A.	N.A.	N.A.	N.A.	N.A.	N.A.	N.A.
V2O3	wt.%	0.04	0.10	0.07	0.12	<0.01	0.05	0.01	0.06	0.08	0.05	0.07	0.10	0.03	0.08	0.01
NiO	wt.%	0.00	0.03	0.03	<0.01	0.01	0.06	0.05	<0.01	<0.01	<0.01	0.10	0.04	0.08	<0.01	0.09
Total	wt.%	100.78	100.10	100.47	100.46	99.68	98.75	99.28	99.22	98.70	99.20	98.88	99.61	97.12	100.02	100.39
Na	ppm	0.04	0.03	0.03	0.03	0.02	0.03	0.02	0.02	0.02	0.02	0.02	0.02	0.02	0.02	0.02
Al	ppm	0.10	0.10	0.12	0.11	0.09	0.13	0.10	0.10	0.11	0.10	0.07	0.08	0.12	0.07	0.08
Mg	ppm	0.85	0.83	0.84	0.85	0.88	0.89	0.84	0.80	0.87	0.86	0.87	0.84	0.86	0.85	0.87
Si	ppm	1.93	1.95	1.93	1.92	1.93	1.89	1.93	1.95	1.93	1.93	1.95	1.94	1.93	1.96	1.97
Ca	ppm	0.85	0.85	0.84	0.86	0.90	0.85	0.90	0.92	0.79	0.84	0.86	0.92	0.86	0.90	0.85
Mn	ppm	0.01	0.01	0.01	0.01	<0.01	<0.01	<0.01	0.01	0.01	0.01	0.01	0.01	0.01	0.01	<0.01
Ti	ppm	0.02	0.03	0.03	0.02	0.02	0.02	0.03	0.02	0.03	0.04	0.02	0.02	0.02	0.02	0.02
Fe2+	ppm	0.18	0.21	0.21	0.17	0.13	0.11	0.16	0.18	0.25	0.21	0.19	0.16	0.17	0.17	0.17
Fe3+	ppm	0.03	<0.01	<0.01	0.02	0.02	0.06	0.01	<0.01	<0.01	<0.01	0.01	0.01	0.01	<0.01	<0.01
Ni	ppm	<0.01	<0.01	<0.01	<0.01	<0.01	<0.01	<0.01	<0.01	<0.01	<0.01	<0.01	<0.01	<0.01	<0.01	<0.01
Cr	ppm	N.A.	N.A.	N.A.	N.A.	N.A.	N.A.	N.A.	N.A.	N.A.	N.A.	N.A.	N.A.	N.A.	N.A.	N.A.
Li	ppm	<0.01	<0.01	<0.01	<0.01	<0.01	<0.01	<0.01	<0.01	<0.01	<0.01	<0.01	<0.01	<0.01	<0.01	<0.01
Sc	ppm	<0.01	<0.01	<0.01	<0.01	<0.01	<0.01	<0.01	<0.01	<0.01	<0.01	<0.01	<0.01	<0.01	<0.01	<0.01
V	ppm	<0.01	<0.01	<0.01	<0.01	<0.01	<0.01	<0.01	<0.01	<0.01	<0.01	<0.01	<0.01	<0.01	<0.01	<0.01
Zn	ppm	<0.01	<0.01	<0.01	<0.01	<0.01	<0.01	<0.01	<0.01	<0.01	<0.01	<0.01	<0.01	<0.01	<0.01	<0.01
Zr	ppm	<0.01	<0.01	<0.01	<0.01	<0.01	<0.01	<0.01	<0.01	<0.01	<0.01	<0.01	<0.01	<0.01	<0.01	<0.01
Mg#		0.82	0.80	0.80	0.83	0.87	0.89	0.84	0.81	0.78	0.81	0.82	0.84	0.83	0.83	0.83

Sample		BM-027	BM-029	BM-029	BM-029	BM-029	BM-029	BM-029	BM-029	BM-029	BM-029	BM-029	BM-029	BM-034	BM-034	BM-042
Drill Hole		FD-6	FD-6	FD-6	FD-6	FD-6	FD-6	FD-6	FD-6	FD-6	FD-6	FD-6	FD-6	FD-12	FD-12	FD-5
Rock Code		Cpxt	Cpxt	Cpxt	Cpxt	Cpxt	Cpxt	Cpxt	Cpxt	Cpxt	Cpxt	Cpxt	Cpxt	Cpxt	Cpxt	Cpxt
SiO2	wt.%	53.47	52.48	51.69	51.03	51.37	51.64	52.16	52.38	53.79	50.56	52.49	51.51	53.31	51.94	50.32
TiO2	wt.%	0.96	0.88	0.80	0.71	0.84	0.80	0.80	0.79	0.82	0.70	0.78	0.79	0.79	0.52	0.66
Al2O3	wt.%	1.98	2.01	1.54	1.70	1.77	1.78	1.45	1.73	1.67	2.15	1.83	1.68	2.11	1.94	3.81
FeO	wt.%	5.52	3.55	6.89	6.15	4.88	5.09	6.11	6.31	5.33	4.70	4.84	4.46	5.46	5.75	6.96
MnO	wt.%	0.16	0.16	0.35	0.06	0.16	0.10	0.11	0.24	0.11	0.17	0.10	0.18	0.14	0.15	0.15
MgO	wt.%	15.43	16.15	16.22	16.76	15.21	15.62	16.68	16.51	16.29	16.78	15.22	14.89	16.59	17.89	17.04
CaO	wt.%	22.50	20.76	18.89	20.03	22.76	21.54	20.67	20.07	21.50	20.10	22.81	22.64	22.40	20.93	19.49
Na2O	wt.%	0.28	0.45	0.27	0.28	0.30	0.28	0.29	0.26	0.30	0.35	0.21	0.28	0.42	0.36	0.36
Cr2O3	wt.%	N.A.	N.A.	N.A.	N.A.	N.A.	N.A.	N.A.	N.A.	N.A.	N.A.	N.A.	N.A.	N.A.	N.A.	N.A.
V2O3	wt.%	0.05	0.04	0.10	0.09	0.01	<0.01	0.01	0.08	0.01	0.06	0.05	0.03	0.04	0.01	0.07
NiO	wt.%	0.02	0.03	0.08	<0.01	<0.01	<0.01	0.03	0.05	0.08	0.01	0.03	<0.01	0.07	0.07	0.02
Total	wt.%	100.35	96.50	96.82	96.80	97.28	96.86	98.30	98.42	99.90	95.59	98.36	96.46	101.32	99.55	98.88
Na	ppm	0.02	0.03	0.02	0.02	0.02	0.02	0.02	0.02	0.02	0.03	0.02	0.02	0.03	0.03	0.03
Al	ppm	0.09	0.09	0.07	0.08	0.08	0.08	0.06	0.08	0.07	0.10	0.08	0.08	0.09	0.08	0.17
Mg	ppm	0.84	0.91	0.92	0.94	0.86	0.88	0.93	0.92	0.89	0.95	0.85	0.85	0.89	0.97	0.94
Si	ppm	1.96	1.98	1.96	1.93	1.94	1.96	1.95	1.95	1.98	1.93	1.96	1.96	1.93	1.90	1.86
Ca	ppm	0.88	0.84	0.77	0.81	0.92	0.87	0.83	0.80	0.85	0.82	0.91	0.92	0.87	0.82	0.77
Mn	ppm	<0.01	0.01	0.01	<0.01	0.01	<0.01	<0.01	0.01	<0.01	0.01	<0.01	0.01	<0.01	<0.01	<0.01
Ti	ppm	0.03	0.03	0.02	0.02	0.02	0.02	0.02	0.02	0.02	0.02	0.02	0.02	0.02	0.01	0.02
Fe2+	ppm	0.17	0.11	0.22	0.15	0.14	0.16	0.17	0.20	0.16	0.12	0.15	0.14	0.12	0.06	0.11
Fe3+	ppm	<0.01	<0.01	<0.01	0.04	0.02	<0.01	0.02	<0.01	<0.01	0.03	<0.01	<0.01	0.04	0.11	0.10
Ni	ppm	<0.01	<0.01	<0.01	<0.01	<0.01	<0.01	<0.01	<0.01	<0.01	<0.01	<0.01	<0.01	<0.01	<0.01	<0.01
Cr	ppm	N.A.	N.A.	N.A.	N.A.	N.A.	N.A.	N.A.	N.A.	N.A.	N.A.	N.A.	N.A.	N.A.	N.A.	N.A.
Li	ppm	<0.01	<0.01	<0.01	<0.01	<0.01	<0.01	<0.01	<0.01	<0.01	<0.01	<0.01	<0.01	<0.01	<0.01	<0.01
Sc	ppm	<0.01	<0.01	<0.01	<0.01	<0.01	<0.01	<0.01	<0.01	<0.01	<0.01	<0.01	<0.01	<0.01	<0.01	<0.01
V	ppm	<0.01	<0.01	<0.01	<0.01	<0.01	<0.01	<0.01	<0.01	<0.01	<0.01	<0.01	<0.01	<0.01	<0.01	<0.01
Zn	ppm	<0.01	<0.01	<0.01	<0.01	<0.01	<0.01	<0.01	<0.01	<0.01	<0.01	<0.01	<0.01	<0.01	<0.01	<0.01
Zr	ppm	<0.01	<0.01	<0.01	<0.01	<0.01	<0.01	<0.01	<0.01	<0.01	<0.01	<0.01	<0.01	<0.01	<0.01	<0.01
Mg#		0.83	0.89	0.81	0.86	0.86	0.85	0.85	0.82	0.84	0.89	0.85	0.86	0.88	0.94	0.89

Sample		BM-042	BM-042	BM-042	BM-042	BM-042	BM-042	BM-042	BM-042	BM-042	BM-042	BM-042	BM-042	BM-042	BM-042	XX-R-10
Drill Hole		FD-5	FD-5	FD-5	FD-5	FD-5	FD-5	FD-5	FD-5	FD-5	FD-5	FD-5	FD-5	FD-5	FD-5	FD-3
Rock Code		Cpxt	Cpxt	Cpxt	Cpxt	Cpxt	Cpxt	Cpxt	Cpxt	Cpxt	Cpxt	Cpxt	Cpxt	Cpxt	Cpxt	Cpxt
SiO2	wt.%	51.36	55.06	55.17	49.89	50.83	50.86	52.08	54.65	53.61	52.76	52.03	52.76	52.16	52.48	51.59
TiO2	wt.%	1.12	0.12	0.10	0.76	0.92	0.95	0.95	0.06	0.17	0.92	1.05	0.88	0.99	0.11	0.62
Al2O3	wt.%	3.17	0.81	0.51	3.33	2.95	2.68	2.06	0.72	0.86	2.28	2.52	1.88	2.39	0.80	2.48
FeO	wt.%	6.57	3.42	3.00	6.52	6.06	6.80	7.87	3.48	4.45	6.05	6.21	5.48	6.37	5.99	6.66
MnO	wt.%	0.13	0.21	0.19	0.18	0.11	0.25	0.16	0.21	0.16	0.16	0.20	0.21	0.13	0.29	0.22
MgO	wt.%	15.66	17.08	17.58	15.57	15.19	14.91	16.21	16.88	16.11	15.19	15.52	15.51	15.41	16.35	15.82
CaO	wt.%	20.95	24.37	24.47	19.61	21.32	21.48	19.69	24.27	23.90	22.54	21.56	22.41	22.06	22.97	19.20
Na2O	wt.%	0.30	0.07	0.05	0.25	0.31	0.34	0.26	0.06	0.08	0.34	0.30	0.36	0.43	0.05	0.26
Cr2O3	wt.%	N.A.	N.A.	N.A.	N.A.	N.A.	N.A.	N.A.	N.A.	N.A.	N.A.	N.A.	N.A.	N.A.	N.A.	N.A.
V2O3	wt.%	0.07	0.03	0.04	0.09	0.06	0.05	0.14	0.06	0.05	0.05	0.08	0.14	0.08	0.05	0.06
NiO	wt.%	0.06	<0.01	<0.01	0.04	0.01	0.03	0.02	0.02	<0.01	<0.01	<0.01	0.01	<0.01	<0.01	0.10
Total	wt.%	99.38	101.16	101.09	96.23	97.77	98.34	99.43	100.41	99.39	100.28	99.48	99.64	100.02	99.07	97.01
Na	ppm	0.02	0.01	<0.01	0.02	0.02	0.02	0.02	<0.01	0.01	0.02	0.02	0.03	0.03	<0.01	0.02
Al	ppm	0.14	0.03	0.02	0.15	0.13	0.12	0.09	0.03	0.04	0.10	0.11	0.08	0.10	0.03	0.11
Mg	ppm	0.86	0.92	0.94	0.89	0.85	0.83	0.90	0.92	0.89	0.83	0.86	0.85	0.85	0.90	0.89
Si	ppm	1.90	1.99	1.99	1.90	1.91	1.91	1.93	1.99	1.98	1.94	1.93	1.95	1.92	1.95	1.96
Ca	ppm	0.83	0.94	0.94	0.80	0.86	0.86	0.78	0.95	0.94	0.89	0.86	0.89	0.87	0.91	0.78
Mn	ppm	<0.01	0.01	0.01	0.01	<0.01	0.01	<0.01	0.01	<0.01	<0.01	0.01	0.01	<0.01	0.01	0.01
Ti	ppm	0.03	<0.01	<0.01	0.02	0.03	0.03	0.03	<0.01	<0.01	0.03	0.03	0.02	0.03	<0.01	0.02
Fe2+	ppm	0.19	0.10	0.09	0.19	0.18	0.18	0.24	0.11	0.14	0.19	0.19	0.17	0.17	0.12	0.21
Fe3+	ppm	0.01	<0.01	<0.01	0.01	0.01	0.03	0.01	<0.01	<0.01	<0.01	<0.01	<0.01	0.03	0.07	<0.01
Ni	ppm	<0.01	<0.01	<0.01	<0.01	<0.01	<0.01	<0.01	<0.01	<0.01	<0.01	<0.01	<0.01	<0.01	<0.01	<0.01
Cr	ppm	N.A.	N.A.	N.A.	N.A.	N.A.	N.A.	N.A.	N.A.	N.A.	N.A.	N.A.	N.A.	N.A.	N.A.	N.A.
Li	ppm	<0.01	<0.01	<0.01	<0.01	<0.01	<0.01	<0.01	<0.01	<0.01	<0.01	<0.01	<0.01	<0.01	<0.01	<0.01
Sc	ppm	<0.01	<0.01	<0.01	<0.01	<0.01	<0.01	<0.01	<0.01	<0.01	<0.01	<0.01	<0.01	<0.01	<0.01	<0.01
V	ppm	<0.01	<0.01	<0.01	<0.01	<0.01	<0.01	<0.01	<0.01	<0.01	<0.01	<0.01	<0.01	<0.01	<0.01	<0.01
Zn	ppm	<0.01	<0.01	<0.01	<0.01	<0.01	<0.01	<0.01	<0.01	<0.01	<0.01	<0.01	<0.01	<0.01	<0.01	<0.01
Zr	ppm	<0.01	<0.01	<0.01	<0.01	<0.01	<0.01	<0.01	<0.01	<0.01	<0.01	<0.01	<0.01	<0.01	<0.01	<0.01
Mg#		0.82	0.90	0.91	0.82	0.83	0.82	0.79	0.90	0.87	0.82	0.82	0.83	0.84	0.89	0.81

Sample		XX-R-10	XX-R-10	XX-R-10	XX-R-10	XX-R-10	XX-R-10	XX-R-10	XX-R-10	XX-R-10	XX-R-10	XX-R-10	XX-R-13	XX-R-13	XX-R-13	XX-R-13
Drill Hole		FD-3	FD-3	FD-3	FD-3	FD-3	FD-3	FD-3	FD-3	FD-3	FD-3	FD-3	FD-5	FD-5	FD-5	FD-5
Rock Code		Cpxt	Cpxt	Cpxt	Cpxt	Cpxt	Cpxt	Cpxt	Cpxt	Cpxt	Cpxt	Cpxt	Cpxt	Cpxt	Cpxt	Cpxt
SiO2	wt.%	51.56	52.72	51.25	52.64	52.22	52.76	52.00	51.87	51.43	52.64	52.67	53.48	51.92	53.07	54.58
TiO2	wt.%	0.65	0.60	0.82	0.82	0.84	0.92	0.68	0.74	0.58	0.87	0.84	0.68	0.78	0.93	0.12
Al2O3	wt.%	2.60	2.15	3.31	2.46	2.32	2.23	2.12	2.57	3.00	2.34	2.58	1.81	1.91	2.18	0.80
FeO	wt.%	6.11	5.50	6.25	5.94	6.20	6.12	6.10	6.09	5.65	7.56	5.76	6.68	9.13	6.14	5.14
MnO	wt.%	0.14	0.16	0.21	0.18	0.25	0.29	0.16	0.15	0.08	0.29	0.15	0.23	0.10	0.23	0.16
MgO	wt.%	16.94	17.15	16.88	15.60	15.83	15.90	16.45	16.69	17.06	16.08	16.06	15.73	15.59	15.71	16.39
CaO	wt.%	20.36	21.62	20.28	21.78	21.88	21.56	21.24	20.53	19.48	20.33	21.10	21.14	20.00	22.36	22.94
Na2O	wt.%	0.28	0.35	0.34	0.33	0.41	0.42	0.33	0.32	0.33	0.29	0.38	0.27	0.29	0.31	0.11
Cr2O3	wt.%	N.A.	N.A.	N.A.	N.A.	N.A.	N.A.	N.A.	N.A.	N.A.	N.A.	N.A.	N.A.	N.A.	N.A.	N.A.
V2O3	wt.%	0.09	0.12	0.06	0.06	0.08	<0.01	0.05	0.07	0.09	0.07	0.12	0.04	0.03	0.12	<0.01
NiO	wt.%	0.00	0.00	0.03	0.03	0.06	0.01	0.11	0.14	0.06	<0.01	<0.01	0.03	0.02	0.02	<0.01
Total	wt.%	98.72	100.36	99.43	99.84	100.10	100.20	99.23	99.18	97.78	100.46	99.65	100.08	99.76	101.07	100.21
Na	ppm	0.02	0.02	0.02	0.02	0.03	0.03	0.02	0.02	0.02	0.02	0.03	0.02	0.02	0.02	0.01
Al	ppm	0.11	0.09	0.14	0.11	0.10	0.10	0.09	0.11	0.13	0.10	0.11	0.08	0.08	0.09	0.03
Mg	ppm	0.94	0.93	0.93	0.86	0.87	0.87	0.91	0.92	0.95	0.88	0.88	0.86	0.86	0.85	0.89
Si	ppm	1.91	1.92	1.88	1.94	1.92	1.94	1.92	1.91	1.92	1.93	1.94	1.97	1.93	1.93	2.00
Ca	ppm	0.81	0.84	0.80	0.86	0.86	0.85	0.84	0.81	0.78	0.80	0.83	0.83	0.80	0.87	0.90
Mn	ppm	<0.01	<0.01	0.01	0.01	0.01	0.01	<0.01	<0.01	<0.01	0.01	<0.01	0.01	<0.01	0.01	<0.01
Ti	ppm	0.02	0.02	0.02	0.02	0.02	0.03	0.02	0.02	0.02	0.02	0.02	0.02	0.02	0.03	<0.01
Fe2+	ppm	0.14	0.11	0.13	0.18	0.14	0.18	0.14	0.15	0.16	0.23	0.18	0.21	0.25	0.18	0.16
Fe3+	ppm	0.05	0.06	0.06	<0.01	0.05	0.01	0.05	0.04	0.02	<0.01	<0.01	<0.01	0.04	<0.01	<0.01
Ni	ppm	<0.01	<0.01	<0.01	<0.01	<0.01	<0.01	<0.01	<0.01	<0.01	<0.01	<0.01	<0.01	<0.01	<0.01	<0.01
Cr	ppm	N.A.	N.A.	N.A.	N.A.	N.A.	N.A.	N.A.	N.A.	N.A.	N.A.	N.A.	N.A.	N.A.	N.A.	N.A.
Li	ppm	<0.01	<0.01	<0.01	<0.01	<0.01	<0.01	<0.01	<0.01	<0.01	<0.01	<0.01	<0.01	<0.01	<0.01	<0.01
Sc	ppm	<0.01	<0.01	<0.01	<0.01	<0.01	<0.01	<0.01	<0.01	<0.01	<0.01	<0.01	<0.01	<0.01	<0.01	<0.01
V	ppm	<0.01	<0.01	<0.01	<0.01	<0.01	<0.01	<0.01	<0.01	<0.01	<0.01	<0.01	<0.01	<0.01	<0.01	<0.01
Zn	ppm	<0.01	<0.01	<0.01	<0.01	<0.01	<0.01	<0.01	<0.01	<0.01	<0.01	<0.01	<0.01	<0.01	<0.01	<0.01
Zr	ppm	<0.01	<0.01	<0.01	<0.01	<0.01	<0.01	<0.01	<0.01	<0.01	<0.01	<0.01	<0.01	<0.01	<0.01	<0.01
Mg#		0.87	0.90	0.88	0.82	0.86	0.83	0.87	0.86	0.86	0.79	0.83	0.81	0.78	0.82	0.85

Sample		XX-R-13	XX-R-13	XX-R-13	XX-R-13	XX-R-13	XX-R-13	XX-R-13	XX-R-13	XX-R-14	XX-R-14	XX-R-14	XX-R-14	XX-R-14	XX-R-14	XX-R-14
Drill Hole		FD-5	FD-5	FD-5	FD-5	FD-5	FD-5	FD-5	FD-5	FD-5	FD-5	FD-5	FD-5	FD-5	FD-5	FD-5
Rock Code		Cpxt	Cpxt	Cpxt	Cpxt	Cpxt	Cpxt	Cpxt	Cpxt	Cpxt	Cpxt	Cpxt	Cpxt	Cpxt	Cpxt	Cpxt
SiO2	wt.%	52.89	51.01	51.93	52.84	52.38	54.81	52.39	51.68	52.22	53.59	52.85	53.10	52.66	53.43	53.80
TiO2	wt.%	0.71	0.81	0.98	0.95	1.07	0.04	0.97	1.07	0.51	0.87	0.92	0.77	0.85	0.78	0.57
Al2O3	wt.%	1.35	2.79	2.32	2.09	2.28	0.73	2.35	2.25	2.45	1.96	2.02	2.04	1.89	1.74	1.78
FeO	wt.%	5.81	6.29	7.08	6.20	5.81	4.71	6.04	6.76	5.63	7.16	6.06	5.90	5.72	5.28	5.99
MnO	wt.%	0.11	0.15	0.26	0.13	0.20	0.13	0.27	0.21	0.11	0.22	0.28	0.26	0.15	0.18	0.23
MgO	wt.%	14.93	15.79	15.02	15.23	14.73	16.08	15.13	15.10	16.97	17.64	16.89	16.00	15.56	16.65	17.20
CaO	wt.%	23.51	21.10	21.79	22.20	22.23	24.51	22.18	22.02	20.15	19.77	21.09	21.85	21.96	20.67	19.96
Na2O	wt.%	0.33	0.27	0.41	0.38	0.38	0.07	0.31	0.37	0.24	0.30	0.33	0.32	0.29	0.31	0.29
Cr2O3	wt.%	N.A.	N.A.	N.A.	N.A.	N.A.	N.A.	N.A.	N.A.	N.A.	N.A.	N.A.	N.A.	N.A.	N.A.	N.A.
V2O3	wt.%	0.05	<0.01	0.08	0.01	0.08	0.05	<0.01	0.06	0.06	0.08	0.11	0.09	0.02	0.04	<0.01
NiO	wt.%	<0.01	0.02	<0.01	<0.01	0.10	0.07	<0.01	0.05	0.05	<0.01	<0.01	0.04	<0.01	<0.01	<0.01
Total	wt.%	99.69	98.23	99.87	100.01	99.24	101.20	99.64	99.55	98.39	101.58	100.55	100.36	99.09	99.07	99.82
Na	ppm	0.02	0.02	0.03	0.03	0.03	<0.01	0.02	0.03	0.02	0.02	0.02	0.02	0.02	0.02	0.02
Al	ppm	0.06	0.12	0.10	0.09	0.10	0.03	0.10	0.10	0.11	0.08	0.09	0.09	0.08	0.08	0.08
Mg	ppm	0.82	0.88	0.83	0.84	0.82	0.87	0.83	0.83	0.94	0.95	0.92	0.87	0.86	0.92	0.94
Si	ppm	1.96	1.91	1.92	1.95	1.95	1.99	1.94	1.92	1.94	1.93	1.93	1.94	1.96	1.97	1.97
Ca	ppm	0.93	0.85	0.86	0.88	0.89	0.95	0.88	0.87	0.80	0.76	0.82	0.86	0.87	0.82	0.78
Mn	ppm	<0.01	<0.01	0.01	<0.01	0.01	<0.01	0.01	0.01	<0.01	0.01	0.01	0.01	<0.01	0.01	0.01
Ti	ppm	0.02	0.02	0.03	0.03	0.03	<0.01	0.03	0.03	0.01	0.02	0.03	0.02	0.02	0.02	0.02
Fe2+	ppm	0.17	0.16	0.19	0.19	0.18	0.14	0.19	0.18	0.17	0.20	0.15	0.18	0.18	0.16	0.18
Fe3+	ppm	0.01	0.04	0.03	<0.01	<0.01	<0.01	<0.01	0.03	<0.01	0.02	0.03	<0.01	<0.01	<0.01	<0.01
Ni	ppm	<0.01	<0.01	<0.01	<0.01	<0.01	<0.01	<0.01	<0.01	<0.01	<0.01	<0.01	<0.01	<0.01	<0.01	<0.01
Cr	ppm	N.A.	N.A.	N.A.	N.A.	N.A.	N.A.	N.A.	N.A.	N.A.	N.A.	N.A.	N.A.	N.A.	N.A.	N.A.
Li	ppm	<0.01	<0.01	<0.01	<0.01	<0.01	<0.01	<0.01	<0.01	<0.01	<0.01	<0.01	<0.01	<0.01	<0.01	<0.01
Sc	ppm	<0.01	<0.01	<0.01	<0.01	<0.01	<0.01	<0.01	<0.01	<0.01	<0.01	<0.01	<0.01	<0.01	<0.01	<0.01
V	ppm	<0.01	<0.01	<0.01	<0.01	<0.01	<0.01	<0.01	<0.01	<0.01	<0.01	<0.01	<0.01	<0.01	<0.01	<0.01
Zn	ppm	<0.01	<0.01	<0.01	<0.01	<0.01	<0.01	<0.01	<0.01	<0.01	<0.01	<0.01	<0.01	<0.01	<0.01	<0.01
Zr	ppm	<0.01	<0.01	<0.01	<0.01	<0.01	<0.01	<0.01	<0.01	<0.01	<0.01	<0.01	<0.01	<0.01	<0.01	<0.01
Mg#		0.83	0.85	0.81	0.81	0.82	0.86	0.82	0.83	0.85	0.83	0.86	0.83	0.83	0.85	0.84

Sample		XX-R-14	XX-R-14	XX-R-14	XX-R-14	XX-R-14	XX-R-14	XX-R-14	XX-R-14	XX-R-14	XX-R-14	BM-009	BM-009	BM-009	BM-009	BM-009
Drill Hole		FD-5	FD-5	FD-5	FD-5	FD-5	FD-5	FD-5	FD-5	FD-5	FD-5	FD-3	FD-3	FD-3	FD-3	FD-3
Rock Code		Cpxt	Cpxt	Cpxt	Cpxt	Cpxt	Cpxt	Cpxt	Cpxt	Cpxt	Cpxt	Ol-Cpxt	Ol-Cpxt	Ol-Cpxt	Ol-Cpxt	Ol-Cpxt
SiO2	wt.%	52.68	52.61	53.43	52.51	52.88	52.75	52.45	52.82	51.36	52.31	51.44	54.63	52.97	53.01	50.58
TiO2	wt.%	1.04	1.07	0.86	0.84	0.89	0.87	0.88	0.91	0.91	0.86	0.69	0.40	0.97	0.76	0.90
Al2O3	wt.%	2.19	2.01	1.92	2.17	2.01	1.97	1.92	2.13	1.78	2.14	3.56	1.64	2.40	1.61	3.03
FeO	wt.%	6.61	7.14	5.50	6.53	7.36	6.44	6.64	6.03	9.06	6.53	5.80	5.12	5.92	6.40	5.90
MnO	wt.%	0.10	0.14	0.18	0.18	0.21	0.16	0.24	0.16	0.13	0.27	0.03	0.17	0.11	0.10	0.07
MgO	wt.%	16.51	17.31	16.41	16.70	16.89	16.53	16.04	16.45	16.27	16.32	17.20	18.89	15.18	15.23	15.01
CaO	wt.%	20.44	19.18	21.62	20.03	19.32	20.95	20.99	21.01	19.63	19.66	17.91	17.64	21.26	22.47	22.02
Na2O	wt.%	0.28	0.26	0.27	0.33	0.29	0.32	0.26	0.30	0.22	0.31	0.63	0.39	0.43	0.32	0.34
Cr2O3	wt.%	N.A.	N.A.	N.A.	N.A.	N.A.	N.A.	N.A.	N.A.	N.A.	N.A.	0.64	0.42	N.A.	N.A.	N.A.
V2O3	wt.%	<0.01	0.01	0.06	0.02	0.04	0.10	0.03	0.07	0.05	0.06	0.03	0.09	<0.01	0.12	0.01
NiO	wt.%	<0.01	0.08	0.04	<0.01	0.07	<0.01	<0.01	<0.01	<0.01	0.05	0.02	<0.01	0.05	0.03	0.07
Total	wt.%	99.85	99.82	100.29	99.31	99.95	100.10	99.43	99.87	99.42	98.52	97.97	99.38	99.29	100.05	97.94
Na	ppm	0.02	0.02	0.02	0.02	0.02	0.02	0.02	0.02	0.02	0.02	0.05	0.03	0.03	0.02	0.03
Al	ppm	0.10	0.09	0.08	0.09	0.09	0.09	0.08	0.09	0.08	0.09	0.16	0.07	0.10	0.07	0.13
Mg	ppm	0.91	0.95	0.90	0.92	0.93	0.90	0.89	0.90	0.90	0.91	0.95	1.03	0.84	0.84	0.84
Si	ppm	1.94	1.93	1.95	1.94	1.94	1.93	1.94	1.94	1.91	1.95	1.91	2.00	1.96	1.96	1.90
Ca	ppm	0.81	0.76	0.85	0.79	0.76	0.82	0.83	0.83	0.78	0.79	0.71	0.69	0.84	0.89	0.89
Mn	ppm	<0.01	<0.01	0.01	0.01	0.01	0.01	0.01	0.01	<0.01	0.01	<0.01	0.01	<0.01	<0.01	<0.01
Ti	ppm	0.03	0.03	0.02	0.02	0.02	0.02	0.02	0.03	0.03	0.02	0.02	0.01	0.03	0.02	0.03
Fe2+	ppm	0.20	0.22	0.17	0.20	0.23	0.18	0.20	0.19	0.21	0.20	0.17	0.16	0.18	0.20	0.14
Fe3+	ppm	<0.01	<0.01	<0.01	<0.01	<0.01	0.02	<0.01	<0.01	0.07	<0.01	0.01	<0.01	<0.01	<0.01	0.04
Ni	ppm	<0.01	<0.01	<0.01	<0.01	<0.01	<0.01	<0.01	<0.01	<0.01	<0.01	<0.01	<0.01	<0.01	<0.01	<0.01
Cr	ppm	N.A.	N.A.	N.A.	N.A.	N.A.	N.A.	N.A.	N.A.	N.A.	N.A.	0.02	0.01	N.A.	N.A.	N.A.
Li	ppm	<0.01	<0.01	<0.01	<0.01	<0.01	<0.01	<0.01	<0.01	<0.01	<0.01	<0.01	<0.01	<0.01	<0.01	<0.01
Sc	ppm	<0.01	<0.01	<0.01	<0.01	<0.01	<0.01	<0.01	<0.01	<0.01	<0.01	<0.01	<0.01	<0.01	<0.01	<0.01
V	ppm	<0.01	<0.01	<0.01	<0.01	<0.01	<0.01	<0.01	<0.01	<0.01	<0.01	<0.01	<0.01	<0.01	<0.01	<0.01
Zn	ppm	<0.01	<0.01	<0.01	<0.01	<0.01	<0.01	<0.01	<0.01	<0.01	<0.01	<0.01	<0.01	<0.01	<0.01	<0.01
Zr	ppm	<0.01	<0.01	<0.01	<0.01	<0.01	<0.01	<0.01	<0.01	<0.01	<0.01	<0.01	<0.01	<0.01	<0.01	<0.01
Mg#		0.82	0.82	0.84	0.82	0.80	0.83	0.81	0.83	0.81	0.82	0.85	0.87	0.82	0.81	0.85

Sample		BM-009	BM-009	BM-009	BM-009	BM-009	BM-009	BM-009	BM-009	BM-009	BM-009	BM-031	BM-031	BM-008	BM-008	BM-030
Drill Hole		FD-3	FD-3	FD-3	FD-3	FD-3	FD-3	FD-3	FD-3	FD-3	FD-3	FD-6	FD-6	FD-3	FD-3	FD-6
Rock Code		Ol-Cpxt	Ol-Cpxt	Ol-Cpxt	Ol-Cpxt	Ol-Cpxt	Ol-Cpxt	Ol-Cpxt	Ol-Cpxt	Ol-Cpxt	Ol-Cpxt	Wrlt	Wrlt	Wrlt	Wrlt	Wrlt
SiO2	wt.%	51.33	50.76	49.97	53.71	52.80	52.63	52.83	49.96	49.96	53.19	52.95	51.97	51.61	52.37	52.90
TiO2	wt.%	0.92	1.27	0.77	1.00	0.93	0.93	0.85	0.83	0.90	0.97	0.73	0.91	0.91	1.03	0.68
Al2O3	wt.%	1.73	2.47	2.59	2.33	2.39	1.98	2.15	2.39	2.08	1.96	1.46	1.38	2.27	2.30	1.69
FeO	wt.%	5.44	6.11	5.22	6.24	7.09	5.90	6.09	6.13	6.75	7.15	5.00	4.79	6.31	6.22	5.64
MnO	wt.%	0.25	0.22	0.17	0.16	0.22	0.27	0.20	0.17	0.22	0.23	0.23	0.20	0.28	0.14	0.13
MgO	wt.%	14.78	14.78	15.70	15.03	16.01	15.34	16.14	14.56	14.88	16.29	16.11	16.26	15.76	15.39	16.24
CaO	wt.%	22.11	21.89	21.45	22.33	21.63	22.13	21.53	20.54	20.77	21.03	22.22	22.02	21.39	21.97	22.21
Na2O	wt.%	0.23	0.24	0.33	0.33	0.39	0.36	0.34	0.30	0.28	0.41	0.31	0.30	0.37	0.36	0.39
Cr2O3	wt.%	N.A.	N.A.	N.A.	N.A.	N.A.	N.A.	N.A.	N.A.	N.A.	N.A.	0.48	0.28	0.40	0.40	0.33
V2O3	wt.%	0.04	0.08	<0.01	0.05	0.12	0.11	0.05	0.03	0.05	0.09	0.06	0.10	0.04	0.06	0.05
NiO	wt.%	<0.01	0.02	0.02	<0.01	0.04	0.02	<0.01	0.06	0.05	0.03	<0.01	<0.01	<0.01	0.05	0.01
Total	wt.%	96.83	97.83	96.21	101.18	101.61	99.66	100.17	94.98	95.93	101.35	99.55	98.21	99.33	100.29	100.26
Na	ppm	0.02	0.02	0.02	0.02	0.03	0.03	0.02	0.02	0.02	0.03	0.02	0.02	0.03	0.03	0.03
Al	ppm	0.08	0.11	0.12	0.10	0.10	0.09	0.09	0.11	0.09	0.08	0.06	0.06	0.10	0.10	0.07
Mg	ppm	0.84	0.83	0.89	0.82	0.86	0.85	0.88	0.84	0.85	0.88	0.89	0.90	0.87	0.84	0.89
Si	ppm	1.96	1.92	1.90	1.96	1.91	1.95	1.94	1.94	1.92	1.93	1.95	1.94	1.91	1.93	1.94
Ca	ppm	0.90	0.89	0.87	0.87	0.84	0.88	0.85	0.85	0.86	0.82	0.88	0.88	0.85	0.87	0.87
Mn	ppm	0.01	0.01	0.01	0.01	0.01	0.01	0.01	0.01	0.01	0.01	0.01	0.01	0.01	<0.01	<0.01
Ti	ppm	0.03	0.04	0.02	0.03	0.03	0.03	0.02	0.02	0.03	0.03	0.02	0.03	0.03	0.03	0.02
Fe2+	ppm	0.17	0.19	0.10	0.19	0.17	0.18	0.18	0.20	0.19	0.19	0.15	0.13	0.16	0.19	0.14
Fe3+	ppm	<0.01	<0.01	0.06	<0.01	0.04	<0.01	0.01	<0.01	0.03	0.03	<0.01	0.02	0.04	<0.01	0.03
Ni	ppm	<0.01	<0.01	<0.01	<0.01	<0.01	<0.01	<0.01	<0.01	<0.01	<0.01	<0.01	<0.01	<0.01	<0.01	<0.01
Cr	ppm	N.A.	N.A.	N.A.	N.A.	N.A.	N.A.	N.A.	N.A.	N.A.	N.A.	0.01	0.01	0.01	0.01	0.01
Li	ppm	<0.01	<0.01	<0.01	<0.01	<0.01	<0.01	<0.01	<0.01	<0.01	<0.01	<0.01	<0.01	<0.01	<0.01	<0.01
Sc	ppm	<0.01	<0.01	<0.01	<0.01	<0.01	<0.01	<0.01	<0.01	<0.01	<0.01	<0.01	<0.01	<0.01	<0.01	<0.01
V	ppm	<0.01	<0.01	<0.01	<0.01	<0.01	<0.01	<0.01	<0.01	<0.01	<0.01	<0.01	<0.01	<0.01	<0.01	<0.01
Zn	ppm	<0.01	<0.01	<0.01	<0.01	<0.01	<0.01	<0.01	<0.01	<0.01	<0.01	<0.01	<0.01	<0.01	<0.01	<0.01
Zr	ppm	<0.01	<0.01	<0.01	<0.01	<0.01	<0.01	<0.01	<0.01	<0.01	<0.01	<0.01	<0.01	<0.01	<0.01	<0.01
Mg#		0.83	0.81	0.90	0.81	0.83	0.82	0.83	0.81	0.82	0.82	0.85	0.87	0.85	0.82	0.86

Sample		BM-030	BM-030	BM-030	BM-038	BM-038	BM-038	BM-038	BM-007	BM-007	BM-007	BM-007	BM-007	BM-007	BM-010	BM-010
Drill Hole		FD-6	FD-6	FD-6	FD-12	FD-12	FD-12	FD-12	FD-3	FD-3	FD-3	FD-3	FD-3	FD-3	FD-3	FD-3
Rock Code		Wrlt	Wrlt	Wrlt	Wrlt	Wrlt	Wrlt	Wrlt	Wrlt	Wrlt	Wrlt	Wrlt	Wrlt	Wrlt	Wrlt	Wrlt
SiO2	wt.%	52.32	52.88	52.91	52.41	53.29	53.90	52.81	53.07	53.77	52.68	53.06	52.65	52.48	53.16	54.01
TiO2	wt.%	0.48	0.61	0.85	0.89	0.63	0.46	0.45	0.63	0.78	0.57	0.60	1.16	0.91	0.62	0.47
Al2O3	wt.%	1.74	1.71	1.62	2.57	1.59	0.75	1.84	1.67	1.51	1.49	1.65	1.99	1.97	1.50	1.25
FeO	wt.%	5.48	5.46	5.22	5.48	5.18	3.99	4.88	5.83	5.86	5.97	5.24	6.17	5.51	5.43	4.96
MnO	wt.%	0.11	0.14	0.23	0.04	0.13	0.29	0.16	0.26	0.16	0.23	0.12	0.22	0.24	0.18	0.11
MgO	wt.%	15.85	15.80	16.32	15.94	16.17	16.55	15.82	16.02	16.53	15.77	15.60	16.79	15.48	16.15	15.90
CaO	wt.%	21.82	21.97	21.69	22.02	22.74	23.70	22.57	21.29	20.60	21.59	22.51	20.34	22.11	21.98	22.80
Na2O	wt.%	0.32	0.30	0.28	0.37	0.31	0.17	0.43	0.24	0.24	0.29	0.21	0.36	0.39	0.33	0.34
Cr2O3	wt.%	0.46	0.34	0.42	0.43	0.62	0.42	0.51	0.50	0.40	0.43	0.54	0.32	0.58	0.33	0.38
V2O3	wt.%	0.12	<0.01	0.07	0.08	0.01	0.01	0.06	0.06	0.01	0.07	0.05	0.03	0.12	0.07	0.01
NiO	wt.%	0.05	<0.01	0.02	<0.01	0.04	0.03	0.06	<0.01	<0.01	<0.01	<0.01	0.01	<0.01	<0.01	0.03
Total	wt.%	98.76	99.21	99.62	100.22	100.70	100.26	99.59	99.55	99.86	99.08	99.57	100.06	99.78	99.75	100.24
Na	ppm	0.02	0.02	0.02	0.03	0.02	0.01	0.03	0.02	0.02	0.02	0.02	0.03	0.03	0.02	0.02
Al	ppm	0.08	0.07	0.07	0.11	0.07	0.03	0.08	0.07	0.07	0.07	0.07	0.09	0.09	0.07	0.05
Mg	ppm	0.88	0.87	0.90	0.87	0.88	0.90	0.87	0.88	0.91	0.87	0.86	0.92	0.85	0.89	0.87
Si	ppm	1.95	1.96	1.95	1.92	1.94	1.97	1.94	1.96	1.98	1.96	1.96	1.93	1.94	1.96	1.98
Ca	ppm	0.87	0.87	0.86	0.86	0.89	0.93	0.89	0.84	0.81	0.86	0.89	0.80	0.87	0.87	0.89
Mn	ppm	<0.01	<0.01	0.01	<0.01	<0.01	0.01	<0.01	0.01	<0.01	0.01	<0.01	0.01	0.01	0.01	<0.01
Ti	ppm	0.01	0.02	0.02	0.02	0.02	0.01	0.01	0.02	0.02	0.02	0.02	0.03	0.03	0.02	0.01
Fe2+	ppm	0.16	0.17	0.16	0.16	0.14	0.12	0.13	0.18	0.18	0.19	0.16	0.19	0.17	0.17	0.15
Fe3+	ppm	0.01	<0.01	<0.01	0.01	0.01	<0.01	0.02	<0.01	<0.01	<0.01	<0.01	<0.01	<0.01	<0.01	<0.01
Ni	ppm	<0.01	<0.01	<0.01	<0.01	<0.01	<0.01	<0.01	<0.01	<0.01	<0.01	<0.01	<0.01	<0.01	<0.01	<0.01
Cr	ppm	0.01	0.01	0.01	0.01	0.02	0.01	0.01	0.01	0.01	0.01	0.02	0.01	0.02	0.01	0.01
Li	ppm	<0.01	<0.01	<0.01	<0.01	<0.01	<0.01	<0.01	<0.01	<0.01	<0.01	<0.01	<0.01	<0.01	<0.01	<0.01
Sc	ppm	<0.01	<0.01	<0.01	<0.01	<0.01	<0.01	<0.01	<0.01	<0.01	<0.01	<0.01	<0.01	<0.01	<0.01	<0.01
V	ppm	<0.01	<0.01	<0.01	<0.01	<0.01	<0.01	<0.01	<0.01	<0.01	<0.01	<0.01	<0.01	<0.01	<0.01	<0.01
Zn	ppm	<0.01	<0.01	<0.01	<0.01	<0.01	<0.01	<0.01	<0.01	<0.01	<0.01	<0.01	<0.01	<0.01	<0.01	<0.01
Zr	ppm	<0.01	<0.01	<0.01	<0.01	<0.01	<0.01	<0.01	<0.01	<0.01	<0.01	<0.01	<0.01	<0.01	<0.01	<0.01
Mg#		0.85	0.84	0.85	0.85	0.86	0.88	0.87	0.83	0.83	0.82	0.84	0.83	0.83	0.84	0.85

Sample		BM-010	BM-010	BM-010	BM-007	BM-007	BM-007	BM-007	BM-007	BM-007	BM-007	BM-007	BM-007	BM-007	BM-007
Drill Hole		FD-3	FD-3	FD-3	FD-3	FD-3	FD-3	FD-3	FD-3	FD-3	FD-3	FD-3	FD-3	FD-3	FD-3
Rock Code		Wrlt	Wrlt	Wrlt	Wrlt	Wrlt	Wrlt	Wrlt	Wrlt	Wrlt	Wrlt	Wrlt	Wrlt	Wrlt	Wrlt
SiO2	wt.%	53.92	50.69	51.96	53.54	52.59	52.67	52.32	53.20	52.52	51.30	52.35	51.51	52.24	52.84	52.39
TiO2	wt.%	0.74	0.76	0.96	0.75	0.87	0.90	0.78	0.76	0.58	0.68	0.96	1.32	1.46	0.78	0.77
Al2O3	wt.%	1.62	3.18	2.47	1.74	2.13	2.33	2.41	2.01	1.58	2.23	2.08	1.94	1.93	1.90	1.88
FeO	wt.%	5.52	6.52	5.76	5.88	6.16	6.24	5.97	5.85	5.87	6.64	6.39	6.46	6.71	5.95	6.00
MnO	wt.%	0.05	0.07	0.16	0.21	0.19	0.15	0.13	0.21	0.22	0.22	0.20	0.21	0.17	0.18	0.17
MgO	wt.%	16.18	16.99	16.04	15.73	16.42	15.90	16.74	15.61	15.89	16.26	15.79	15.98	15.15	15.84	15.67
CaO	wt.%	21.33	20.02	21.84	22.42	20.96	22.23	21.32	22.32	22.41	20.50	21.88	20.43	21.21	21.91	21.86
Na2O	wt.%	0.28	0.26	0.32	0.28	0.32	0.31	0.32	0.37	0.22	0.29	0.33	0.27	0.35	0.30	0.37
Cr2O3	wt.%	0.38	0.46	0.41	N.A.	N.A.	N.A.	N.A.	N.A.	N.A.	N.A.	N.A.	N.A.	N.A.	N.A.	N.A.
V2O3	wt.%	0.07	0.04	0.06	0.01	<0.01	0.08	0.06	<0.01	<0.01	0.08	0.11	0.03	0.06	0.08	0.06
NiO	wt.%	0.03	<0.01	0.01	<0.01	0.05	<0.01	0.13	<0.01	<0.01	0.04	0.04	0.06	<0.01	0.09	0.09
Total	wt.%	100.11	98.99	99.99	100.56	99.70	100.81	100.17	100.33	99.29	98.24	100.11	98.20	99.27	99.86	99.25
Na	ppm	0.02	0.02	0.02	0.02	0.02	0.02	0.02	0.03	0.02	0.02	0.02	0.02	0.03	0.02	0.03
Al	ppm	0.07	0.14	0.11	0.07	0.09	0.10	0.10	0.09	0.07	0.10	0.09	0.09	0.08	0.08	0.08
Mg	ppm	0.89	0.94	0.88	0.86	0.90	0.86	0.91	0.85	0.88	0.91	0.87	0.89	0.84	0.87	0.87
Si	ppm	1.98	1.87	1.91	1.96	1.94	1.92	1.91	1.95	1.94	1.92	1.93	1.93	1.95	1.95	1.94
Ca	ppm	0.84	0.79	0.86	0.88	0.83	0.87	0.84	0.88	0.89	0.82	0.86	0.82	0.85	0.86	0.87
Mn	ppm	<0.01	<0.01	<0.01	0.01	0.01	<0.01	<0.01	0.01	0.01	0.01	0.01	0.01	0.01	0.01	0.01
Ti	ppm	0.02	0.02	0.03	0.02	0.02	0.02	0.02	0.02	0.02	0.02	0.03	0.04	0.04	0.02	0.02
Fe2+	ppm	0.17	0.13	0.15	0.18	0.18	0.16	0.13	0.18	0.16	0.16	0.17	0.20	0.21	0.18	0.17
Fe3+	ppm	<0.01	0.08	0.03	<0.01	0.01	0.03	0.05	<0.01	0.03	0.05	0.03	<0.01	<0.01	<0.01	0.02
Ni	ppm	<0.01	<0.01	<0.01	<0.01	<0.01	<0.01	<0.01	<0.01	<0.01	<0.01	<0.01	<0.01	<0.01	<0.01	<0.01
Cr	ppm	0.01	0.01	0.01	N.A.	N.A.	N.A.	N.A.	N.A.	N.A.	N.A.	N.A.	N.A.	N.A.	N.A.	N.A.
Li	ppm	<0.01	<0.01	<0.01	<0.01	<0.01	<0.01	<0.01	<0.01	<0.01	<0.01	<0.01	<0.01	<0.01	<0.01	<0.01
Sc	ppm	<0.01	<0.01	<0.01	<0.01	<0.01	<0.01	<0.01	<0.01	<0.01	<0.01	<0.01	<0.01	<0.01	<0.01	<0.01
V	ppm	<0.01	<0.01	<0.01	<0.01	<0.01	<0.01	<0.01	<0.01	<0.01	<0.01	<0.01	<0.01	<0.01	<0.01	<0.01
Zn	ppm	<0.01	<0.01	<0.01	<0.01	<0.01	<0.01	<0.01	<0.01	<0.01	<0.01	<0.01	<0.01	<0.01	<0.01	<0.01
Zr	ppm	<0.01	<0.01	<0.01	<0.01	<0.01	<0.01	<0.01	<0.01	<0.01	<0.01	<0.01	<0.01	<0.01	<0.01	<0.01
Mg#		0.84	0.88	0.86	0.83	0.83	0.84	0.87	0.83	0.85	0.85	0.84	0.82	0.80	0.83	0.84

Sample		BM-007	BM-007	BM-008	BM-008	BM-008	BM-008	BM-008	BM-008	BM-008	BM-008	BM-008	BM-010	BM-010	BM-010	BM-010
Drill Hole		FD-3	FD-3	FD-3	FD-3	FD-3	FD-3	FD-3	FD-3	FD-3	FD-3	FD-3	FD-3	FD-3	FD-3	FD-3
Rock Code		Wrlt	Wrlt	Wrlt	Wrlt	Wrlt	Wrlt	Wrlt	Wrlt	Wrlt	Wrlt	Wrlt	Wrlt	Wrlt	Wrlt	Wrlt
SiO2	wt.%	51.99	52.95	51.63	51.94	51.77	51.00	52.62	53.46	51.75	49.85	51.70	54.46	52.80	52.01	53.28
TiO2	wt.%	0.58	0.68	2.29	0.99	0.89	1.18	1.01	1.03	1.10	0.94	0.92	0.63	0.94	1.05	0.78
Al2O3	wt.%	1.76	1.92	2.06	2.56	2.53	2.43	2.46	2.06	2.37	2.35	2.43	1.41	2.13	2.23	1.69
FeO	wt.%	6.01	6.01	7.19	6.92	6.99	8.48	6.45	6.29	6.32	6.72	7.17	4.63	5.60	6.16	5.38
MnO	wt.%	0.23	0.11	0.26	0.07	0.18	0.10	0.28	0.22	0.19	0.12	0.12	0.17	0.18	0.15	0.15
MgO	wt.%	16.43	15.81	15.84	16.92	17.14	15.16	15.65	16.59	16.21	15.82	17.11	17.09	15.60	15.48	16.08
CaO	wt.%	21.19	22.24	21.46	20.23	19.46	21.23	21.30	21.59	20.60	19.64	20.07	21.23	21.77	21.75	22.48
Na2O	wt.%	0.39	0.34	0.29	0.30	0.38	0.38	0.40	0.31	0.37	0.26	0.39	0.24	0.32	0.33	0.29
Cr2O3	wt.%	N.A.	N.A.	N.A.	N.A.	N.A.	N.A.	N.A.	N.A.	N.A.	N.A.	N.A.	N.A.	N.A.	N.A.	N.A.
V2O3	wt.%	0.04	0.03	0.06	0.02	0.04	<0.01	0.06	0.07	0.09	0.03	0.02	0.02	0.08	0.06	0.08
NiO	wt.%	0.02	0.02	0.07	0.02	<0.01	<0.01	0.01	<0.01	<0.01	<0.01	0.04	<0.01	0.01	<0.01	<0.01
Total	wt.%	98.62	100.11	101.15	99.95	99.37	99.95	100.25	101.61	99.00	95.72	99.97	99.89	99.41	99.22	100.21
Na	ppm	0.03	0.02	0.02	0.02	0.03	0.03	0.03	0.02	0.03	0.02	0.03	0.02	0.02	0.02	0.02
Al	ppm	0.08	0.08	0.09	0.11	0.11	0.11	0.11	0.09	0.10	0.11	0.10	0.06	0.09	0.10	0.07
Mg	ppm	0.91	0.87	0.86	0.93	0.94	0.84	0.86	0.89	0.90	0.91	0.93	0.93	0.86	0.86	0.88
Si	ppm	1.93	1.94	1.89	1.91	1.91	1.89	1.93	1.93	1.92	1.91	1.89	1.99	1.95	1.93	1.95
Ca	ppm	0.84	0.87	0.84	0.80	0.77	0.84	0.84	0.84	0.82	0.81	0.79	0.83	0.86	0.86	0.88
Mn	ppm	0.01	<0.01	0.01	<0.01	0.01	<0.01	0.01	0.01	0.01	<0.01	<0.01	0.01	0.01	<0.01	<0.01
Ti	ppm	0.02	0.02	0.06	0.03	0.02	0.03	0.03	0.03	0.03	0.03	0.03	0.02	0.03	0.03	0.02
Fe2+	ppm	0.13	0.17	0.20	0.17	0.16	0.18	0.20	0.18	0.18	0.19	0.14	0.14	0.17	0.19	0.16
Fe3+	ppm	0.06	0.01	0.02	0.04	0.05	0.08	<0.01	0.01	0.02	0.03	0.08	<0.01	<0.01	0.01	0.00
Ni	ppm	<0.01	<0.01	<0.01	<0.01	<0.01	<0.01	<0.01	<0.01	<0.01	<0.01	<0.01	<0.01	<0.01	<0.01	<0.01
Cr	ppm	N.A.	N.A.	N.A.	N.A.	N.A.	N.A.	N.A.	N.A.	N.A.	N.A.	N.A.	N.A.	N.A.	N.A.	N.A.
Li	ppm	<0.01	<0.01	<0.01	<0.01	<0.01	<0.01	<0.01	<0.01	<0.01	<0.01	<0.01	<0.01	<0.01	<0.01	<0.01
Sc	ppm	<0.01	<0.01	<0.01	<0.01	<0.01	<0.01	<0.01	<0.01	<0.01	<0.01	<0.01	<0.01	<0.01	<0.01	<0.01
V	ppm	<0.01	<0.01	<0.01	<0.01	<0.01	<0.01	<0.01	<0.01	<0.01	<0.01	<0.01	<0.01	<0.01	<0.01	<0.01
Zn	ppm	<0.01	<0.01	<0.01	<0.01	<0.01	<0.01	<0.01	<0.01	<0.01	<0.01	<0.01	<0.01	<0.01	<0.01	<0.01
Zr	ppm	<0.01	<0.01	<0.01	<0.01	<0.01	<0.01	<0.01	<0.01	<0.01	<0.01	<0.01	<0.01	<0.01	<0.01	<0.01
Mg#		0.87	0.84	0.82	0.85	0.85	0.82	0.81	0.83	0.84	0.83	0.87	0.87	0.83	0.82	0.84

Sample		BM-010	BM-010	BM-010	BM-010	BM-010	BM-010	BM-030	BM-030	BM-030	BM-030	BM-030	BM-030	BM-030	BM-030	BM-030
Drill Hole		FD-3	FD-3	FD-3	FD-3	FD-3	FD-3	FD-6	FD-6	FD-6	FD-6	FD-6	FD-6	FD-6	FD-6	FD-6
Rock Code		Wrlt	Wrlt	Wrlt	Wrlt	Wrlt	Wrlt	Wrlt	Wrlt	Wrlt	Wrlt	Wrlt	Wrlt	Wrlt	Wrlt	Wrlt
SiO2	wt.%	53.85	54.27	53.31	52.34	53.29	52.23	51.27	52.22	51.26	50.87	51.98	51.09	50.94	51.21	52.06
TiO2	wt.%	0.67	0.66	0.79	1.06	0.98	1.08	0.71	0.85	0.95	0.96	0.96	0.91	0.72	0.86	0.79
Al2O3	wt.%	1.39	1.47	2.02	2.59	2.58	2.63	1.86	1.73	1.83	2.01	2.20	2.11	1.95	1.58	1.82
FeO	wt.%	5.50	5.62	6.08	5.49	5.96	5.59	5.29	5.36	5.71	5.75	5.70	5.39	5.48	5.24	5.51
MnO	wt.%	0.18	0.12	0.18	0.22	0.13	0.22	0.16	0.13	0.15	0.16	0.21	0.18	0.15	0.11	0.17
MgO	wt.%	16.81	16.62	15.62	15.89	16.08	16.26	15.15	15.46	15.06	15.03	15.38	14.76	16.48	15.38	15.13
CaO	wt.%	21.16	21.15	21.45	22.27	22.08	22.14	22.10	21.88	22.66	21.59	22.07	22.15	20.17	22.20	21.89
Na2O	wt.%	0.34	0.32	0.27	0.40	0.28	0.35	0.33	0.37	0.35	0.33	0.29	0.36	0.26	0.23	0.34
Cr2O3	wt.%	N.A.	N.A.	N.A.	N.A.	N.A.	N.A.	N.A.	N.A.	N.A.	N.A.	N.A.	N.A.	N.A.	N.A.	N.A.
V2O3	wt.%	0.08	0.03	0.02	0.06	0.01	0.02	0.05	0.02	0.02	0.02	0.11	0.07	<0.01	0.07	0.03
NiO	wt.%	<0.01	<0.01	<0.01	<0.01	<0.01	0.10	<0.01	0.07	0.04	<0.01	<0.01	<0.01	<0.01	0.01	<0.01
Total	wt.%	99.99	100.24	99.74	100.32	101.39	100.61	96.92	98.11	98.02	96.73	98.88	97.00	96.15	96.90	97.73
Na	ppm	0.02	0.02	0.02	0.03	0.02	0.02	0.02	0.03	0.03	0.02	0.02	0.03	0.02	0.02	0.02
Al	ppm	0.06	0.06	0.09	0.11	0.11	0.11	0.08	0.08	0.08	0.09	0.10	0.09	0.09	0.07	0.08
Mg	ppm	0.92	0.91	0.86	0.87	0.87	0.88	0.86	0.86	0.84	0.85	0.85	0.83	0.93	0.87	0.85
Si	ppm	1.97	1.98	1.97	1.91	1.93	1.90	1.94	1.96	1.93	1.94	1.94	1.94	1.94	1.94	1.96
Ca	ppm	0.83	0.83	0.85	0.87	0.86	0.86	0.90	0.88	0.91	0.88	0.88	0.90	0.82	0.90	0.88
Mn	ppm	0.01	<0.01	0.01	0.01	<0.01	0.01	0.01	<0.01	<0.01	0.01	0.01	0.01	<0.01	<0.01	0.01
Ti	ppm	0.02	0.02	0.02	0.03	0.03	0.03	0.02	0.02	0.03	0.03	0.03	0.03	0.02	0.02	0.02
Fe2+	ppm	0.17	0.17	0.19	0.14	0.18	0.13	0.16	0.17	0.14	0.18	0.18	0.17	0.16	0.16	0.17
Fe3+	ppm	<0.01	<0.01	<0.01	0.03	<0.01	0.04	0.01	<0.01	0.04	0.01	<0.01	<0.01	0.02	0.01	<0.01
Ni	ppm	<0.01	<0.01	<0.01	<0.01	<0.01	<0.01	<0.01	<0.01	<0.01	<0.01	<0.01	<0.01	<0.01	<0.01	<0.01
Cr	ppm	N.A.	N.A.	N.A.	N.A.	N.A.	N.A.	N.A.	N.A.	N.A.	N.A.	N.A.	N.A.	N.A.	N.A.	N.A.
Li	ppm	<0.01	<0.01	<0.01	<0.01	<0.01	<0.01	<0.01	<0.01	<0.01	<0.01	<0.01	<0.01	<0.01	<0.01	<0.01
Sc	ppm	<0.01	<0.01	<0.01	<0.01	<0.01	<0.01	<0.01	<0.01	<0.01	<0.01	<0.01	<0.01	<0.01	<0.01	<0.01
V	ppm	<0.01	<0.01	<0.01	<0.01	<0.01	<0.01	<0.01	<0.01	<0.01	<0.01	<0.01	<0.01	<0.01	<0.01	<0.01
Zn	ppm	<0.01	<0.01	<0.01	<0.01	<0.01	<0.01	<0.01	<0.01	<0.01	<0.01	<0.01	<0.01	<0.01	<0.01	<0.01
Zr	ppm	<0.01	<0.01	<0.01	<0.01	<0.01	<0.01	<0.01	<0.01	<0.01	<0.01	<0.01	<0.01	<0.01	<0.01	<0.01
Mg#		0.84	0.84	0.82	0.86	0.83	0.87	0.85	0.84	0.86	0.83	0.83	0.83	0.86	0.85	0.83

Sample		BM-030	BM-030	BM-030	BM-030	BM-030	BM-030	BM-030	BM-030	BM-031	BM-031	BM-031	BM-031	BM-031	BM-031	BM-031
Drill Hole		FD-6	FD-6	FD-6	FD-6	FD-6	FD-6	FD-6	FD-6	FD-6	FD-6	FD-6	FD-6	FD-6	FD-6	FD-6
Rock Code		Wrlt	Wrlt	Wrlt	Wrlt	Wrlt	Wrlt	Wrlt	Wrlt	Wrlt	Wrlt	Wrlt	Wrlt	Wrlt	Wrlt	Wrlt
SiO2	wt.%	50.84	53.40	51.85	52.02	53.22	53.25	52.21	52.99	51.43	48.87	50.97	52.96	52.25	52.18	52.76
TiO2	wt.%	0.67	0.75	0.95	0.62	0.66	0.69	0.80	0.80	1.00	0.79	0.92	0.31	0.61	0.70	0.75
Al2O3	wt.%	1.78	1.59	2.17	1.51	1.52	1.62	1.88	1.81	2.14	1.92	1.91	0.76	1.50	1.68	1.55
FeO	wt.%	5.57	5.77	6.74	7.81	5.74	6.18	7.32	6.21	6.72	6.00	5.13	4.01	4.87	4.96	4.55
MnO	wt.%	0.11	0.18	0.07	0.26	0.23	0.20	0.21	0.17	0.30	0.16	0.13	0.15	0.20	0.17	0.22
MgO	wt.%	16.34	16.31	15.82	15.21	16.16	15.97	15.77	16.10	15.24	15.80	14.90	16.06	16.01	15.81	15.74
CaO	wt.%	21.16	22.36	21.75	22.23	21.36	22.17	21.81	21.86	20.45	21.42	22.40	22.82	20.24	21.66	21.70
Na2O	wt.%	0.31	0.34	0.38	0.20	0.36	0.31	0.33	0.33	0.38	0.26	0.33	0.18	0.20	0.28	0.29
Cr2O3	wt.%	N.A.	N.A.	N.A.	N.A.	N.A.	N.A.	N.A.	N.A.	N.A.	N.A.	N.A.	N.A.	N.A.	N.A.	N.A.
V2O3	wt.%	0.07	<0.01	0.15	0.06	0.03	0.08	0.10	0.05	0.01	<0.01	<0.01	0.02	0.02	0.13	0.06
NiO	wt.%	0.03	<0.01	0.11	<0.01	0.03	<0.01	<0.01	0.04	<0.01	0.05	<0.01	0.07	0.09	<0.01	<0.01
Total	wt.%	96.88	100.70	99.97	99.91	99.31	100.45	100.42	100.36	97.67	95.27	96.71	97.32	95.99	97.56	97.62
Na	ppm	0.02	0.02	0.03	0.01	0.03	0.02	0.02	0.02	0.03	0.02	0.02	0.01	0.01	0.02	0.02
Al	ppm	0.08	0.07	0.09	0.07	0.07	0.07	0.08	0.08	0.10	0.09	0.09	0.03	0.07	0.07	0.07
Mg	ppm	0.92	0.89	0.87	0.84	0.89	0.87	0.86	0.88	0.86	0.91	0.84	0.90	0.91	0.89	0.88
Si	ppm	1.92	1.95	1.91	1.93	1.97	1.95	1.92	1.94	1.94	1.88	1.94	1.99	2.00	1.96	1.98
Ca	ppm	0.86	0.87	0.86	0.88	0.85	0.87	0.86	0.86	0.83	0.88	0.91	0.92	0.83	0.87	0.87
Mn	ppm	<0.01	0.01	<0.01	0.01	0.01	0.01	0.01	0.01	0.01	0.01	<0.01	<0.01	0.01	0.01	0.01
Ti	ppm	0.02	0.02	0.03	0.02	0.02	0.02	0.02	0.02	0.03	0.02	0.03	0.01	0.02	0.02	0.02
Fe2+	ppm	0.11	0.15	0.15	0.19	0.18	0.18	0.16	0.17	0.21	0.07	0.15	0.13	0.16	0.16	0.14
Fe3+	ppm	0.06	0.02	0.06	0.06	<0.01	0.01	0.06	0.02	<0.01	0.13	0.01	<0.01	<0.01	<0.01	<0.01
Ni	ppm	<0.01	<0.01	<0.01	<0.01	<0.01	<0.01	<0.01	<0.01	<0.01	<0.01	<0.01	<0.01	<0.01	<0.01	<0.01
Cr	ppm	N.A.	N.A.	N.A.	N.A.	N.A.	N.A.	N.A.	N.A.	N.A.	N.A.	N.A.	N.A.	N.A.	N.A.	N.A.
Li	ppm	<0.01	<0.01	<0.01	<0.01	<0.01	<0.01	<0.01	<0.01	<0.01	<0.01	<0.01	<0.01	<0.01	<0.01	<0.01
Sc	ppm	<0.01	<0.01	<0.01	<0.01	<0.01	<0.01	<0.01	<0.01	<0.01	<0.01	<0.01	<0.01	<0.01	<0.01	<0.01
V	ppm	<0.01	<0.01	<0.01	<0.01	<0.01	<0.01	<0.01	<0.01	<0.01	<0.01	<0.01	<0.01	<0.01	<0.01	<0.01
Zn	ppm	<0.01	<0.01	<0.01	<0.01	<0.01	<0.01	<0.01	<0.01	<0.01	<0.01	<0.01	<0.01	<0.01	<0.01	<0.01
Zr	ppm	<0.01	<0.01	<0.01	<0.01	<0.01	<0.01	<0.01	<0.01	<0.01	<0.01	<0.01	<0.01	<0.01	<0.01	<0.01
Mg#		0.89	0.85	0.85	0.82	0.83	0.83	0.84	0.84	0.80	0.93	0.85	0.88	0.85	0.85	0.86

Sample		BM-031	BM-031	BM-031	BM-031	BM-031	BM-031	BM-031	BM-031	BM-031	BM-031	BM-031	BM-038	BM-038	BM-038	BM-038
Drill Hole		FD-6	FD-6	FD-6	FD-6	FD-6	FD-6	FD-6	FD-6	FD-6	FD-6	FD-6	FD-12	FD-12	FD-12	FD-12
Rock Code		Wrlt	Wrlt	Wrlt	Wrlt	Wrlt	Wrlt	Wrlt	Wrlt	Wrlt	Wrlt	Wrlt	Wrlt	Wrlt	Wrlt	Wrlt
SiO2	wt.%	52.10	52.14	52.31	52.39	51.37	52.10	51.97	52.37	52.81	52.21	53.69	53.28	50.52	52.14	51.00
TiO2	wt.%	0.64	0.97	1.16	1.00	0.88	0.43	0.49	0.61	0.83	0.79	0.57	0.47	1.23	0.80	0.87
Al2O3	wt.%	1.30	1.97	2.13	2.01	1.93	1.39	1.58	1.57	1.59	2.12	1.59	1.71	1.85	2.20	2.63
FeO	wt.%	4.80	6.44	6.03	6.46	5.51	5.14	6.22	5.39	6.23	5.98	5.43	4.19	5.66	4.97	4.83
MnO	wt.%	0.22	0.30	0.18	0.13	0.19	0.19	0.08	0.16	0.20	0.14	0.11	0.16	0.18	0.08	0.16
MgO	wt.%	16.49	15.88	15.51	15.71	15.71	17.28	16.88	16.47	16.08	16.12	17.50	16.13	16.20	15.66	15.28
CaO	wt.%	21.52	21.45	22.47	21.90	21.34	21.32	20.27	20.87	21.50	21.63	20.39	22.82	21.36	21.85	21.52
Na2O	wt.%	0.22	0.26	0.33	0.32	0.24	0.20	0.35	0.30	0.39	0.35	0.26	0.28	0.27	0.34	0.39
Cr2O3	wt.%	N.A.	N.A.	N.A.	N.A.	N.A.	N.A.	N.A.	N.A.	N.A.	N.A.	N.A.	N.A.	N.A.	N.A.	N.A.
V2O3	wt.%	0.01	0.03	0.06	0.09	0.09	0.03	0.04	0.01	0.06	0.03	0.03	<0.01	<0.01	<0.01	0.10
NiO	wt.%	0.08	<0.01	0.06	0.07	<0.01	0.03	0.02	0.03	0.05	<0.01	<0.01	<0.01	<0.01	0.06	0.13
Total	wt.%	97.38	99.44	100.25	100.06	97.26	98.10	97.89	97.77	99.73	99.36	99.57	99.04	97.26	98.09	96.89
Na	ppm	0.02	0.02	0.02	0.02	0.02	0.01	0.03	0.02	0.03	0.03	0.02	0.02	0.02	0.02	0.03
Al	ppm	0.06	0.09	0.09	0.09	0.09	0.06	0.07	0.07	0.07	0.09	0.07	0.07	0.08	0.10	0.12
Mg	ppm	0.92	0.88	0.85	0.86	0.88	0.96	0.94	0.92	0.88	0.89	0.96	0.89	0.91	0.87	0.86
Si	ppm	1.96	1.93	1.92	1.93	1.94	1.94	1.94	1.96	1.95	1.93	1.97	1.97	1.91	1.95	1.93
Ca	ppm	0.87	0.85	0.88	0.86	0.86	0.85	0.81	0.84	0.85	0.86	0.80	0.90	0.86	0.87	0.87
Mn	ppm	0.01	0.01	0.01	<0.01	0.01	0.01	<0.01	<0.01	0.01	<0.01	<0.01	<0.01	0.01	<0.01	0.01
Ti	ppm	0.02	0.03	0.03	0.03	0.03	0.01	0.01	0.02	0.02	0.02	0.02	0.01	0.03	0.02	0.02
Fe2+	ppm	0.14	0.18	0.17	0.18	0.17	0.11	0.15	0.17	0.17	0.15	0.17	0.13	0.12	0.16	0.15
Fe3+	ppm	0.01	0.02	0.02	0.02	<0.01	0.05	0.04	<0.01	0.02	0.03	<0.01	<0.01	0.06	<0.01	<0.01
Ni	ppm	<0.01	<0.01	<0.01	<0.01	<0.01	<0.01	<0.01	<0.01	<0.01	<0.01	<0.01	<0.01	<0.01	<0.01	<0.01
Cr	ppm	N.A.	N.A.	N.A.	N.A.	N.A.	N.A.	N.A.	N.A.	N.A.	N.A.	N.A.	N.A.	N.A.	N.A.	N.A.
Li	ppm	<0.01	<0.01	<0.01	<0.01	<0.01	<0.01	<0.01	<0.01	<0.01	<0.01	<0.01	<0.01	<0.01	<0.01	<0.01
Sc	ppm	<0.01	<0.01	<0.01	<0.01	<0.01	<0.01	<0.01	<0.01	<0.01	<0.01	<0.01	<0.01	<0.01	<0.01	<0.01
V	ppm	<0.01	<0.01	<0.01	<0.01	<0.01	<0.01	<0.01	<0.01	<0.01	<0.01	<0.01	<0.01	<0.01	<0.01	<0.01
Zn	ppm	<0.01	<0.01	<0.01	<0.01	<0.01	<0.01	<0.01	<0.01	<0.01	<0.01	<0.01	<0.01	<0.01	<0.01	<0.01
Zr	ppm	<0.01	<0.01	<0.01	<0.01	<0.01	<0.01	<0.01	<0.01	<0.01	<0.01	<0.01	<0.01	<0.01	<0.01	<0.01
Mg#		0.87	0.83	0.84	0.83	0.84	0.90	0.86	0.84	0.84	0.85	0.85	0.87	0.88	0.85	0.85

Sample		BM-038	BM-038	BM-038	BM-038	BM-038	BM-038	XX-R-29	XX-R-29	XX-R-29	XX-R-29	XX-R-29	XX-R-29	XX-R-29
Drill Hole		FD-12	FD-12	FD-12	FD-12	FD-12	FD-12	FD-12	FD-12	FD-12	FD-12	FD-12	FD-12	FD-12
Rock Code		Wrlt	Wrlt	Wrlt	Wrlt	Wrlt	Wrlt	Wrlt	Wrlt	Wrlt	Wrlt	Wrlt	Wrlt	Wrlt
SiO2	wt.%	53.15	53.67	53.13	53.01	53.25	52.13	52.58	51.94	54.38	53.58	53.66	52.44	51.05
TiO2	wt.%	0.61	0.51	0.71	0.55	0.81	0.65	0.55	0.55	0.66	0.67	0.67	1.00	0.80
Al2O3	wt.%	1.60	1.30	1.97	1.89	1.93	1.61	1.64	2.11	1.10	1.78	1.60	2.86	1.82
FeO	wt.%	4.54	4.53	5.16	4.32	4.55	4.64	5.26	4.82	3.84	4.28	4.76	5.02	6.70
MnO	wt.%	0.07	0.14	0.16	0.14	0.10	0.16	0.13	0.07	0.19	0.07	0.17	0.16	0.19
MgO	wt.%	16.58	16.52	16.19	16.56	16.54	16.69	15.73	17.07	16.34	15.93	15.91	15.06	15.36
CaO	wt.%	23.24	23.41	22.98	22.66	23.32	23.12	22.57	21.22	23.63	23.04	23.16	22.40	22.30
Na2O	wt.%	0.34	0.27	0.33	0.34	0.34	0.32	0.36	0.27	0.27	0.27	0.34	0.36	0.27
Cr2O3	wt.%	N.A.	N.A.	N.A.	N.A.	N.A.	N.A.	N.A.	N.A.	N.A.	N.A.	N.A.	N.A.	N.A.
V2O3	wt.%	0.03	0.04	0.04	0.04	<0.01	0.06	0.04	<0.01	0.05	<0.01	0.06	0.02	0.04
NiO	wt.%	0.03	<0.01	<0.01	0.05	0.07	<0.01	0.01	<0.01	<0.01	<0.01	<0.01	0.05	0.10	0.02
Total	wt.%	100.19	100.39	100.66	99.56	100.89	99.37	98.90	98.05	100.45	99.62	100.40	99.42	98.55
Na	*	0.02	0.02	0.02	0.02	0.02	0.02	0.03	0.02	0.02	0.02	0.02	0.03	0.02
Al	*	0.07	0.06	0.08	0.08	0.08	0.07	0.07	0.09	0.05	0.08	0.07	0.12	0.08
Mg	*	0.90	0.90	0.88	0.91	0.89	0.91	0.87	0.95	0.89	0.87	0.87	0.83	0.86
Si	*	1.94	1.96	1.93	1.94	1.93	1.92	1.95	1.93	1.98	1.97	1.96	1.94	1.91
Ca	*	0.91	0.91	0.90	0.89	0.91	0.91	0.90	0.84	0.92	0.91	0.91	0.89	0.89
Mn	*	<0.01	<0.01	<0.01	<0.01	<0.01	<0.01	<0.01	<0.01	0.01	<0.01	0.01	<0.01	0.01
Ti	*	0.02	0.01	0.02	0.02	0.02	0.02	0.02	0.02	0.02	0.02	0.02	0.03	0.02
Fe2+	*	0.09	0.12	0.13	0.11	0.10	0.06	0.14	0.11	0.12	0.13	0.15	0.16	0.14
Fe3+	*	0.04	0.02	0.03	0.02	0.04	0.08	0.02	0.04	<0.01	<0.01	<0.01	<0.01	0.07
Ni	*	<0.01	<0.01	<0.01	<0.01	<0.01	<0.01	<0.01	<0.01	<0.01	<0.01	<0.01	<0.01	<0.01
Cr	*	N.A.	N.A.	N.A.	N.A.	N.A.	N.A.	N.A.	N.A.	N.A.	N.A.	N.A.	N.A.	N.A.
Li	*	<0.01	<0.01	<0.01	<0.01	<0.01	<0.01	<0.01	<0.01	<0.01	<0.01	<0.01	<0.01	<0.01
Sc	*	<0.01	<0.01	<0.01	<0.01	<0.01	<0.01	<0.01	<0.01	<0.01	<0.01	<0.01	<0.01	<0.01
V	*	<0.01	<0.01	<0.01	<0.01	<0.01	<0.01	<0.01	<0.01	<0.01	<0.01	<0.01	<0.01	<0.01
Zn	*	<0.01	<0.01	<0.01	<0.01	<0.01	<0.01	<0.01	<0.01	<0.01	<0.01	<0.01	<0.01	<0.01
Zr	*	<0.01	<0.01	<0.01	<0.01	<0.01	<0.01	<0.01	<0.01	<0.01	<0.01	<0.01	<0.01	<0.01
Mg#	*	0.90	0.89	0.87	0.89	0.90	0.94	0.86	0.89	0.88	0.87	0.86	0.84	0.86

Appendix 2: Amphibole compositions.

Sample		BM-013	BM-013	BM-016	BM-016	BM-016	XX-R-16	XX-R-16	XX-R-16	XX-R-16	BM-011	BM-011	BM-011	BM-011
Drill Hole		FD-9	FD-9	FD-9	FD-9	FD-9	FD-5	FD-5	FD-5	FD-5	FD-3	FD-3	FD-3	FD-3
Rock Code		Cpxt	Cpxt	Cpxt	Cpxt	Cpxt	Cpxt	Cpxt	Cpxt	Cpxt	Cpxt	Cpxt	Cpxt	Cpxt
SiO2	wt.%	58.20	58.44	56.51	56.42	55.87	59.07	57.97	58.27	58.59	57.28	56.44	57.28	57.43
TiO2	wt.%	0.04	0.07	0.10	0.04	0.02	<0.01	<0.01	<0.01	0.03	<0.01	0.01	0.02	<0.01
Al2O3	wt.%	0.16	0.09	1.56	1.34	1.06	0.02	0.05	0.02	0.07	0.21	0.25	0.27	0.05
FeO	wt.%	6.51	6.62	8.65	8.87	8.91	6.63	7.68	7.03	7.74	5.67	7.50	6.42	5.70
MnO	wt.%	0.15	0.13	0.19	0.23	0.21	0.16	0.18	0.13	0.30	0.11	0.08	0.12	0.15
MgO	wt.%	20.70	20.12	18.35	17.79	18.01	20.57	20.43	20.19	20.33	20.88	19.85	20.39	21.18
CaO	wt.%	12.80	12.71	11.85	12.27	12.56	12.82	12.38	12.17	12.15	12.91	12.47	12.78	12.86
Na2O	wt.%	0.09	0.12	0.54	0.32	0.22	0.00	0.08	0.06	0.05	0.05	0.05	0.12	0.07
K2O	wt.%	0.09	0.04	0.08	0.10	0.07	0.03	<0.01	0.05	<0.01	0.05	0.09	0.06	0.06
F	wt.%	<0.01	<0.01	<0.01	<0.01	<0.01	<0.01	<0.01	<0.01	<0.01	<0.01	<0.01	<0.01	<0.01
Cl	wt.%	0.01	0.02	<0.01	<0.01	0.05	<0.01	<0.01	0.01	0.02	0.01	<0.01	<0.01	<0.01
V2O3	wt.%	<0.01	0.04	0.05	0.03	0.04	0.04	<0.01	<0.01	0.04	<0.01	0.03	<0.01	<0.01
NiO	wt.%	0.06	<0.01	<0.01	0.01	0.01	0.01	0.04	<0.01	0.02	<0.01	<0.01	0.07	<0.01
Total	wt.%	98.81	98.40	97.87	97.42	97.03	99.35	98.80	97.94	99.35	97.17	96.75	97.50	97.49
OH	ppm	2.00	2.00	2.00	2.00	1.99	2.00	2.00	2.00	2.00	2.00	2.00	2.00	2.00
Cl	ppm	<0.01	<0.01	<0.01	<0.01	0.01	<0.01	<0.01	<0.01	<0.01	<0.01	<0.01	<0.01	<0.01
F	ppm	<0.01	<0.01	<0.01	<0.01	<0.01	<0.01	<0.01	<0.01	<0.01	<0.01	<0.01	<0.01	<0.01
Si	ppm	8.01	8.07	7.93	7.96	7.94	8.07	8.01	8.08	8.04	7.99	7.98	7.99	7.99
Al	ppm	0.03	0.02	0.26	0.22	0.18	<0.01	0.01	<0.01	0.01	0.03	0.04	0.04	0.01
Ti	ppm	<0.01	0.01	0.01	<0.01	<0.01	<0.01	<0.01	<0.01	<0.01	<0.01	<0.01	<0.01	<0.01
V	ppm	<0.01	<0.01	0.01	<0.01	<0.01	<0.01	<0.01	<0.01	<0.01	<0.01	<0.01	<0.01	<0.01
Sc	ppm	<0.01	<0.01	<0.01	<0.01	<0.01	<0.01	<0.01	<0.01	<0.01	<0.01	<0.01	<0.01	<0.01
Cr	ppm	<0.01	<0.01	<0.01	<0.01	<0.01	<0.01	<0.01	<0.01	<0.01	<0.01	<0.01	<0.01	<0.01
Mn3+	ppm	<0.01	<0.01	<0.01	<0.01	<0.01	<0.01	<0.01	<0.01	<0.01	<0.01	<0.01	<0.01	<0.01
Zr	ppm	<0.01	<0.01	<0.01	<0.01	<0.01	<0.01	<0.01	<0.01	<0.01	<0.01	<0.01	<0.01	<0.01
Mg	ppm	4.25	4.14	3.84	3.74	3.82	4.19	4.21	4.18	4.16	4.35	4.18	4.24	4.39
Zn	ppm	<0.01	<0.01	<0.01	<0.01	<0.01	<0.01	<0.01	<0.01	<0.01	<0.01	<0.01	<0.01	<0.01
Ni	ppm	0.01	<0.01	<0.01	<0.01	<0.01	<0.01	<0.01	<0.01	<0.01	<0.01	<0.01	0.01	<0.01
Co	ppm	<0.01	<0.01	<0.01	<0.01	<0.01	<0.01	<0.01	<0.01	<0.01	<0.01	<0.01	<0.01	<0.01
Fe2+	ppm	0.75	0.76	1.01	1.05	1.06	0.76	0.89	0.82	0.89	0.66	0.89	0.75	0.66
Mn2+	ppm	0.02	0.02	0.02	0.03	0.03	0.02	0.02	0.01	0.04	0.01	0.01	0.01	0.02
Li	ppm	<0.01	<0.01	<0.01	<0.01	<0.01	<0.01	<0.01	<0.01	<0.01	<0.01	<0.01	<0.01	<0.01
Ca	ppm	1.89	1.88	1.78	1.86	1.91	1.88	1.83	1.81	1.79	1.93	1.89	1.91	1.92
Sr	ppm	<0.01	<0.01	<0.01	<0.01	<0.01	<0.01	<0.01	<0.01	<0.01	<0.01	<0.01	<0.01	<0.01
Ba	ppm	<0.01	<0.01	<0.01	<0.01	<0.01	<0.01	<0.01	<0.01	<0.01	<0.01	<0.01	<0.01	<0.01
Na	ppm	0.03	0.03	0.15	0.09	0.06	<0.01	0.02	0.02	0.01	0.01	0.01	0.03	0.02
K	ppm	0.02	0.01	0.02	0.02	0.01	<0.01	<0.01	0.01	<0.01	0.01	0.02	0.01	0.01
Rb	ppm	<0.01	<0.01	<0.01	<0.01	<0.01	<0.01	<0.01	<0.01	<0.01	<0.01	<0.01	<0.01	<0.01
Cs	ppm	<0.01	<0.01	<0.01	<0.01	<0.01	<0.01	<0.01	<0.01	<0.01	<0.01	<0.01	<0.01	<0.01
Mg#		0.85	0.84	0.79	0.78	0.78	0.85	0.83	0.84	0.82	0.87	0.83	0.85	0.87

Sample		BM-019	BM-019	BM-042	BM-042	BM-042	BM-042	BM-042	BM-027	BM-027	BM-027	BM-009	BM-009	BM-010
Drill Hole		FD-9	FD-9	FD-5	FD-5	FD-5	FD-5	FD-5	FD-6	FD-6	FD-6	FD-3	FD-3	FD-3
Rock Code		Cpxt	Cpxt	Cpxt	Cpxt	Cpxt	Cpxt	Cpxt	Cpxt	Cpxt	Cpxt	Ol-Cpxt	Ol-Cpxt	Wrlt
SiO2	wt.%	57.95	58.42	57.54	57.67	56.20	58.45	57.65	58.06	57.66	56.98	55.60	56.62	58.30
TiO2	wt.%	0.04	<0.01	<0.01	<0.01	0.09	0.01	<0.01	<0.01	<0.01	<0.01	0.03	0.03	<0.01
Al2O3	wt.%	0.09	0.07	0.18	0.13	1.84	0.04	0.06	0.12	0.14	0.09	0.50	0.10	0.11
FeO	wt.%	5.93	5.39	7.71	6.63	6.57	6.43	7.51	6.46	5.81	5.72	5.61	5.40	5.94
MnO	wt.%	0.01	0.20	0.17	0.14	0.21	0.13	0.13	0.19	0.19	0.09	0.17	0.18	0.17
MgO	wt.%	21.21	21.70	19.84	20.12	20.25	20.57	20.02	19.98	19.88	19.96	20.32	19.91	20.88
CaO	wt.%	12.70	12.80	12.66	12.77	12.54	13.13	12.71	12.97	12.88	13.12	12.66	12.80	12.50
Na2O	wt.%	0.08	0.11	0.03	0.15	0.35	0.02	0.23	0.05	0.12	0.06	0.06	0.14	0.02
K2O	wt.%	0.09	0.05	0.05	0.03	<0.01	0.03	0.03	0.06	0.06	0.03	0.05	0.06	0.07
F	wt.%	<0.01	<0.01	<0.01	<0.01	<0.01	<0.01	<0.01	<0.01	<0.01	<0.01	<0.01	<0.01	<0.01
Cl	wt.%	0.01	<0.01	<0.01	0.07	0.01	0.01	0.01	0.01	<0.01	0.02	<0.01	<0.01	<0.01
V2O3	wt.%	0.01	<0.01	0.04	0.02	0.09	0.03	<0.01	0.03	<0.01	0.05	0.02	<0.01	0.01
NiO	wt.%	<0.01	<0.01	<0.01	<0.01	0.04	0.07	0.03	<0.01	0.09	0.01	<0.01	0.04	0.01
Total	wt.%	98.11	98.73	98.22	97.73	98.19	98.91	98.37	97.89	96.82	96.12	95.02	95.28	97.98
OH	ppm	2.00	2.00	2.00	1.98	2.00	2.00	2.00	2.00	2.00	1.99	2.00	2.00	2.00
Cl	ppm	<0.01	<0.01	<0.01	0.02	<0.01	<0.01	<0.01	<0.01	<0.01	0.01	<0.01	<0.01	<0.01
F	ppm	<0.01	<0.01	<0.01	<0.01	<0.01	<0.01	<0.01	<0.01	<0.01	<0.01	<0.01	<0.01	<0.01
Si	ppm	8.01	8.01	8.01	8.04	7.81	8.03	8.01	8.06	8.07	8.04	7.95	8.05	8.05
Al	ppm	0.01	0.01	0.03	0.02	0.30	0.01	0.01	0.02	0.02	0.01	0.08	0.02	0.02
Ti	ppm	<0.01	<0.01	<0.01	<0.01	0.01	<0.01	<0.01	<0.01	<0.01	<0.01	<0.01	<0.01	<0.01
V	ppm	<0.01	<0.01	<0.01	<0.01	0.01	<0.01	<0.01	<0.01	<0.01	0.01	<0.01	<0.01	<0.01
Sc	ppm	<0.01	<0.01	<0.01	<0.01	<0.01	<0.01	<0.01	<0.01	<0.01	<0.01	<0.01	<0.01	<0.01
Cr	ppm	<0.01	<0.01	<0.01	<0.01	<0.01	<0.01	<0.01	<0.01	<0.01	<0.01	<0.01	<0.01	<0.01
Mn3+	ppm	<0.01	<0.01	<0.01	<0.01	<0.01	<0.01	<0.01	<0.01	<0.01	<0.01	<0.01	<0.01	<0.01
Zr	ppm	<0.01	<0.01	<0.01	<0.01	<0.01	<0.01	<0.01	<0.01	<0.01	<0.01	<0.01	<0.01	<0.01
Mg	ppm	4.37	4.43	4.12	4.18	4.19	4.22	4.15	4.13	4.15	4.20	4.33	4.22	4.30
Zn	ppm	<0.01	<0.01	<0.01	<0.01	<0.01	<0.01	<0.01	<0.01	<0.01	<0.01	<0.01	<0.01	<0.01
Ni	ppm	<0.01	<0.01	<0.01	<0.01	<0.01	0.01	<0.01	<0.01	0.01	<0.01	<0.01	<0.01	<0.01
Co	ppm	<0.01	<0.01	<0.01	<0.01	<0.01	<0.01	<0.01	<0.01	<0.01	<0.01	<0.01	<0.01	<0.01
Fe2+	ppm	0.69	0.62	0.90	0.77	0.76	0.74	0.87	0.75	0.68	0.67	0.67	0.64	0.69
Mn2+	ppm	<0.01	0.02	0.02	0.02	0.02	0.01	0.02	0.02	0.02	0.01	0.02	0.02	0.02
Li	ppm	<0.01	<0.01	<0.01	<0.01	<0.01	<0.01	<0.01	<0.01	<0.01	<0.01	<0.01	<0.01	<0.01
Ca	ppm	1.88	1.88	1.89	1.91	1.87	1.93	1.89	1.93	1.93	1.99	1.94	1.95	1.85
Sr	ppm	<0.01	<0.01	<0.01	<0.01	<0.01	<0.01	<0.01	<0.01	<0.01	<0.01	<0.01	<0.01	<0.01
Ba	ppm	<0.01	<0.01	<0.01	<0.01	<0.01	<0.01	<0.01	<0.01	<0.01	<0.01	<0.01	<0.01	<0.01
Na	ppm	0.02	0.03	0.01	0.04	0.10	0.01	0.06	0.01	0.03	0.02	0.02	0.04	0.01
K	ppm	0.02	0.01	0.01	0.01	<0.01	0.01	<0.01	0.01	0.01	0.01	0.01	0.01	0.01
Rb	ppm	<0.01	<0.01	<0.01	<0.01	<0.01	<0.01	<0.01	<0.01	<0.01	<0.01	<0.01	<0.01	<0.01
Cs	ppm	<0.01	<0.01	<0.01	<0.01	<0.01	<0.01	<0.01	<0.01	<0.01	<0.01	<0.01	<0.01	<0.01
Mg#		0.86	0.88	0.82	0.84	0.85	0.85	0.83	0.85	0.86	0.86	0.87	0.87	0.86

Sample		BM-010	BM-010	BM-010	BM-010	BM-010	XX-R-029	XX-R-029	BM-007	BM-007	BM-007	BM-007	BM-007	BM-008
Drill Hole		FD-3	FD-3	FD-3	FD-3	FD-3	FD-12	FD-12	FD-3	FD-3	FD-3	FD-3	FD-3	FD-3
Rock Code		Wrlt	Wrlt	Wrlt	Wrlt	Wrlt	Wrlt	Wrlt	Wrlt	Wrlt	Wrlt	Wrlt	Wrlt	Wrlt
SiO2	wt.%	57.85	58.77	58.12	57.53	57.39	58.71	58.92	58.06	58.64	56.47	58.57	58.00	58.15
TiO2	wt.%	0.03	<0.01	0.04	0.13	0.06	0.04	<0.01	0.05	<0.01	0.09	<0.01	0.01	0.04
Al2O3	wt.%	0.06	0.10	0.13	0.27	0.17	0.08	0.04	0.15	0.04	0.08	0.08	0.11	0.06
FeO	wt.%	5.44	5.38	5.85	5.86	6.27	4.65	4.08	5.60	4.30	7.69	4.48	5.71	4.48
MnO	wt.%	0.09	0.18	0.29	0.24	0.21	0.07	0.19	0.10	0.15	0.17	0.12	0.14	0.20
MgO	wt.%	20.93	21.08	20.71	20.62	20.60	22.08	21.95	21.20	21.84	20.60	21.99	21.74	21.37
CaO	wt.%	13.06	12.84	12.77	12.71	12.65	13.35	13.50	12.95	13.44	12.59	13.20	13.11	13.38
Na2O	wt.%	0.07	0.12	0.09	0.14	0.12	0.02	0.00	0.01	0.05	0.00	0.04	0.00	0.04
K2O	wt.%	0.01	0.04	0.05	0.05	0.08	0.01	0.01	0.02	<0.01	0.01	0.03	<0.01	<0.01
F	wt.%	<0.01	<0.01	<0.01	<0.01	<0.01	<0.01	<0.01	<0.01	<0.01	<0.01	<0.01	<0.01	<0.01
Cl	wt.%	<0.01	0.02	0.00	<0.01	0.02	<0.01	<0.01	<0.01	0.02	0.02	<0.01	0.01	<0.01
V2O3	wt.%	0.02	0.03	<0.01	<0.01	0.06	0.02	0.01	0.02	0.01	<0.01	0.02	<0.01	0.06
NiO	wt.%	0.16	<0.01	<0.01	0.09	<0.01	<0.01	0.02	0.02	<0.01	0.02	0.03	0.03	0.02
Total	wt.%	97.71	98.55	98.04	97.62	97.62	99.03	98.73	98.17	98.48	97.71	98.54	98.87	97.79
OH	ppm	2.00	2.00	2.00	2.00	1.99	2.00	2.00	2.00	2.00	2.00	2.00	2.00	2.00
Cl	ppm	<0.01	<0.01	<0.01	<0.01	0.01	<0.01	<0.01	<0.01	<0.01	<0.01	<0.01	<0.01	<0.01
F	ppm	<0.01	<0.01	<0.01	<0.01	<0.01	<0.01	<0.01	<0.01	<0.01	<0.01	<0.01	<0.01	<0.01
Si	ppm	8.02	8.06	8.04	8.00	8.00	8.00	8.03	8.01	8.02	7.92	8.01	7.96	8.02
Al	ppm	0.01	0.02	0.02	0.04	0.03	0.01	0.01	0.02	0.01	0.01	0.01	0.02	0.01
Ti	ppm	<0.01	<0.01	<0.01	0.01	0.01	<0.01	<0.01	0.01	<0.01	0.01	<0.01	<0.01	<0.01
V	ppm	<0.01	<0.01	<0.01	<0.01	0.01	<0.01	<0.01	<0.01	<0.01	<0.01	<0.01	<0.01	0.01
Sc	ppm	<0.01	<0.01	<0.01	<0.01	<0.01	<0.01	<0.01	<0.01	<0.01	<0.01	<0.01	<0.01	<0.01
Cr	ppm	<0.01	<0.01	<0.01	<0.01	<0.01	<0.01	<0.01	<0.01	<0.01	<0.01	<0.01	<0.01	<0.01
Mn3+	ppm	<0.01	<0.01	<0.01	<0.01	<0.01	<0.01	<0.01	<0.01	<0.01	<0.01	<0.01	<0.01	<0.01
Zr	ppm	<0.01	<0.01	<0.01	<0.01	<0.01	<0.01	<0.01	<0.01	<0.01	<0.01	<0.01	<0.01	<0.01
Mg	ppm	4.33	4.31	4.27	4.27	4.28	4.49	4.46	4.36	4.46	4.31	4.48	4.45	4.40
Zn	ppm	<0.01	<0.01	<0.01	<0.01	<0.01	<0.01	<0.01	<0.01	<0.01	<0.01	<0.01	<0.01	<0.01
Ni	ppm	0.02	<0.01	<0.01	0.01	<0.01	<0.01	<0.01	<0.01	<0.01	<0.01	<0.01	<0.01	<0.01
Co	ppm	<0.01	<0.01	<0.01	<0.01	<0.01	<0.01	<0.01	<0.01	<0.01	<0.01	<0.01	<0.01	<0.01
Fe2+	ppm	0.63	0.62	0.68	0.68	0.73	0.53	0.47	0.65	0.49	0.90	0.51	0.65	0.52
Mn2+	ppm	0.01	0.02	0.03	0.03	0.03	0.01	0.02	0.01	0.02	0.02	0.01	0.02	0.02
Li	ppm	<0.01	<0.01	<0.01	<0.01	<0.01	<0.01	<0.01	<0.01	<0.01	<0.01	<0.01	<0.01	<0.01
Ca	ppm	1.94	1.89	1.89	1.89	1.89	1.95	1.97	1.91	1.97	1.89	1.93	1.93	1.98
Sr	ppm	<0.01	<0.01	<0.01	<0.01	<0.01	<0.01	<0.01	<0.01	<0.01	<0.01	<0.01	<0.01	<0.01
Ba	ppm	<0.01	<0.01	<0.01	<0.01	<0.01	<0.01	<0.01	<0.01	<0.01	<0.01	<0.01	<0.01	<0.01
Na	ppm	0.02	0.03	0.02	0.04	0.03	0.01	<0.01	<0.01	0.01	<0.01	0.01	<0.01	0.01
K	ppm	<0.01	0.01	0.01	0.01	0.01	<0.01	<0.01	<0.01	<0.01	<0.01	<0.01	<0.01	<0.01
Rb	ppm	<0.01	<0.01	<0.01	<0.01	<0.01	<0.01	<0.01	<0.01	<0.01	<0.01	<0.01	<0.01	<0.01
Cs	ppm	<0.01	<0.01	<0.01	<0.01	<0.01	<0.01	<0.01	<0.01	<0.01	<0.01	<0.01	<0.01	<0.01
Mg#		0.87	0.87	0.86	0.86	0.85	0.89	0.91	0.87	0.90	0.83	0.90	0.87	0.89

Appendix 3: Sulfide compositions.

- Pyrrhotite:

Sample		BM-038	BM-038	BM-038	BM-038	BM-013	BM-013	XX-R-16	XX-R-16	BM-042	BM-042	BM-042	BM-042	BM-041
Drill Hole		FD-12	FD-12	FD-12	FD-12	FD-9	FD-9	FD-5	FD-5	FD-5	FD-5	FD-5	FD-5	FD-5
Rock Code		Wrlt	Wrlt	Wrlt	Wrlt	Cpxt	Cpxt	Cpxt	Cpxt	Cpxt	Cpxt	Cpxt	Cpxt	Wrlt
Mineral		Po	Po	Po	Po	Po	Po	Po	Po	Po	Po	Po	Po	Po
As	wt.%	<0.01	<0.01	<0.01	<0.01	<0.01	<0.01	<0.01	<0.01	<0.01	<0.01	<0.01	<0.01	<0.01
Zn	wt.%	0.01	<0.01	<0.01	<0.01	0.01	<0.01	<0.01	<0.01	<0.01	<0.01	<0.01	0.03	<0.01
S	wt.%	39.85	40.22	38.36	40.02	40.51	40.58	40.73	38.36	39.56	39.33	39.66	39.36	38.94
Pb	wt.%	0.21	0.11	0.11	0.10	0.14	0.06	0.17	0.11	0.15	0.23	0.07	0.14	0.07
Fe	wt.%	52.39	50.83	52.27	54.35	55.67	55.30	56.40	54.65	58.32	58.16	58.62	57.65	58.26
Cu	wt.%	<0.01	<0.01	0.12	0.21	<0.01	<0.01	<0.01	<0.01	<0.01	<0.01	<0.01	<0.01	<0.01
Pt	wt.%	<0.01	<0.01	<0.01	0.01	<0.01	<0.01	<0.01	<0.01	<0.01	<0.01	<0.01	<0.01	<0.01
Cr	wt.%	0.02	0.05	0.62	0.04	0.01	<0.01	<0.01	<0.01	0.01	<0.01	<0.01	<0.01	0.03
Co	wt.%	0.04	0.13	0.06	0.10	0.05	0.10	0.08	0.03	0.08	0.11	0.09	0.09	0.12
Ni	wt.%	2.27	2.94	2.20	2.78	1.56	2.31	0.57	1.13	0.66	0.36	0.38	0.40	0.51
Total	wt.%	94.78	94.28	93.74	97.61	97.95	98.34	97.94	94.27	98.77	98.19	98.83	97.66	97.93

Sample		BM-041	BM-041	BM-041	BM-027	BM-027	BM-027	BM-027	BM-009	BM-009	BM-030	BM-030	BM-010	BM-010
Drill Hole		FD-5	FD-5	FD-5	FD-6	FD-6	FD-6	FD-6	FD-3	FD-3	FD-6	FD-6	FD-3	FD-3
Rock Code		Wrlt	Wrlt	Wrlt	Cpxt	Cpxt	Cpxt	Cpxt	Ol-Cpxt	Ol-Cpxt	Wrlt	Wrlt	Wrlt	Wrlt
Mineral		Po	Po	Po	Po	Po	Po	Po	Po	Po	Po	Po	Po	Po
As	wt.%	<0.01	<0.01	<0.01	<0.01	<0.01	<0.01	<0.01	<0.01	<0.01	<0.01	<0.01	<0.01	<0.01
Zn	wt.%	0.02	0.01	0.01	<0.01	<0.01	<0.01	<0.01	0.05	0.09	<0.01	<0.01	<0.01	<0.01
S	wt.%	39.08	38.88	39.17	37.66	38.17	38.32	38.88	40.48	39.66	37.67	37.67	38.98	39.17
Pb	wt.%	0.18	0.14	0.19	0.07	0.17	0.06	0.16	0.13	0.11	0.12	0.12	0.13	0.20
Fe	wt.%	57.81	58.47	57.36	58.71	59.21	59.62	58.87	56.05	56.81	58.91	58.91	58.74	58.26
Cu	wt.%	0.29	0.04	0.02	<0.01	<0.01	0.03	<0.01	0.02	<0.01	0.05	0.05	<0.01	<0.01
Pt	wt.%	<0.01	<0.01	0.02	<0.01	<0.01	<0.01	<0.01	<0.01	<0.01	<0.01	<0.01	<0.01	<0.01
Cr	wt.%	<0.01	<0.01	0.02	0.01	<0.01	<0.01	<0.01	<0.01	0.01	<0.01	<0.01	<0.01	0.01
Co	wt.%	0.13	0.07	0.08	0.06	0.07	0.09	0.08	0.07	0.06	0.09	0.09	0.06	0.07
Ni	wt.%	0.54	0.38	0.48	0.63	0.64	0.16	0.32	0.86	0.48	0.39	0.39	0.47	0.51
Total	wt.%	98.04	97.97	97.34	97.13	98.26	98.28	98.31	97.65	97.22	97.22	97.22	98.38	98.22

Sample		BM-010	BM-010	BM-041	BM-041	BM-042	BM-042	BM-042	BM-042	BM-013	BM-013	BM-013	XX-R-30	BM-033
Drill Hole		FD-3	FD-3	FD-5	FD-5	FD-5	FD-5	FD-5	FD-5	FD-9	FD-9	FD-9	FD-12	FD-12
Rock Code		Wrlt	Wrlt	Wrlt	Wrlt	Cpxt	Cpxt	Cpxt	Cpxt	Cpxt	Cpxt	Cpxt	Dun	Ol-Cpxt
Mineral		Po	Po	Po	Po	Po	Po	Po	Po	Po	Po	Po	Po	Po
As	wt.%	<0.01	<0.01	<0.01	<0.01	<0.01	<0.01	<0.01	<0.01	<0.01	<0.01	<0.01	<0.01	<0.01
Zn	wt.%	<0.01	<0.01	0.01	0.01	0.05	<0.01	<0.01	0.03	0.01	<0.01	<0.01	0.06	0.08
S	wt.%	39.19	39.07	38.38	38.25	39.10	39.21	38.86	38.97	38.92	38.11	39.85	48.24	34.83
Pb	wt.%	0.14	0.03	0.20	0.03	0.09	0.15	0.16	0.15	0.16	0.14	0.05	0.08	0.16
Fe	wt.%	57.90	58.20	57.80	58.16	58.77	58.76	58.80	58.56	57.75	62.41	61.17	50.43	60.71
Cu	wt.%	<0.01	<0.01	<0.01	<0.01	<0.01	<0.01	<0.01	<0.01	<0.01	<0.01	<0.01	0.08	0.02
Pt	wt.%	<0.01	<0.01	<0.01	0.01	<0.01	<0.01	<0.01	<0.01	<0.01	<0.01	<0.01	<0.01	0.01
Cr	wt.%	0.02	<0.01	0.02	<0.01	<0.01	0.01	<0.01	0.01	<0.01	<0.01	<0.01	<0.01	0.03
Co	wt.%	0.12	0.08	0.09	0.05	0.06	0.07	0.09	0.06	0.10	0.14	0.06	0.06	0.07
Ni	wt.%	0.65	0.64	0.46	0.49	0.57	0.44	0.29	0.32	0.70	0.75	0.51	0.38	0.45
Total	wt.%	98.01	98.01	96.95	97.00	98.63	98.64	98.20	98.08	97.63	101.55	101.64	99.33	96.36

Sample		BM-033	XX-R-03	XX-R-03	XX-R-03	XX-R-03	XX-R-03	XX-R-03	XX-R-03	XX-R-03	XX-R-03	XX-R-03	XX-R-03	XX-R-03
Drill Hole		FD-12	FD-2	FD-2	FD-2	FD-2	FD-2	FD-2	FD-2	FD-2	FD-2	FD-2	FD-2	FD-2
Rock Code		Ol-Cpxt	Cpxt	Cpxt	Cpxt	Cpxt	Cpxt	Cpxt	Cpxt	Cpxt	Cpxt	Cpxt	Cpxt	Cpxt
Mineral		Po	Po	Po	Po	Po	Po	Po	Po	Po	Po	Po	Po	Po
As	wt.%	<0.01	<0.01	<0.01	<0.01	<0.01	<0.01	<0.01	<0.01	<0.01	<0.01	<0.01	<0.01	<0.01
Zn	wt.%	<0.01	<0.01	<0.01	0.09	0.13	<0.01	<0.01	<0.01	<0.01	0.09	0.13	<0.01	<0.01
S	wt.%	39.87	38.75	39.21	38.11	39.88	38.37	38.52	38.75	39.21	38.11	39.88	38.37	38.52
Pb	wt.%	0.14	0.08	0.13	0.15	0.19	0.17	0.07	0.08	0.13	0.15	0.19	0.17	0.07
Fe	wt.%	60.77	57.22	57.22	58.76	56.34	56.87	58.64	57.22	57.22	58.76	56.34	56.87	58.64
Cu	wt.%	<0.01	<0.01	<0.01	<0.01	<0.01	<0.01	<0.01	<0.01	<0.01	<0.01	<0.01	<0.01	<0.01
Pt	wt.%	<0.01	<0.01	<0.01	<0.01	<0.01	<0.01	<0.01	<0.01	<0.01	<0.01	<0.01	<0.01	<0.01
Cr	wt.%	<0.01	<0.01	0.03	<0.01	<0.01	0.01	0.01	<0.01	0.03	<0.01	<0.01	0.01	0.01
Co	wt.%	0.05	0.07	0.04	0.07	0.09	0.08	0.04	0.07	0.04	0.07	0.09	0.08	0.04
Ni	wt.%	0.51	0.79	0.46	0.70	0.50	1.10	0.38	0.79	0.46	0.70	0.50	1.10	0.38
Total	wt.%	101.35	96.92	97.09	97.87	97.13	96.60	97.67	96.92	97.09	97.87	97.13	96.60	97.67

- Pentlandite:

Sample		BM-042	BM-042	BM-027	BM-027	BM-027	BM-027	BM-034	BM-010	BM-010	BM-042	BM-042	BM-042	BM-013
Drill Hole		FD-5	FD-5	FD-6	FD-6	FD-6	FD-6	FD-12	FD-3	FD-3	FD-5	FD-5	FD-5	FD-9
Rock Code		Cpxt	Cpxt	Cpxt	Cpxt	Cpxt	Cpxt	Cpxt	Wrlt	Wrlt	Cpxt	Cpxt	Cpxt	Cpxt
Mineral		Pn	Pn	Pn	Pn	Pn	Pn	Pn	Pn	Pn	Pn	Pn	Pn	Pn
As	wt.%	<0.01	<0.01	<0.01	<0.01	<0.01	<0.01	<0.01	<0.01	<0.01	<0.01	<0.01	<0.01	<0.01
Zn	wt.%	<0.01	<0.01	<0.01	<0.01	0.02	0.07	0.06	<0.01	<0.01	0.03	<0.01	<0.01	0.05
S	wt.%	33.77	33.36	31.99	32.14	32.26	32.46	39.92	32.61	32.78	32.75	33.77	35.00	32.98
Pb	wt.%	0.04	0.17	0.10	0.02	0.11	0.01	0.22	0.19	0.06	0.02	0.13	0.03	0.18
Fe	wt.%	30.03	26.74	27.72	27.81	27.79	27.71	24.54	27.58	27.60	27.43	27.31	29.12	24.73
Cu	wt.%	<0.01	<0.01	<0.01	<0.01	<0.01	<0.01	<0.01	<0.01	<0.01	<0.01	<0.01	<0.01	<0.01
Pt	wt.%	<0.01	<0.01	<0.01	<0.01	<0.01	<0.01	<0.01	<0.01	<0.01	<0.01	<0.01	<0.01	<0.01
Cr	wt.%	0.02	0.01	<0.01	<0.01	0.02	0.03	0.01	<0.01	<0.01	0.03	<0.01	<0.01	0.01
Co	wt.%	2.02	1.87	1.60	1.90	2.04	1.77	1.23	2.68	2.69	2.08	2.25	2.63	1.58
Ni	wt.%	28.80	34.34	34.58	35.48	34.73	34.79	29.99	34.86	34.65	40.13	38.30	34.45	35.07
Total	wt.%	94.67	96.49	96.00	97.34	96.96	96.84	95.97	97.91	97.79	102.46	101.77	101.23	94.60

Sample		BM-013	BM-013	BM-013	BM-013	BM-013	BM-013	BM-013	BM-013	BM-033	BM-010	BM-010
Drill Hole		FD-9	FD-9	FD-9	FD-9	FD-9	FD-9	FD-9	FD-9	FD-12	FD-3	FD-3
Rock Code		Cpxt	Cpxt	Cpxt	Cpxt	Cpxt	Cpxt	Cpxt	Cpxt	Ol-Cpxt	Wrlt	Wrlt
Mineral		Pn	Pn	Pn	Pn	Pn	Pn	Pn	Pn	Pn	Pn	Pn
As	wt.%	<0.01	<0.01	<0.01	<0.01	<0.01	<0.01	<0.01	<0.01	<0.01	<0.01	<0.01
Zn	wt.%	<0.01	<0.01	<0.01	<0.01	0.01	0.03	<0.01	<0.01	0.01	<0.01	0.06
S	wt.%	32.42	32.62	33.60	33.64	34.15	33.57	33.21	34.62	34.53	33.28	31.47
Pb	wt.%	0.06	0.07	0.20	0.12	0.04	0.08	0.17	0.20	0.09	0.15	0.07
Fe	wt.%	26.89	27.09	25.74	26.69	26.39	28.42	28.90	27.38	28.75	28.98	31.23
Cu	wt.%	<0.01	<0.01	<0.01	<0.01	<0.01	<0.01	<0.01	<0.01	<0.01	<0.01	<0.01
Pt	wt.%	<0.01	<0.01	<0.01	<0.01	<0.01	<0.01	<0.01	<0.01	<0.01	<0.01	<0.01
Cr	wt.%	0.01	<0.01	0.01	<0.01	<0.01	0.01	<0.01	<0.01	0.01	0.01	<0.01
Co	wt.%	0.72	1.39	1.15	0.52	0.79	0.78	0.91	0.96	2.35	2.75	2.37
Ni	wt.%	38.46	39.57	38.51	39.59	36.51	38.38	37.55	36.31	34.45	36.14	33.80
Total	wt.%	98.56	100.74	99.20	100.56	97.89	101.26	100.75	99.46	100.19	101.32	99.01

- Chalcopyrite:

Sample		XX-R-13	XX-R-13	BM-007	XX-R-16	XX-R-16	XX-R-16	XX-R-16	XX-R-28	XX-R-28	XX-R-28	XX-R-28	BM-038	BM-042
Drill Hole		FD-5	FD-5	FD-3	FD-5	FD-5	FD-5	FD-5	FD-7	FD-7	FD-7	FD-7	FD-12	FD-5
Rock Code		Cpxt	Cpxt	Wrlt	Cpxt	Cpxt	Cpxt	Cpxt	Cpxt	Cpxt	Cpxt	Cpxt	Wrlt	Cpxt
Mineral		Ccp	Ccp	Ccp	Ccp	Ccp	Ccp	Ccp	Ccp	Ccp	Ccp	Ccp	Ccp	Ccp
As	wt.%	<0.01	<0.01	<0.01	<0.01	<0.01	<0.01	<0.01	<0.01	<0.01	<0.01	<0.01	<0.01	<0.01
Zn	wt.%	<0.01	<0.01	<0.01	0.12	0.05	0.14	<0.01	0.07	0.08	0.14	0.06	<0.01	<0.01
S	wt.%	34.77	34.15	34.31	34.26	34.28	33.90	34.24	34.11	33.94	34.14	34.23	33.69	34.20
Pb	wt.%	0.11	0.11	0.20	0.03	0.20	0.13	0.14	0.05	0.05	0.19	0.08	0.15	0.07
Fe	wt.%	29.60	29.28	29.41	29.44	29.87	29.57	29.19	29.60	29.73	29.27	29.40	28.70	29.42
Cu	wt.%	34.32	34.00	34.32	34.56	34.84	33.93	34.35	34.24	34.65	34.63	34.48	32.99	34.68
Pt	wt.%	<0.01	<0.01	<0.01	<0.01	<0.01	<0.01	<0.01	<0.01	<0.01	<0.01	<0.01	<0.01	<0.01
Cr	wt.%	<0.01	0.01	<0.01	0.02	<0.01	0.01	<0.01	<0.01	0.01	<0.01	<0.01	0.18	<0.01
Co	wt.%	<0.01	0.05	0.05	0.03	0.03	0.04	0.01	0.06	0.03	0.05	0.02	0.04	0.05
Ni	wt.%	<0.01	0.10	<0.01	<0.01	<0.01	<0.01	<0.01	<0.01	<0.01	0.02	<0.01	<0.01	<0.01
Total	wt.%	98.80	97.70	98.28	98.45	99.26	97.73	97.93	98.13	98.48	98.44	98.27	95.75	98.43

Sample		BM-042	BM-042	BM-034	BM-041	BM-041	BM-041	BM-041	BM-038	BM-038	BM-038	BM-034	BM-010	BM-010
Drill Hole		FD-5	FD-5	FD-12	FD-5	FD-5	FD-5	FD-5	FD-12	FD-12	FD-12	FD-12	FD-3	FD-3
Rock Code		Cpxt	Cpxt	Cpxt	Wrlt	Wrlt	Wrlt	Wrlt	Wrlt	Wrlt	Wrlt	Cpxt	Wrlt	Wrlt
Mineral		Ccp	Ccp	Ccp	Ccp	Ccp	Ccp	Ccp	Ccp	Ccp	Ccp	Ccp	Ccp	Ccp
As	wt.%	<0.01	<0.01	<0.01	<0.01	<0.01	<0.01	<0.01	<0.01	<0.01	<0.01	<0.01	<0.01	<0.01
Zn	wt.%	0.07	0.10	0.08	0.11	0.03	<0.01	0.09	0.05	0.10	0.05	0.18	0.01	<0.01
S	wt.%	34.23	34.34	34.80	33.95	34.11	34.12	34.25	34.20	34.16	33.68	34.49	34.15	34.13
Pb	wt.%	0.05	0.13	0.06	<0.01	0.13	0.15	0.13	0.14	0.08	0.10	0.07	0.12	0.19
Fe	wt.%	29.85	29.75	29.81	29.51	29.74	29.45	30.02	29.47	29.76	29.41	29.75	29.49	29.87
Cu	wt.%	34.57	34.51	34.67	34.53	34.42	34.43	34.31	34.15	34.07	33.88	34.63	34.35	34.61
Pt	wt.%	<0.01	<0.01	<0.01	<0.01	<0.01	<0.01	<0.01	<0.01	<0.01	<0.01	<0.01	<0.01	<0.01
Cr	wt.%	0.01	<0.01	0.01	0.02	<0.01	0.01	<0.01	<0.01	0.03	0.01	<0.01	0.02	<0.01
Co	wt.%	0.04	0.05	0.04	0.01	0.03	0.04	0.03	0.04	0.04	0.06	0.03	0.04	0.06
Ni	wt.%	0.08	<0.01	0.03	<0.01	0.01	<0.01	<0.01	<0.01	0.01	<0.01	<0.01	<0.01	<0.01
Total	wt.%	98.90	98.88	99.50	98.12	98.46	98.19	98.82	98.05	98.25	97.19	99.16	98.18	98.87

Sample		BM-041	BM-041	BM-041	BM-042	BM-042	BM-013	BM-013	BM-013	BM-013	BM-013	BM-013	XX-R-30	XX-R-30	XX-R-30	BM-033	BM-010	BM-010
Drill Hole		FD-5	FD-5	FD-5	FD-5	FD-5	FD-9	FD-9	FD-9	FD-9	FD-9	FD-9	FD-12	FD-12	FD-12	FD-12	FD-3	FD-3
Rock Code		Wrlt	Wrlt	Wrlt	Cpxt	Cpxt	Cpxt	Cpxt	Cpxt	Cpxt	Cpxt	Cpxt	Dun	Dun	Dun	Ol-Cpxt	Wrlt	Wrlt
Mineral		Ccp	Ccp	Ccp	Ccp	Ccp	Ccp	Ccp	Ccp	Ccp	Ccp	Ccp	Ccp	Ccp	Ccp	Ccp	Ccp	Ccp
As	wt.%	<0.01	<0.01	<0.01	<0.01	<0.01	<0.01	<0.01	<0.01	<0.01	<0.01	<0.01	<0.01	<0.01	<0.01	<0.01	<0.01	<0.01
Zn	wt.%	0.09	0.11	0.12	<0.01	0.13	0.18	0.19	0.06	0.16	0.10	0.61	0.08	<0.01	0.10	0.08	0.03	<0.01
S	wt.%	34.16	34.24	34.33	33.88	34.25	32.34	31.87	32.40	32.90	34.67	34.38	34.31	33.38	34.22	34.13	34.79	34.43
Pb	wt.%	0.11	0.09	0.17	0.01	0.16	0.12	0.12	0.13	0.08	0.08	0.16	0.09	0.13	0.17	0.17	0.16	0.13
Fe	wt.%	29.64	29.17	29.71	29.22	29.21	28.96	28.46	28.95	29.29	32.64	31.80	32.40	32.41	31.85	29.84	32.32	32.60
Cu	wt.%	34.43	34.14	34.32	34.38	34.18	34.14	33.66	33.75	34.39	35.21	33.94	33.94	32.94	32.88	31.01	33.67	34.61
Pt	wt.%	<0.01	<0.01	<0.01	<0.01	<0.01	<0.01	<0.01	<0.01	<0.01	<0.01	<0.01	<0.01	<0.01	<0.01	<0.01	<0.01	<0.01
Cr	wt.%	0.03	0.01	<0.01	0.01	<0.01	<0.01	<0.01	<0.01	0.02	0.02	<0.01	<0.01	0.02	<0.01	<0.01	<0.01	0.01
Co	wt.%	0.02	0.03	0.02	0.01	0.06	0.02	0.02	0.03	0.02	0.05	0.08	0.03	0.06	0.04	0.06	0.05	0.05
Ni	wt.%	0.02	<0.01	<0.01	0.02	0.10	0.01	<0.01	<0.01	0.02	<0.01	<0.01	0.04	<0.01	0.01	0.04	<0.01	0.04
Total	wt.%	98.49	97.79	98.67	97.52	98.08	95.76	94.33	95.32	96.87	102.76	100.98	100.89	98.95	99.28	95.32	101.02	101.87

- Pyrite:

Sample		XX-R-013	XX-R-013	XX-R-013	XX-R-013	XX-R-013	XX-R-016	XX-R-016	XX-R-016	XX-R-016	XX-R-028	XX-R-028	XX-R-028	XX-R-028
Drill Hole		FD-5	FD-5	FD-5	FD-5	FD-5	FD-5	FD-5	FD-5	FD-5	FD-7	FD-7	FD-7	FD-7
Rock Code		Cpxt	Cpxt	Cpxt	Cpxt	Cpxt	Cpxt	Cpxt	Cpxt	Cpxt	Cpxt	Cpxt	Cpxt	Cpxt
Mineral		Py	Py	Py	Py	Py	Py	Py	Py	Py	Py	Py	Py	Py
As	wt.%	<0.01	<0.01	<0.01	<0.01	<0.01	<0.01	<0.01	<0.01	<0.01	<0.01	<0.01	<0.01	<0.01
Zn	wt.%	0.05	0.01	<0.01	0.03	0.06	0.02	<0.01	<0.01	0.04	<0.01	<0.01	<0.01	0.04
S	wt.%	52.60	51.11	51.00	52.92	50.39	51.76	50.45	52.75	51.95	51.94	52.50	52.24	52.07
Pb	wt.%	0.15	0.06	0.18	0.23	0.10	0.16	0.10	0.15	0.12	0.19	0.14	0.21	<0.01
Fe	wt.%	45.49	44.51	44.95	44.89	44.35	44.97	44.41	46.18	44.61	44.69	43.73	45.26	45.30
Cu	wt.%	0.11	0.03	0.02	0.04	0.06	<0.01	<0.01	0.10	0.18	<0.01	<0.01	<0.01	0.03
Pt	wt.%	<0.01	<0.01	<0.01	<0.01	<0.01	<0.01	<0.01	<0.01	<0.01	<0.01	<0.01	<0.01	<0.01
Cr	wt.%	<0.01	<0.01	<0.01	0.02	<0.01	<0.01	<0.01	<0.01	<0.01	<0.01	0.01	0.03	0.01
Co	wt.%	0.07	0.05	0.06	0.04	0.04	0.07	0.03	0.07	0.04	0.06	0.11	0.08	0.03
Ni	wt.%	0.45	0.47	0.64	0.20	0.44	0.35	0.60	0.03	0.30	0.66	1.93	0.54	0.57
Total	wt.%	98.92	96.23	96.84	98.37	95.43	97.34	95.59	99.28	97.23	97.54	98.41	98.37	98.04

Sample		XX-R-028	XX-R-028	XX-R-028	BM-034	BM-034	XX-R-013	XX-R-013	XX-R-013	XX-R-013	XX-R-013	XX-R-013	XX-R-007	XX-R-007
Drill Hole		FD-7	FD-7	FD-7	FD-12	FD-12	FD-5	FD-5	FD-5	FD-5	FD-5	FD-5	FD-2	FD-2
Rock Code		Cpxt	Cpxt	Cpxt	Cpxt	Cpxt	Cpxt	Cpxt	Cpxt	Cpxt	Cpxt	Cpxt	Cpxt	Cpxt
Mineral		Py	Py	Py	Py	Py	Py	Py	Py	Py	Py	Py	Py	Py
As	wt.%	<0.01	<0.01	<0.01	<0.01	<0.01	<0.01	<0.01	<0.01	<0.01	<0.01	<0.01	<0.01	<0.01
Zn	wt.%	<0.01	<0.01	<0.01	<0.01	<0.01	<0.01	<0.01	0.05	0.04	<0.01	<0.01	<0.01	0.01
S	wt.%	52.38	52.23	52.43	52.38	52.34	50.88	51.63	51.26	52.60	50.37	51.27	49.67	50.72
Pb	wt.%	0.15	0.17	0.18	0.35	0.09	0.13	0.17	0.19	0.07	0.11	0.20	0.16	0.15
Fe	wt.%	45.74	45.41	44.21	45.01	45.35	45.75	45.35	45.87	46.12	45.85	45.38	44.59	44.90
Cu	wt.%	<0.01	0.03	<0.01	0.10	0.19	0.12	0.10	0.16	0.05	0.08	0.03	<0.01	<0.01
Pt	wt.%	<0.01	<0.01	<0.01	<0.01	<0.01	<0.01	<0.01	<0.01	<0.01	<0.01	<0.01	<0.01	<0.01
Cr	wt.%	<0.01	<0.01	<0.01	<0.01	<0.01	<0.01	<0.01	0.02	<0.01	0.01	<0.01	<0.01	0.02
Co	wt.%	0.08	0.05	0.02	0.05	0.09	0.07	0.04	0.05	0.09	0.07	0.05	0.03	0.05
Ni	wt.%	0.29	0.45	1.52	0.17	0.12	0.54	0.40	0.32	0.16	0.21	0.81	0.99	1.50
Total	wt.%	98.64	98.34	98.36	98.05	98.18	97.48	97.70	97.92	99.12	96.70	97.75	95.44	97.35

Sample		XX-R-007	XX-R-007	XX-R-003	XX-R-003	XX-R-003	XX-R-003	XX-R-003	XX-R-003	XX-R-007	XX-R-007	XX-R-007	XX-R-003	XX-R-003
Drill Hole		FD-2	FD-2	FD-2	FD-2	FD-2	FD-2	FD-2	FD-2	FD-2	FD-2	FD-2	FD-2	FD-2
Rock Code		Cpxt	Cpxt	Cpxt	Cpxt	Cpxt	Cpxt	Cpxt	Cpxt	Cpxt	Cpxt	Cpxt	Cpxt	Cpxt
Mineral		Py	Py	Py	Py	Py	Py	Py	Py	Py	Py	Py	Py	Py
As	wt.%	<0.01	<0.01	<0.01	<0.01	<0.01	<0.01	<0.01	<0.01	<0.01	<0.01	<0.01	<0.01	<0.01
Zn	wt.%	<0.01	<0.01	<0.01	<0.01	0.10	<0.01	<0.01	0.03	<0.01	0.01	<0.01	<0.01	<0.01
S	wt.%	48.55	50.97	51.28	51.47	51.69	51.51	51.88	51.25	49.67	50.72	50.97	51.28	51.47
Pb	wt.%	0.12	0.11	0.16	0.11	0.10	0.05	0.12	0.16	0.16	0.15	0.11	0.16	0.11
Fe	wt.%	44.82	44.69	44.72	44.79	45.49	45.23	45.60	46.01	44.59	44.90	44.69	44.72	44.79
Cu	wt.%	<0.01	0.16	<0.01	<0.01	<0.01	<0.01	<0.01	<0.01	<0.01	<0.01	0.16	<0.01	<0.01
Pt	wt.%	<0.01	<0.01	<0.01	<0.01	<0.01	<0.01	<0.01	<0.01	<0.01	<0.01	<0.01	<0.01	<0.01
Cr	wt.%	<0.01	<0.01	<0.01	0.01	0.01	0.01	<0.01	<0.01	<0.01	0.02	<0.01	<0.01	0.01
Co	wt.%	0.06	0.08	0.09	0.05	0.06	0.06	0.05	0.07	0.03	0.05	0.08	0.09	0.05
Ni	wt.%	0.91	1.14	1.11	1.63	0.55	0.47	0.51	0.40	0.99	1.50	1.14	1.11	1.63
Total	wt.%	94.46	97.14	97.36	98.05	98.00	97.32	98.16	97.91	95.44	97.35	97.14	97.36	98.05

Sample		XX-R-003	XX-R-003	XX-R-003	XX-R-003	XX-R-030	XX-R-007	XX-R-007	XX-R-007	XX-R-007	XX-R-007	BM-031
Drill Hole		FD-2	FD-2	FD-2	FD-2	FD-12	FD-2	FD-2	FD-2	FD-2	FD-2	FD-6
Rock Code		Cpxt	Cpxt	Cpxt	Cpxt	Dun	Cpxt	Cpxt	Cpxt	Cpxt	Cpxt	Wrlt
Mineral		Py	Py	Py	Py	Py	Py	Py	Py	Py	Py	Py
As	wt.%	<0.01	<0.01	<0.01	<0.01	<0.01	<0.01	<0.01	<0.01	<0.01	<0.01	<0.01
Zn	wt.%	0.10	<0.01	<0.01	0.03	0.02	<0.01	0.04	<0.01	0.06	0.02	<0.01
S	wt.%	51.69	51.51	51.88	51.25	53.32	49.05	51.13	50.33	51.83	52.29	51.57
Pb	wt.%	0.10	0.05	0.12	0.16	0.16	0.17	0.23	0.12	0.14	0.13	0.12
Fe	wt.%	45.49	45.23	45.60	46.01	46.66	44.69	45.42	45.51	45.46	46.34	45.39
Cu	wt.%	<0.01	<0.01	<0.01	<0.01	0.19	0.52	0.54	0.25	0.08	0.11	0.01
Pt	wt.%	<0.01	<0.01	<0.01	<0.01	<0.01	<0.01	<0.01	<0.01	<0.01	<0.01	<0.01
Cr	wt.%	0.01	0.01	<0.01	<0.01	0.02	<0.01	<0.01	0.01	<0.01	<0.01	0.03
Co	wt.%	0.06	0.06	0.05	0.07	0.03	0.09	0.07	0.07	0.06	0.06	0.07
Ni	wt.%	0.55	0.47	0.51	0.40	0.20	0.40	0.08	0.45	0.85	<0.01	0.16
Total	wt.%	98.00	97.32	98.16	97.91	100.60	94.91	97.52	96.74	98.48	98.95	97.35

CONCLUSÕES

As conclusões deste estudo são as seguintes:

1. O depósito magmático de sulfetos de Ni-Cu Caboclo dos Mangueiros representa recente descoberta situada na borda noroeste do cráton do São Francisco, um cenário amplamente reconhecido em depósitos de Ni-Cu-EGP pelo mundo;
2. O corpo de minério está hospedado em uma intrusão relativamente pequena, consistindo de um *sill* (soleira) alongado em forma de barco (*boat-shape*) na direção WNW-ESE, com seções transversais de poucas centenas de metros de profundidade, aproximadamente 2 km de comprimento e 500 m de largura;
3. A intrusão ultramáfica que hospeda o depósito Caboclo dos Mangueiros está fracionada da porção norte, onde prevalece dunito e wehrlito, para a porção sul onde clinopiroxenito é abundante;
4. Composições de elementos maiores nas rochas ultramáficas são controladas pelas proporções de olivina e clinopiroxênio, que seguem sequência de cristalização consistindo de Ol => Ol + Cpx => Cpx;
5. A abundância de rochas ultramáficas e a variação composicional de #Mg em clinopiroxênio cumulus, de 0.78 a 0.94, suportam composição moderada a primitiva para o magma parental;
6. A sequência de cristalização indica composição insaturada em sílica para o magma parental e a inexistência de cristais cúmulus de ortopiroxênio sugere que o magma parental se manteve com esta característica composicional, sem assimilação significativa de rochas crustais silicosas durante ascenção e alojamento na crosta;
7. Perfis normalizados ao manto primitivo, de elementos traço resistentes à alteração estimados para o magma parental, indicam composição enriquecida em ETRL, o que é refletido em perfis normalizados ao manto primitivo de elementos traço resistentes à alteração, para as rochas cumuláticas ultramáficas juntamente com anomalias negativas de Nb e Ta;
8. A distribuição dos ETRL normalizados ao manto primitivo nas rochas cumuláticas ultramáficas é parcialmente controlada pela proporção modal de clinopiroxênio;
9. As texturas e as quantidades de sulfeto, acima da proporção cotética, no depósito magmático de sulfetos de Ni-Cu Caboclo dos Mangueiros sugerem alojamento de magma carreando gotículas imiscíveis de sulfeto através de estrutura de conduto que posteriormente solidificou-se como um *sill* alongado em forma de barco;
10. Os conteúdos de sulfeto acima da proporção cotética também sugerem que grandes volumes de sulfetos tenham sido transportados pelo sistema magmático;
11. A composição dos sulfetos depletada em EGP, proveniente de um magma parental com composição moderada a primitiva, é sugestiva que tenha ocorrido segregação prévia de sulfetos em profundidade;
12. Características composicionais dos isótopos de enxofre do depósito refletem fonte mantélica para os sulfetos sem adição significativa de enxofre derivado da crosta;

13. Assembleias metamórficas descritas para as rochas crustais, cumulados ultramáficos e para as rochas da zona de borda sugerem que a intrusão ultramáfica e as rochas crustais foram submetidas ao mesmo evento de tectonismo e metamorfismo de fácies xisto verde associado. Ainda assim a estrutura magmática primária da intrusão se manteve preservada;
14. Embora a similaridade na distribuição dos elementos traços entre as rochas da zona de borda e os cumulados ultramáficos sugiram que são originários de magmas parentais composicionalmente similares, dados adicionais são necessários para a caracterização robusta desta zona da intrusão;
15. O posicionamento do depósito Caboclo dos Mangueiros na evolução tectônica do cráton do São Francisco ainda não é definido devido à falta de uma idade absoluta para a intrusão ultramáfica; e
16. A abundância de anomalias magnéticas inexplicadas no cenário regional do depósito Caboclo dos Mangueiros, juntamente com o cenário tectônico o qual está situado indicam alto potencial para depósitos de Ni-Cu-EGP nesta região.